

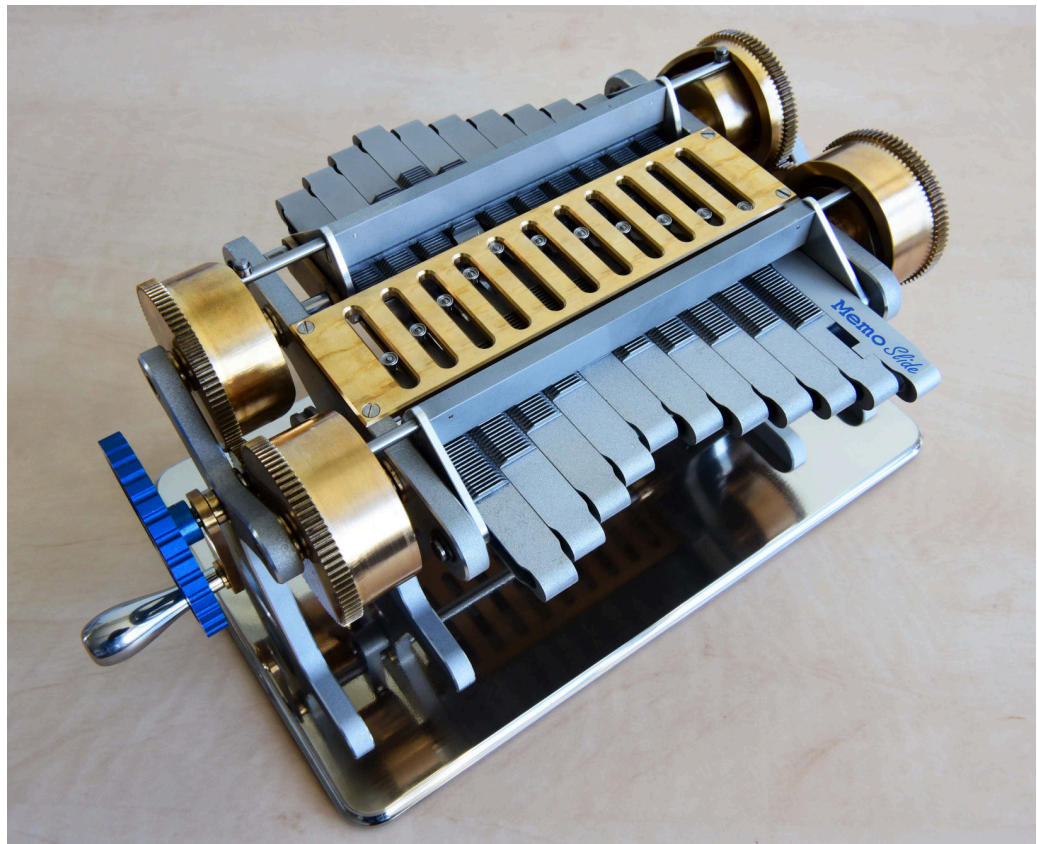
Follow-The-Leader Control:

A mechanical control mechanism for path following deployment of surgical instruments

Principle validation & concept design

MASTER THESIS

STEFAN GOTTENBOS



ABSTRACT

Surgical procedures are shifting towards Minimal Invasive Surgery (MIS). Surgeons are currently limited in their actions by the straight rigid instruments available to them. Devices capable of navigating along curved trajectories increase a surgeon's workspace, which can benefit surgical performance.

This paper shortly goes over the state of the art of Highly Redundant Devices (HRD) capable of Follow-The-Leader (FTL) behaviour. In literature virtual and physical control methods are used. Virtual control relies on computer control in combination with actuators. The actuators control the tip segments via cables running the length of the device. Physical control stores and transfers shape information in a mechanical configuration. From the state of the art it was found that physical control has the potential of reducing the amount of actuators severely. However, it was also found that these mechanisms are, up to now, placed inside the tip. The integration of the physical control inside the tip leads to problems with stiffness, accumulating errors and minimisation. A combination of attributes from both virtual and physical control resulted in a novel mechanical FTL control principle: MemoSlide. This principle essentially captures a software algorithm in a mechanism. The suggested control principle reduces the number of actuators needed for FTL control.

A Proof of Concept (PoC) demonstrator model, showcasing the MemoSlide principle in a plane, is designed and fabricated. Friction, Jamming and Locking were identified as crucial aspects to consider while implementing the MemoSlide principle. Experience gained during fabrication and evaluation resulted in a set of design guidelines and a simplification of the MemoSlide principle. Application of the simplified principle and the design guidelines resulted in a conceptual design of a control module. The control module is intended to control a steerable surgical tool tip as inspiration for future applications of the MemoSlide principle.

PREFACE

Before you lies my Master Thesis "Follow-The-Leader Control: A mechanical control mechanism for path following deployment of surgical instruments", the product of my graduation project. This thesis is written to complete the graduation requirements of the Bio Inspired Technology specialisation within the BioMechanical Engineering department of the TU Delft. I was engaged in my graduation project during the period of September 2015 to August 2016.

With this preface, I want to thank a few people who helped and inspired me to complete it. First of all I'd like to thank my professor Paul Breedveld for the interesting graduation subject and the inspired talks we had during the course of my graduation. Furthermore, I want to thank my daily supervisor Paul Henselmans for the regular meetings and constructive feedback which kept me on track, his enthusiasm and patience with me when I dropped in outside our scheduled meetings. Additionally I'd like to thank David Jager for his expertise in fine mechanical fabrication, contributions to the design phase and attention to detail which made the realisation of a beautiful prototype possible.

Thanks to our study group on the fourth floor of 3Me for all the fun during coffee breaks and lunches. And most of all the peer pressure which contributed to the completion of this thesis.

Lastly, I want to thank my family for helping me become the person I am today. Special thanks to my girlfriend for all her support and encouragements which were instrumental to finishing my graduation project.

Stefan Gottenbos

Delft, August 2016

CONTENTS

I Introduction 9

I-A Motive 9

I-B State of the art 10

I-C Problem definition 11

I-D Goal 11

I-E Structure 11

II Principle 11

II-A Actuation 11

II-B Dots/Blocks representation 11

II-C Algorithm 13

II-C1 Steering 13

II-C2 Lock memory 13

II-C3 Memory slide 13

II-C4 Lock shape 13

II-C5 Memory reset 13

III PoC demonstrator 13

III-A Design guidelines 13

III-B Mechanical representation D/B 13

III-B1 Basic constraints 13

III-B2 Dots/Blocks interaction 14

III-C Functions 15

III-D Prototype 18

III-E Evaluation 18

III-E1 Principle 18

III-E2 Design guidelines 18

III-F Alterations 22

IV Concept design 22

IV-A 2D to 3D translation 22

IV-B Design guidelines 22

IV-B1 Tip 22

IV-B2 Stiff tip control 23

IV-B3 Friction 23

IV-B4 Jamming 23

IV-B5 Locking 23

IV-C Concept design 23

IV-C1 Basic constraints/interaction 25

IV-C2 Locking 25

IV-C3 Steering 25

IV-C4 Memory slide 25

IV-C5 Timing 25

V Discussion 25

V-A Principle 25

V-B PoC validation 27

V-C Future work 27

VI Conclusion 28

References 28

Appendix A: Friction accumulation 29

Appendix B: Literature paper 31

Appendix C: Work drawings 45

LIST OF FIGURES

1 Follow-The-Leader locomotion modes of snakes. 9

2 OC Robotics X125 series II [1]. 10

3 Highly Articulated Robotic Probe (HARP) [3] . 10

4 Concentric Tube Robot (CTR) [2]. 10

5 A 20 DoF cable ring steerable tip [4]. 10

6 Remote actuated steerable tip model. 12

7 D/B representation 12

8 The algorithm cycle, D/B representation 12

9 Mechanical FTL principle algorithm 13

10 Shape and memory fingers, basic constraints . . 14

11 Shape/memory finger interaction, 3D view. . . . 14

12 Shape and memory interaction phases. 15

13 Guidance plates 15

14 Steering input sub-functions. 16

15 Locking system. 16

16 Locking system actuation. 16

17 Memory slide and locking system actuation. . . . 17

18 Algorithm time-line. 17

19 The PoC demonstrator: 'MemoSlide' 18

20 A single algorithm cycle, top view. 19

21 Complex shape transfer 20

22 Tilt-jamming, problem and solution 21

23 Friction accumulation, problem and solution . . . 21

24 One-way slide algorithm, D/B representation . . 22

25 Simplified mechanical FTL principle algorithm . 22

26 MemoSlide control module configuration options. 23

27 Artists impression steerable device. 23

28 Concept design tip control module. 24

29 Basic constraints and interactions of parts 24

30 Joystick, schematic side and top views 26

31 Timing phase conceptual design, top view. . . . 26

32 MemoSlide modules implementation options. . . 26

33 Friction accumulation, problem and solution . . . 30

34 The 'MemoSlide', exploded view. 45

Mechanical Follow-The-Leader Principle, Validation & Concept Design

Stefan Gottenbos, *MSc student, TU Delft*

Abstract—Surgical procedures are shifting towards Minimal Invasive Surgery (MIS). Surgeons are currently limited in their actions by the straight rigid instruments available to them. Devices capable of navigating along curved trajectories increase a surgeon’s workspace, which can benefit surgical performance.

This paper shortly goes over the state of the art of Highly Redundant Devices (HRD) capable of Follow-The-Leader (FTL) behaviour. In literature virtual and physical control methods are used. Virtual control relies on computer control in combination with actuators. The actuators control the tip segments via cables running the length of the device. Physical control stores and transfers shape information in a mechanical configuration. From the state of the art it was found that physical control has the potential of reducing the amount of actuators severely. However, it was also found that these mechanisms are, up to now, placed inside the tip. The integration of the physical control inside the tip leads to problems with stiffness, accumulating errors and minimisation. A combination of attributes from both virtual and physical control resulted in a novel mechanical FTL control principle: MemoSlide. This principle essentially captures a software algorithm in a mechanism. The suggested control principle reduces the number of actuators needed for FTL control.

A Proof of Concept (PoC) demonstrator model, showcasing the MemoSlide principle in a plane, is designed and fabricated. Friction, Jamming and Locking were identified as crucial aspects to consider while implementing the MemoSlide principle. Experience gained during fabrication and evaluation resulted in a set of design guidelines and a simplification of the MemoSlide principle. Application of the simplified principle and the design guidelines resulted in a conceptual design of a control module. The control module is intended to control a steerable surgical tool tip as inspiration for future applications of the MemoSlide principle.

Index Terms—Follow-The-Leader, FTL, highly redundant devices, HRD, surgical instrumentation, pathway surgery, minimal invasive surgery, MIS, prototyping.

I. INTRODUCTION

A. Motive

In recent years, many surgical procedures have shifted from open to Minimal Invasive Surgery (MIS). In MIS, surgical instruments are inserted through small incisions into the body. Current surgical instruments are mostly long, slender rigid instruments. The instruments pivot at the incision location, and insertion angle, depth and tip orientation are the only methods to control the tool at the tip. This limits the surgical workspace to locations reachable via a straight path from incision to target. This implies the need for instruments capable of following non-straight, curved paths.

To enable a surgeon to operate on an obscured target, an instrument requires additional Degrees of Freedom (DoF) to



Fig. 1: Follow-The-Leader locomotion modes of snakes.
The body follows the path of the head.

manoeuvre around an obstacle along a curved path. These additional DoF are referred to as redundant DoF because they are not required for tip positioning, but can influence the instrument’s shape between base and tip. The human elbow, for example, provides us with such a redundant DoF to enable picking up an object behind an obstacle. In more complex tasks, the available workspace can be restricted further by more and closer boundaries. When more DoF are added, more obstacles can be avoided and the boundaries can become narrower. Highly Redundant Devices (HRD) have numerous redundant DoF and are therefore highly flexible.

Surgery on an obscured target requires the instruments to be able to propagate along complex trajectories containing multiple curves. This means that an adequate control strategy needs to be deployed to control the numerous redundant DoF. Such a control strategy is called Follow-The-Leader control, which can best be compared with the locomotion of a snake. A snake can navigate complex, cluttered environments by steering its head while its body follows around obstacles, illustrated in Fig. 1.

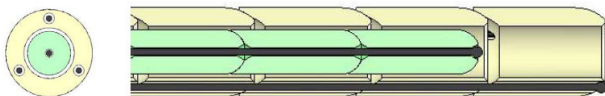
When the snake propels itself forward, it shifts the shape of its body backwards. Similarly, a FTL controlled device must advance its entire body while the device shape is transferred backwards. The device shape will then remain stationary with respect to the environment. Devices capable of FTL behaviour are identified in a literature survey by S. Gottenbos [5]. A self-guided surgical device must be self-supported to enable following of complex trajectories in space without relying on interaction with the environment.



Fig. 2: OC Robotics X125 series II [1].
A series of individually remote actuated segments

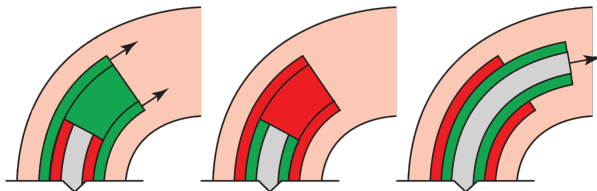


(a) HARP around a model heart.



(b) HARP internal structure, cross section view.

The play can be seen between the green inner and yellow outer snake.



(c) Physical shape memory approach.

Fig. 3: Highly Articulated Robotic Probe (HARP) [3]

Two 'snakes' of serially connected segments can be rigidified separately by cable tension and slide along each other. The inner snake has a single cable running through it. The outer snake has three cables running through it. Two tubes are alternately made rigid and flexible, the rigid (red) tube acts as a guide for the flexible (green) tube. The flexible tube is pushed forwards and is then made rigid to act as a new guide for the other tube [6].

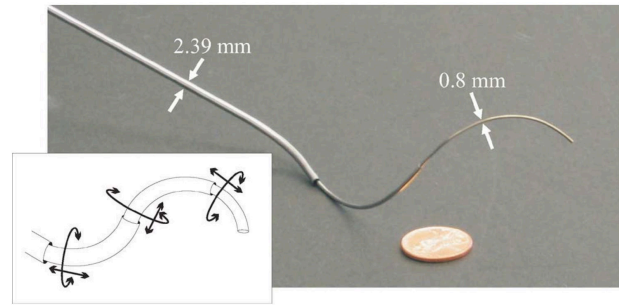


Fig. 4: Concentric Tube Robot (CTR) [2].
The flexible interactions between parallel pre-curved tubes determine the device shape.

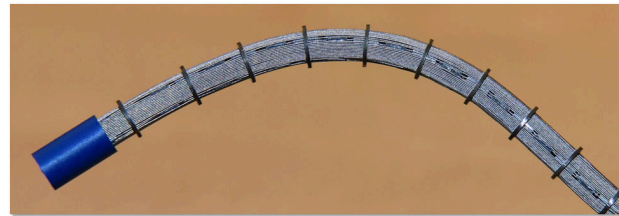


Fig. 5: A 20 DoF cable ring steerable tip [4].

B. State of the art

Two separate methods of achieving FTL control have been identified by A. Loeve [6]: *Virtual* [1], [2] shape memory control and *physical* [3] shape memory control. Virtual shape memory control relies fully on digital control theory. In this method, the shape information is stored in a computer and transferred to the HRD via actuators. Software calculates which actuators need to be activated at what input to achieve FTL-behaviour. Physical shape control relies on a mechanical approach. The shape information is stored in a mechanical configuration and also transferred to the HRD via a mechanical mechanism. Physical shape control requires simple to no control software.

A robot of OC Robotics, the OC Robotics X125 series II [1] illustrated in Fig. 2 uses virtual control. The tip of this device consists of a series of connected segments. These segments can be independently controlled via their own cable sets that run along the length of the device. The cables are actuated by electric motors in the base on the device.

Another device that uses virtual memory control is the Concentric Tube Robot (CTR) [2] illustrated in Fig. 4. The CTR employs the flexible interactions between parallel pre-curved tubes for shape control. The tubes translate and rotate with respect to each other which affects the entire shape of the device. The resultant shape of two or more pre-curved tubes inserted into each other is a product of the force equilibrium of the pre-curvature and stiffness characteristics of the tubes. As the entire shape of the device is affected by the re-orientation or re-positioning of a single tube, unstable configurations can occur while working towards the goal configuration. In such unstable configurations a small change in an input variable can result in a large displacement of the device shape [7]. CTRs are therefore generally not capable of performing pure

FTL behaviour. Instead approximate following of the path, with small tracking errors of under 3 mm, can be obtained [8]. However in very specific combinations of pre-curvatures and control strategies some paths can be followed with pure FTL behaviour [9].

The Highly Articulated Robotic Probe (HARP) [3] employs physical shape memory control. The HARP deployed along a complex trajectory around a heart model is illustrated in Fig. 3a. The HARP consists of two co-axially placed stacks of segments serially linked with cables, the so called inner and outer 'snakes', illustrated in Fig. 3b. Tension on the inner cable makes the inner snake stiff, releasing tension makes it flexible again. The outer snake rigidity is controlled by tensioning and relaxing the 3 outer cables.

Physically shape controlled devices [3], [6] incorporate the shape memory control into the mechanical design. A physically controlled device consists of sets of two or more tubes, with a steerable tip. The tubes can be made rigid or flexible at will. By having one tube rigid and one tube flexible, the rigid tube can act as a guide for the flexible tube as illustrated in Fig. 3c [6]. Pushing the flexible tube forward beyond the length of the rigid tube, the tip can be used to steer the flexible tube in a desired direction. By alternating the rigid and flexible state of both tubes, the process can repeat itself resulting in FTL behaviour. Due to the necessity of alternating the rigidity and the time this action costs this is a relatively slow method. An extensive overview of possible rigidifying mechanisms is created by A. Loeve [6].

C. Problem definition

Approximate FTL behaviour with a small instrument can be achieved by CTR's employing virtual control. However, pure FTL behaviour can not be achieved except for specific trajectory and configuration combinations. The serial tip of OC Robotics did achieve pure FTL deployment. Therefore, the serial remote actuation principle seen in the OC Robotics X125 series II was miniaturised at the TU Delft to a compact cable ring mechanism [4]. A 10 segment, 20 DoF, Ø6 mm steerable tip is constructed at the TU Delft, illustrated in Fig. 5. However, this remotely actuated tip requires control of 40 individual cables. Virtual shape memory control can provide the control required for FTL behaviour, yet this would require at least 20 actuators.

The physical shape memory control of the HARP reduces the number of actuators considerably. A disadvantage, due to the discrete nature of the device links sliding relatively, is the interplay between the outer and inner links illustrated in Fig. 3b. This play is necessary to allow the relative sliding when the device is curved. However, this play acts as a damper on the shape information stored in the snakes. With each step a small portion of the shape information is lost. The storage of shape information relies on the friction contacts between the snake segments. A large enough disturbance force can corrupt the stored device shape permanently. The fact that the shape memory control system resides inside the steerable tip limits the tracking accuracy and the potential for minimisation.

A physical shape memory control system outside the device body could function without the play required in the HARP,

preventing the decay of shape information with each step. A remotely actuated steerable tip with a physical shape memory control module could provide a dextrous surgical device, without the need for a large amount of electric actuators.

D. Goal

The goal of this paper is to introduce and validate a novel fully mechanical shape memory control principle, the "MemoSlide" principle, that eliminates the need for large numbers of electric actuators. To encourage implementation of this principle a plausible concept design is presented intended to control a remotely actuated 20 DoF steerable cable ring instrument tip.

E. Structure

This paper will introduce the MemoSlide principle first in section II. A PoC prototype is designed to validate the MemoSlide principle. The design guidelines, design and evaluation which resulted in the PoC demonstrator model are described in section III. The lessons learned during fabrication and evaluation of the PoC demonstrator are used to generate a conceptual design of a control module in section IV. Achievements and problems encountered are discussed in section V. The paper is concluded in section VI.

II. PRINCIPLE

A. Actuation

To introduce the MemoSlide principle a simple representation of a remotely actuated 2D steerable device is illustrated in Fig. 6, consisting of 5 segments with each 1 DoF. These segments are all independently actuated by their individual cable-sets. When all cable-ends are at the base line, visualised using green dots on a dotted line, the device is straight (Fig. 6a). The tip is steered by displacing the corresponding cables (Fig. 6b). Controlling the (relative) displacements of the control dots determines the shape of the device. Follow-the-leader behaviour is obtained when the displacements of the cables shift one segment backwards (in Fig 7 this is downward), while the entire device moves one segment length forward (in Fig 7 this is to the right), see Fig. 6c.

Observing Fig. 6 we can see the cable control input on the top side of the device is a mirror image of the bottom side. Connecting these displacements via two pulleys reduces the control input to the linear displacement of just a single control dot. Further explanation of the principle will use a single set of green control dots corresponding to the bottom cable control input.

B. Dots/Blocks representation

As a tool to introduce the shape memory control principle a simplified 2D representation is used. Based on the green control dots of Fig. 6 the actuating input is reduced to the position of these green *Dots* in the so-called Dots/Blocks (D/B) representation. The Dots are corresponding to the control input of the cables, and can only translate horizontally, illustrated in Fig. 7a. The Blocks represent the physical memory bank. They

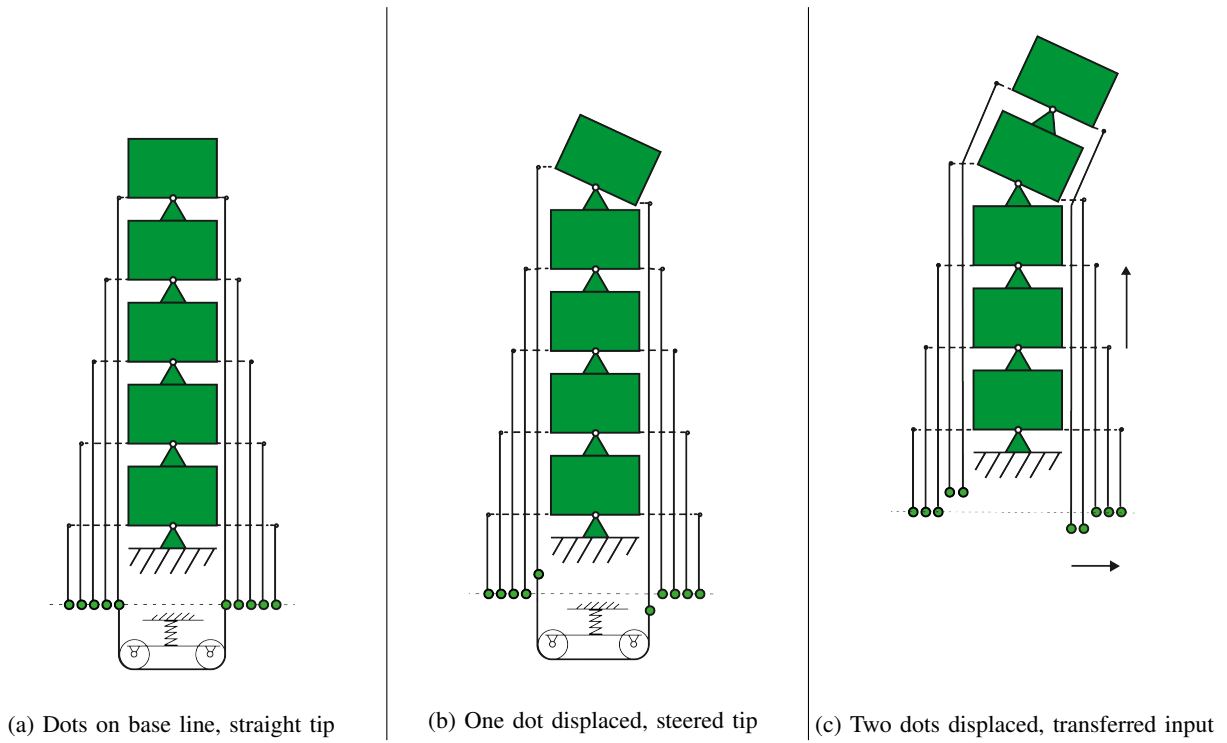


Fig. 6: Remote actuated steerable tip model.

A schematic representation of a 5 DoF steerable tip is remotely actuated using cables. The cable ends are marked with dots.

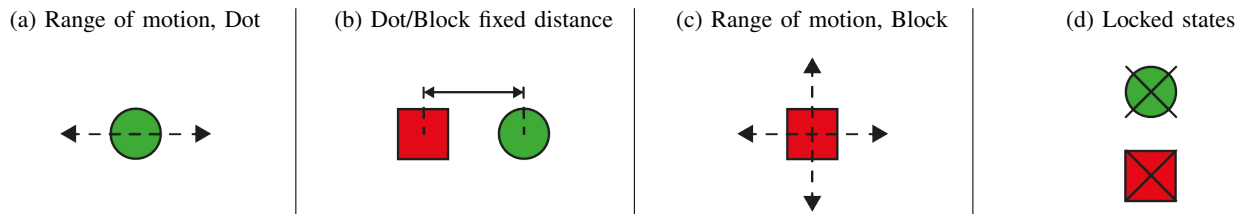


Fig. 7: D/B representation

An abstract representation of the control input of a steerable tip.

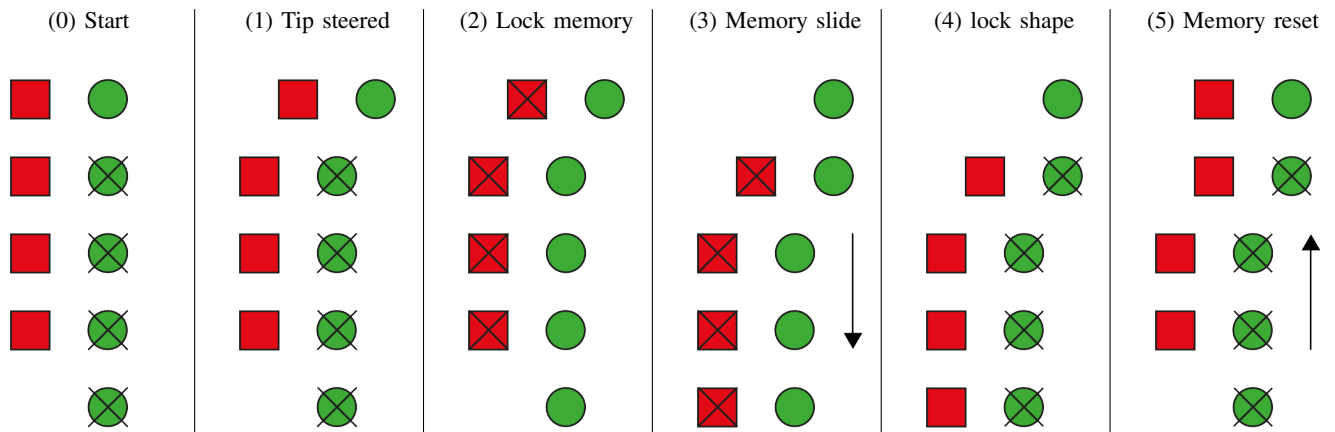


Fig. 8: The algorithm cycle, D/B representation

Schematic representation of the algorithm steps of the control principle.

copy the movements of the dots by keeping a fixed distance from the dots they are in-line with, illustrated in Fig. 7b. Moreover, the blocks can slide vertically, to align with the dots above or below them, illustrated in Fig. 7c. Furthermore, the dots and blocks can be in a locked state, meaning they cannot slide horizontally, illustrated by a cross in Fig. 7d. Translating Fig. 6 into the D/B representation results into Fig. 8.

C. Algorithm

The algorithm to enable FTL-control can now be described by two phases, the steering phase and the shape transfer phase (Fig. 9). The steering phase requires input from the user. The shape transfer phase consists of four sequential actions that transfer the shape of the device.

Algorithm:

Input	
1) Input shape from user:	<i>Steering</i>
Shape transfer	
2) Store shape in memory:	<i>Lock memory</i>
3) Transfer shape to next segment:	<i>Memory slide</i>
4) Store transferred shape:	<i>Lock shape</i>
5) Restore memory to start:	<i>Memory reset</i>

Fig. 9: Mechanical FTL principle algorithm

One full cycle of the algorithm is illustrated by the D/B representation in Fig. 8. Starting with the straight tip configuration seen in Fig. 6 corresponding with 8.0 in the D/B representation. The input and shape transfer steps each facilitate the transition between two mechanism states illustrated in Fig. 8.0-8.5. In the straight starting configuration, Fig. 8.0, all Dots are locked in position except for the first, the user controlled Dot.

1) *Steering*: Fig. 8.0 → 8.1

The tip receives the steering input from the user as a displacement of the first Dot.

2) *Lock memory*: Fig. 8.1 → 8.2

Once the steering input is given the shape information is stored in the Blocks by locking their configuration. Sequentially, the Dots are unlocked.

3) *Memory slide*: Fig. 8.2 → 8.3

Moving the locked Blocks down to align with the subsequent Dots imposes the shape information onto the Dots, transferring the shape information.

4) *Lock shape*: Fig. 8.3 → 8.4

The newly transferred device shape is stored in the Dots by locking their configuration. Subsequently the Blocks are unlocked.

5) *Memory reset*: Fig. 8.4 → 8.5

Moving the unlocked Blocks back upwards resets the memory bank in order to receive the next steering input.

III. POC DEMONSTRATOR

A Proof of Concept (PoC) prototype is required to validate whether the principle can be executed by a purely mechanical device. To facilitate further development the prototype is desired to clearly show the working principle and function as a demonstrator model. Due to the crucial step of the memory bank sliding back and forth the PoC demonstrator is named: "MemoSlide". Several design iterations resulted in the final design presented in this section.

A. Design guidelines

The PoC demonstrator was subject to a set of design guidelines. These guidelines are qualitative in nature due to the novelty of the working principle. To obtain a clear demonstrator model these guidelines focus on the usability and recognisability of the principle at work. The goal of the PoC demonstrator is to obtain a mechanical, insightful, table-top device, scaled for easy manual manipulation. Furthermore the parts representing the Dots and Blocks are desired to move in a 2D plane. $N = 10$ memory segments are chosen to represent a tip with 10 steerable segments capable of complex shapes. Maximal steering action corresponds to a 4 mm displacement of a Dot. The total Dot Range of Motion (RoM) consists of the middle configuration and 3 full steps to either side, [-12 to +12] mm.

B. Mechanical representation D/B

To create a PoC demonstrator the basic constraints and the interactions between the Dots and Blocks as described in the D/B representation must be translated to their mechanical equivalent. First, the required Dots/Blocks *basic constraints* and the *Dots/Blocks interaction* are detailed.

1) *Basic constraints*: As seen in the D/B representation, the Dots have 1 DoF, in a line, with a maximal RoM of [-12 to +12] mm from the centre point. A Dot is represented by a ball bearing with a $\varnothing 4$ mm outer diameter. It is supported by a slender beam, a 'shape finger'. This shape finger lays on two axes that run through a groove in the shape finger. The shape finger can slide along those axes, while the RoM is enforced by the groove length. One of these axes rotates, actuating the shape transfer algorithm steps. To prevent the shape fingers from interacting with the rotating axis which support it a bushing is fitted inside the groove, illustrated in Fig. 10.a. Frames supporting the axes restrict movement perpendicular to the desired direction by sandwiching 11 fingers between the side plates, illustrated in Fig. 10.c.

The Blocks have 2 DoFs. One mimics the Dots in horizontal direction, the other DoF is in the vertical direction to align with the next Dot. A similar slender beam, a 'memory finger', with a groove supported by 2 axes can allow both DoFs. A memory finger is illustrated on its supporting axes in Fig. 10.b. 10 memory fingers form the entire memory bank and are sandwiched between the restricting frames, illustrated in Fig. 10.d. Moving the restricting frames along the axes lengths controls the perpendicular movement of the Blocks.

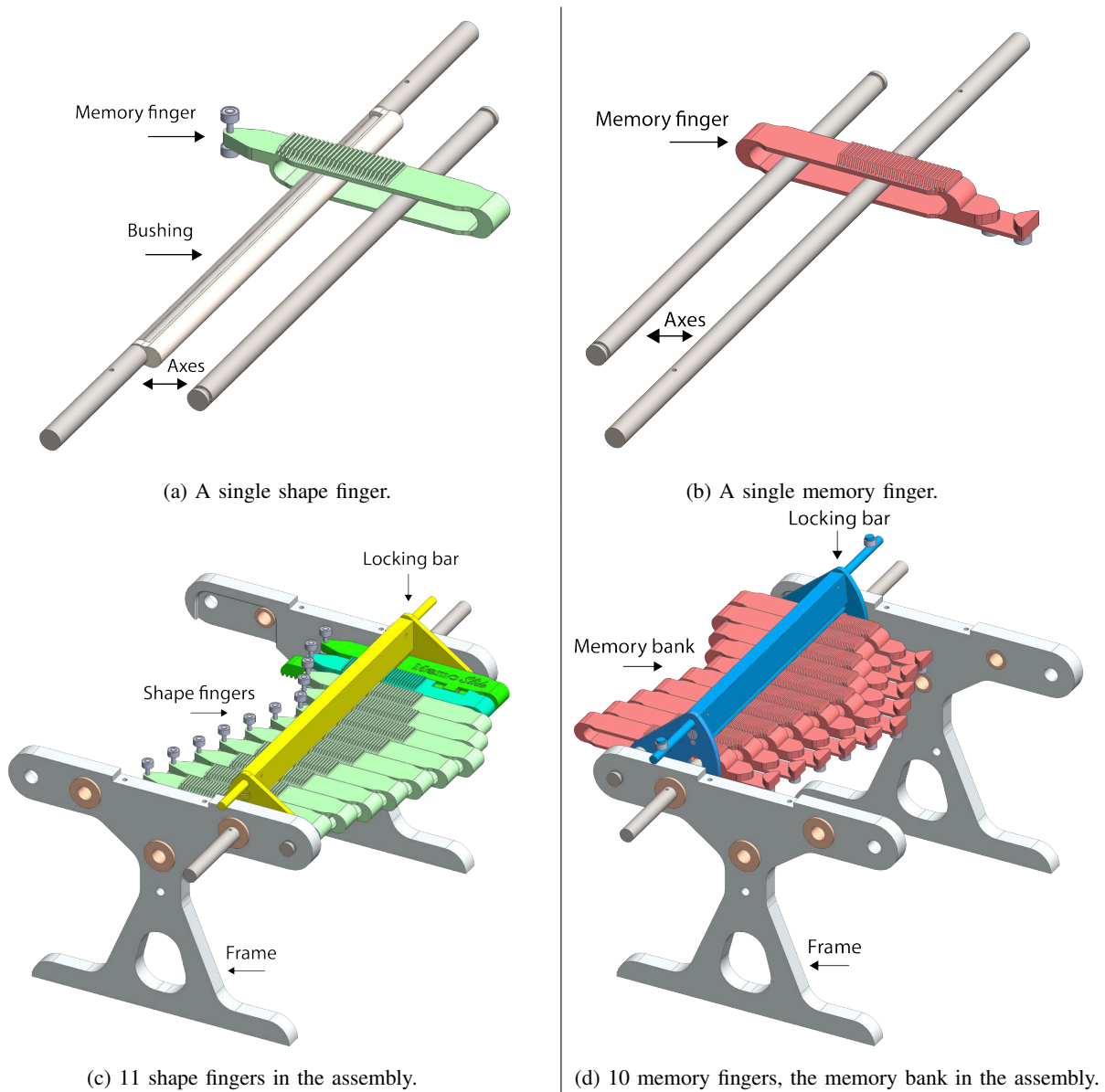


Fig. 10: Shape and memory fingers, basic constraints

The required DoFs of the dots and blocks are achieved using 'fingers' sliding along 2 axes, constrained by frames.

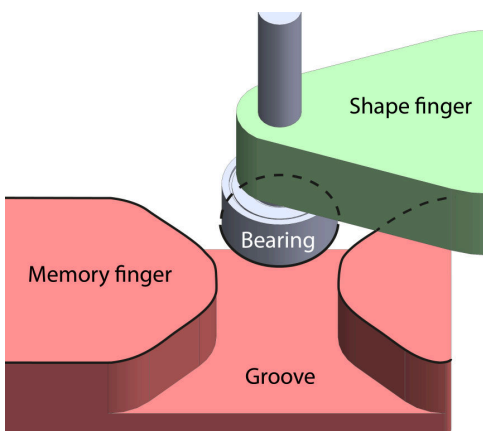


Fig. 11: Shape/memory finger interaction, 3D view.

2) *Dots/Blocks interaction*: The interaction between the Dots (shape fingers) and Blocks, (memory fingers) lies at the core of this principle. As introduced in the D/B representation the shape fingers (Dots) and memory fingers (Blocks) must have a fixed distance when aligned. Furthermore, when the memory is sliding downward the shape finger must assume the fixed displacement of the memory finger. This transfer of shape information is illustrated by the transition from Fig. 8.2 to 8.3.

A method to achieve this behaviour mechanically is to create a funnel-shaped groove on the memory fingers, illustrated in Fig. 11. The interaction is shown in a 2D view in Fig. 12. The ball bearing, functioning as Dot, is constrained when aligned with the memory groove (Fig. 12.1). However, when the locked memory fingers start sliding vertically the grooves contact the next bearings, illustrated in Fig. 12.2. The in-

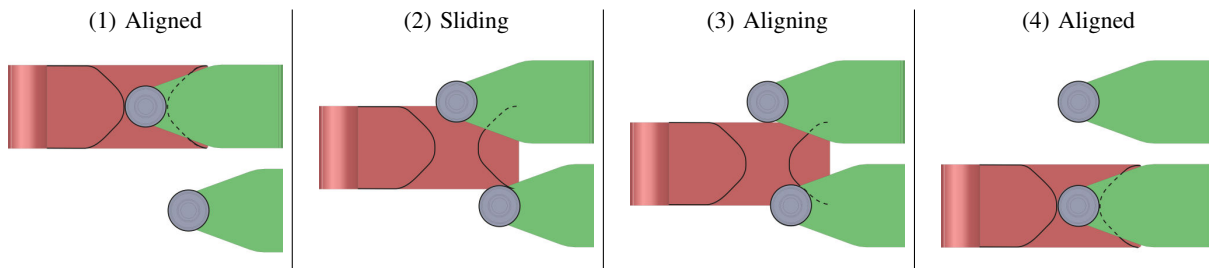


Fig. 12: Shape and memory interaction phases.

The bearing/groove interaction during the memory slide, the bearing is forced to align with the groove.

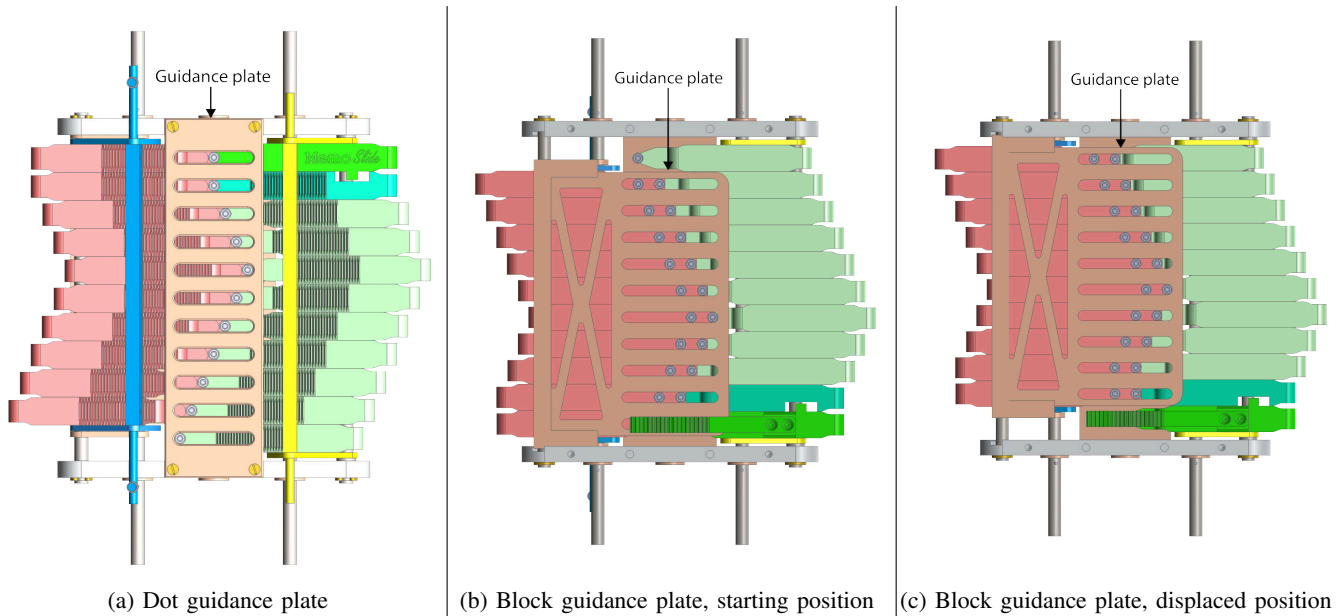


Fig. 13: Guidance plates

The grooved plates guiding the shape Dot and memory Block bearings

teraction forces move the bearing horizontally (Fig. 12.3) to eventually align with the groove, illustrated in Fig. 12.4. The alignment action is limited in the offset it is able to handle. Therefore, the steering input must be limited to accommodate for this restriction.

Strict linear guidance is required for the shape control Dots. This is realised by implementing a plate with grooves that guide the Dot bearings as illustrated in Fig. 13.a. With the local guidance present the transmission of sideways movement to a translation perpendicular in direction was achieved using groove edges at an angle of 45 deg. Resulting in a 1:1 ratio between perpendicular motions. The range of viable groove angles is not further investigated in this study.

The memory fingers require linear guidance as well. Two bearings are mounted on the underside of the fingers. The bearings are guided by a separate plate with grooves below the memory bank. Since the memory fingers have an additional DoF the guidance plate must be able to slide vertically. The vertical DoF is achieved by mounting the guidance plate on the same axes supporting the memory fingers. The plate guiding the memory fingers is illustrated in Fig. 13, the start and displaced positions are illustrated in respectively Fig. 13.b and 13.c.

C. Functions

The algorithm steps must be captured in mechanical structures. These structures are described according to the corresponding actions they perform: *Steering*, *Locking*, *Memory slide* and *Timing*. As each function is described the integrated design will be presented.

Steering: A rack and pinion transmission is used to control the first shape control finger, illustrated in Fig. 14. The pinion is connected to the steering wheel, the rack is connected to the first shape control finger illustrated in Fig. 14.a. The maximal steering input is limited by a pin/slot connection between the steering finger and the second, following, shape finger. The input limiting tab/slot connection is illustrated in Fig. 14.b. A discrete steering input is created using a spring loaded rattle system inspired by the Curta mechanical calculator, illustrated in Fig. 14.a [?]. The discrete steering input corresponds to the discretisation of the locking system, which is discussed next.

Locking: The locking of the fingers is done by a discrete, shape closed locking system as illustrated in Fig. 15. The

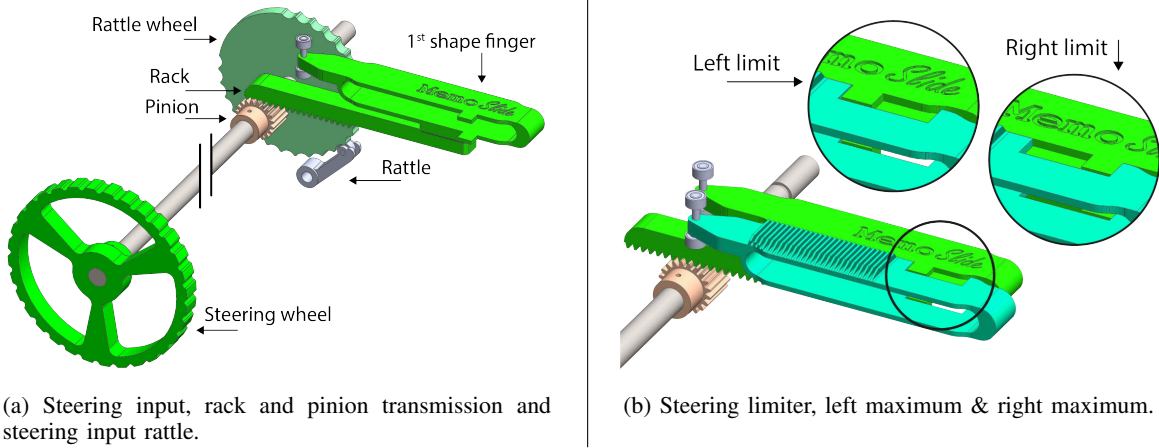


Fig. 14: Steering input sub-functions.

The steering input is given to the first shape finger using a rack and pinion transmission. The steering input is discretised using a rattle system. The steering input is limited by the tab/groove connection.

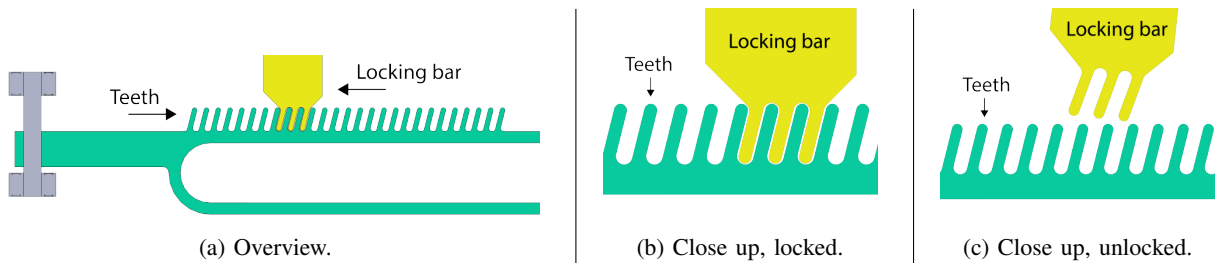


Fig. 15: Locking system.

The fingers' locations are locked using a downward facing teeth bar lowered into a row of upwards teeth, interlocking constrains horizontal movement.

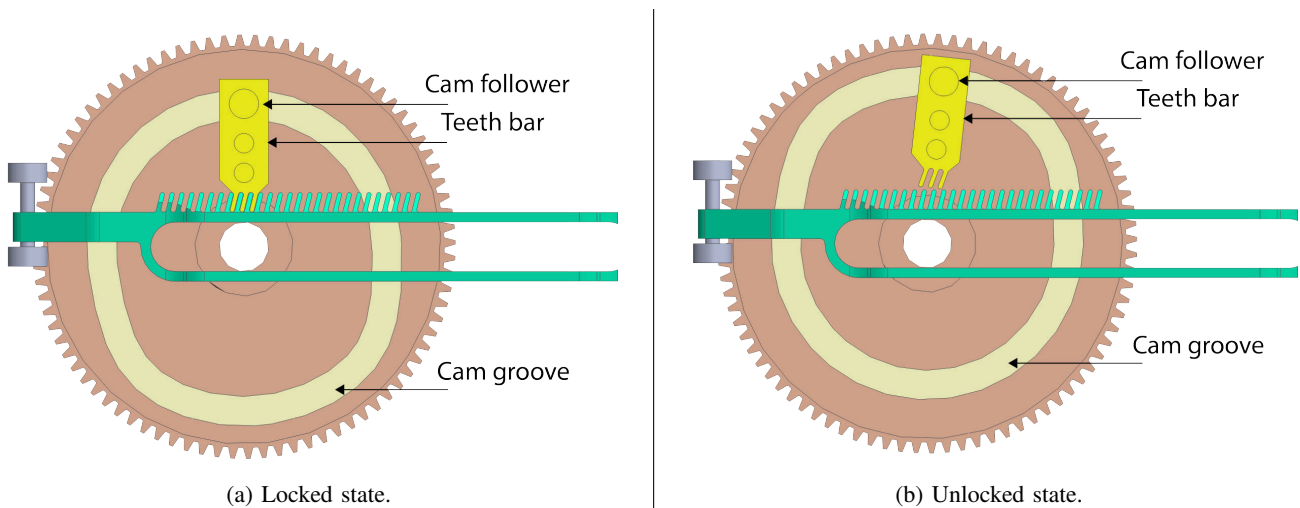


Fig. 16: Locking system actuation.

The teeth bar is actuated by a radial cam/follower system.

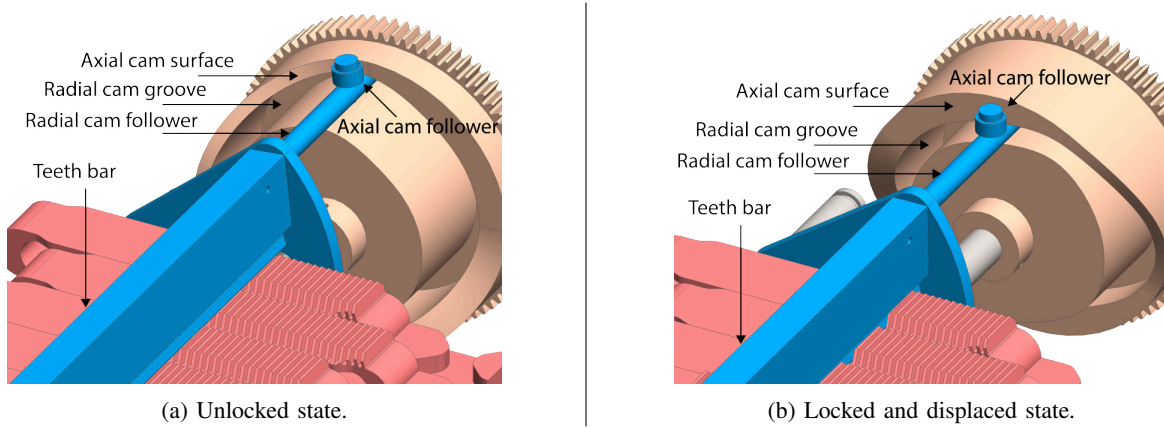


Fig. 17: Memory slide and locking system actuation. Addition of a axial component to the memory cam actuates the memory sliding motion.

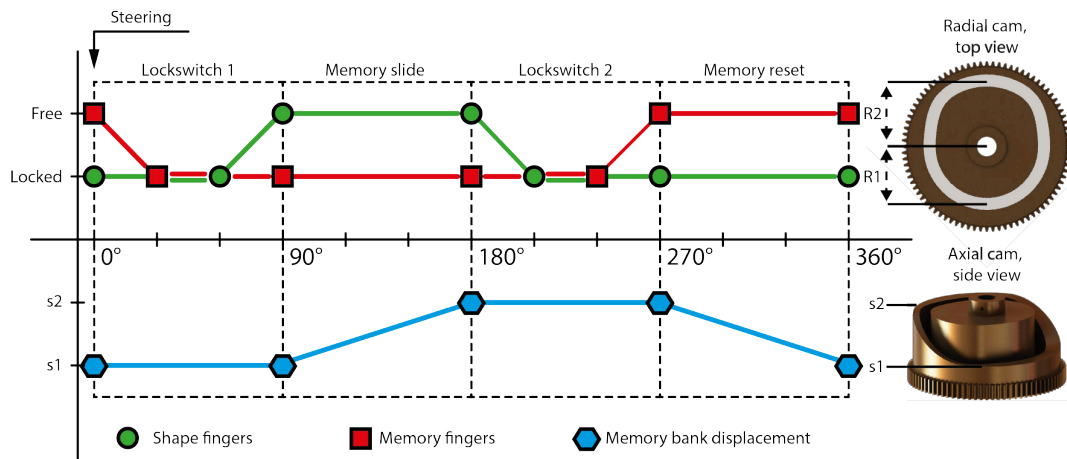


Fig. 18: Algorithm time-line.

After the steering input, the actuating cams are rotated. *Lock switch 1* stores the shape information. *Memory slide* transfers the shape information. *Lock switch 2* stores the transferred shape information. *Memory reset* slides the memory bank back, ready to repeat the cycle.

fingers' locations can be stored at discrete intervals of 1 mm by interlocking a row of teeth on the fingers with a matching set of teeth on a locking bar actuated with respect to the frame, illustrated in Fig. 15.b. The teeth are 0.45 mm wide, 2 mm high and angled to accommodate the insertion angle of the locking bar teeth. If the locking bar is lifted, the teeth no longer interlock and the fingers are unlocked as illustrated in Fig. 15.c.

The locking bars are actuated using a radial cam-follower system. The locked and unlocked state are illustrated in Fig. 16.a and Fig. 16.b respectively.

Memory slide: All memory fingers must be translated simultaneously. The previously mentioned restricting frames must be pushed back and forth. This motion is actuated by an axial cam integrated with the radial cams of the locking system. To aid the following of this axial cam, a ball bearing is mounted on the cam follower. The simultaneous locking and pushing actions are illustrated in Fig. 17.

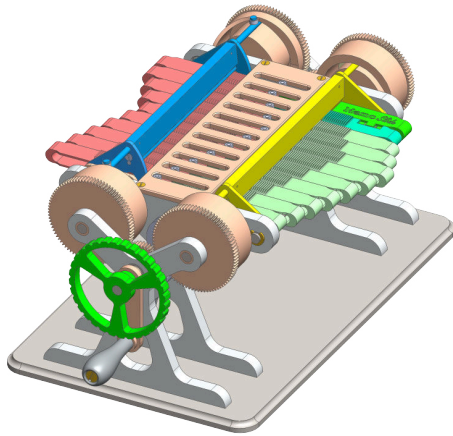
Timing: The timing is crucial for the functioning of the principle. The steering moment is emphasized by another spring loaded rattle on one of the cams. Both the locking and sliding action are actuated by cams, in turn actuated by a clockwise rotating crank. The 4 algorithm phases can be clearly seen in the algorithm time-line, illustrated in Fig. 18. The algorithm time-line directly dictates the required cam dimensions by translating the discrete states to fluent curves of the cam surface.

The *Lock switch 1* takes place in the first quarter of cam rotation. The memory fingers are locked, storing the shape information, before the shape fingers are unlocked.

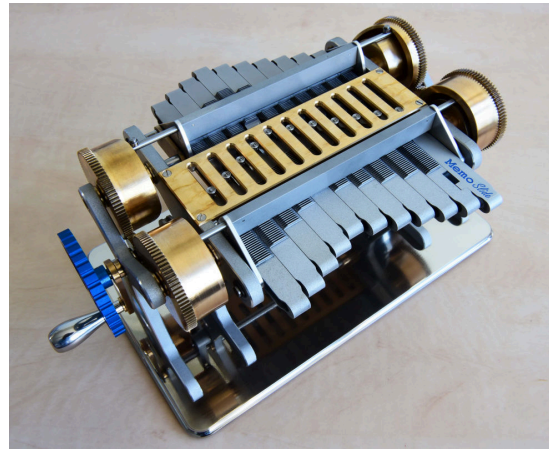
The *Memory slide*, in the second quarter, displaces the memory bank. Thus Transferring the shape information to the unlocked shape fingers.

The *Lock switch 2*, in the third quarter, stores the transferred shape information by locking the shape fingers. Again information transfer is guaranteed by the locking of the shape fingers before the memory fingers are unlocked.

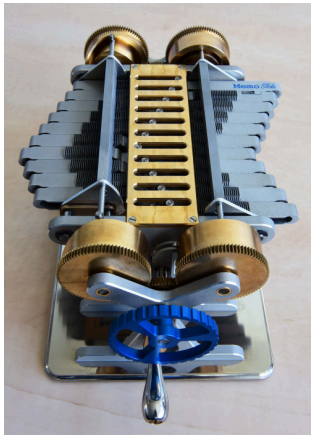
In the final quarter, the *Memory reset*, the unlocked memory bank is slid back to receive a new steering input.



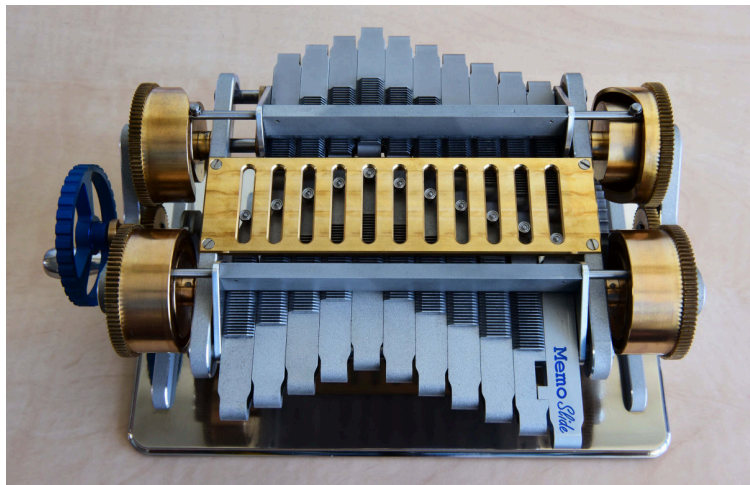
(a) Solidworks model, isometric view



(b) Photo, isometric view



(c) Photo, front view



(d) Photo, side view

Fig. 19: The PoC demonstrator: 'MemoSlide'

The assembled PoC demonstrator clearly highlights the cams and guidance plate due to the contrasts between the used materials.

D. Prototype

Integration of all functions described previously results in the complete prototype illustrated in Fig. 19. The prototype has a footprint of about an A5 piece of paper and a height of 101.5 mm. The SolidWorks model (Fig. 19.a), a photo of the complete PoC demonstrator model (Fig. 19.b), a front view (Fig. 19.c) and a side view (Fig. 19.d) are illustrated. To give an impression of the number of parts and their assembly, an exploded view is illustrated in Fig. 34 in appendix C. Work drawings specifying all components of the PoC demonstrator are included in Appendix C. Materials choices are made to obtain favourable sliding contact interactions, minimising friction forces. Aluminium is used for the fingers, locking systems and frames to minimise weight. Bronze is used for all parts involved in sliding contacts: the cams, gears and guidance plates. All axes are made of stainless steel due to its strength and low coefficients of friction with both aluminium and bronze.

E. Evaluation

1) *Principle:* After some iterations, including the addition of the sliding guidance plates, the PoC demonstrator works smoothly. The steering input is stored and transferred fluently throughout the shape fingers. By rotating the crank counter-clockwise the shape transfer algorithm can be reversed. The shape is transferred towards the tip of the device, this is a crucial feature to enable retraction of a deployed device. It can be concluded that the principle proposed in this paper is valid.

A photo series of the start, steering phase and one algorithm cycle, analogous to Fig. 8 is illustrated in Fig. 20. A complex shape is followed by the PoC demonstrator, illustrated as yellow dots in Fig. 21.

2) *Design guidelines:* Preliminary testing during fabrication revealed problems with the force distribution during the *Memory slide* and *Memory reset* phases.

During the sliding phases all fingers assume a new position due to the interactions between bearings and grooves located on the shape and memory fingers, respectively. The forces

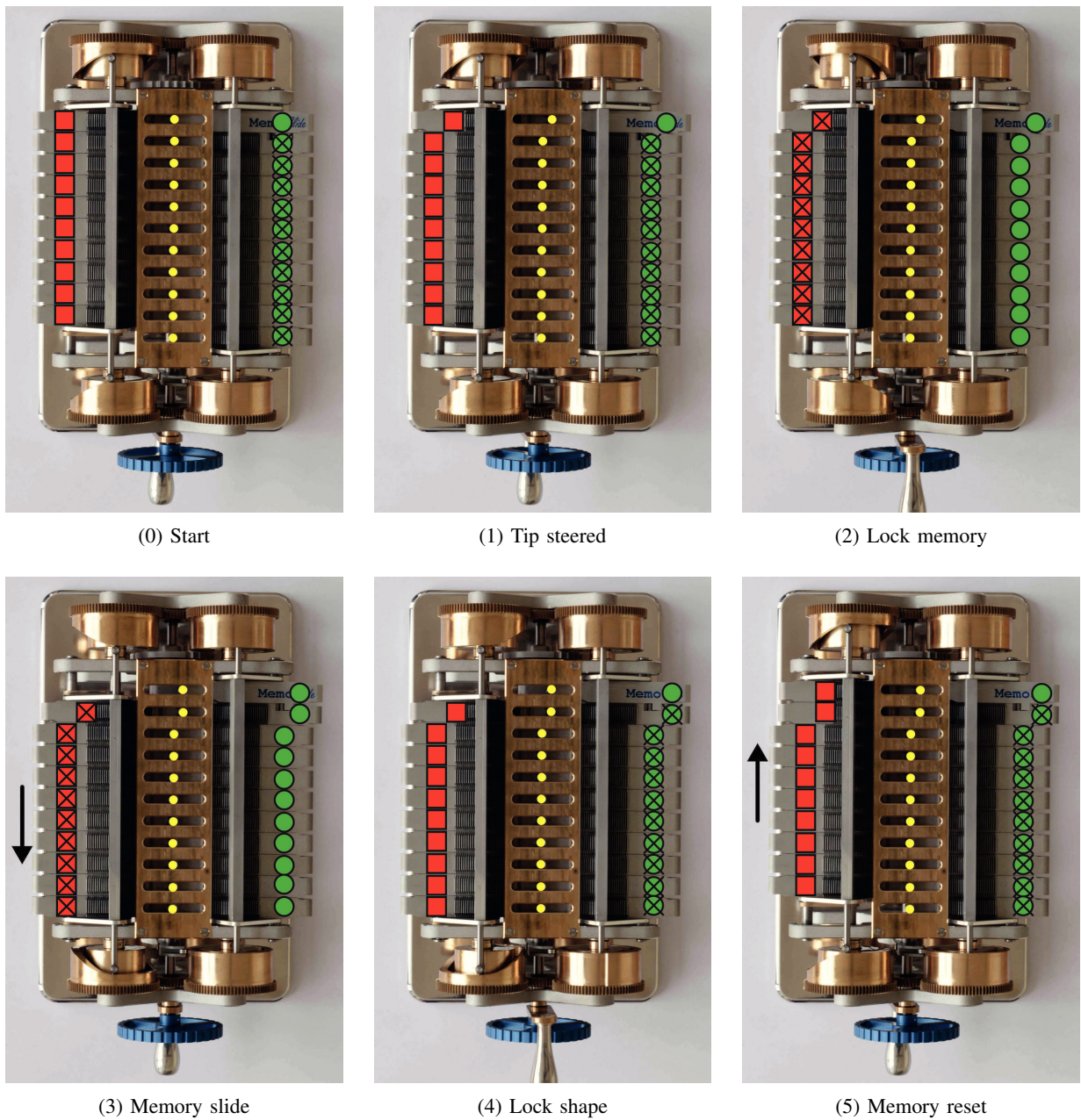


Fig. 20: A single algorithm cycle, top view.

The D/B representation is superimposed on the PoC demonstrator during a single algorithm cycle.

at play at this interaction are illustrated in Fig. 22.a. A Free Body Diagram (FBD) of a shape finger illustrates the forces acting on it in Fig. 22.b. The angled interaction force can be decomposed in a force horizontally and vertically. The horizontal force is the force effectively pushing the finger to its new position. The vertical force is an undesired side effect. This force causes a rotational moment in the 2D plane the finger is constrained to. The rotation caused by the moment created jams the fingers within their restricting frames, schematically illustrated in Fig. 22.c. For this reason, the guiding plates were added. Local support provided by the guidance plate prevents a moment from being created and therefore preventing tilt-jamming.

Another phenomenon encountered was the accumulation of

normal forces between the moving memory fingers, illustrated in Fig. 23.a. These normal forces are directly responsible for the friction forces occurring between the fingers. The friction accumulating between the sliding fingers caused the mechanism to seize in operation without local guidance.

During the Memory slide phase the entire memory bank with all 10 fingers are slid sideways simultaneously. During this sliding motion, the force needed to move the last finger must be transmitted through the second to last finger, and so on, all the way to the first of the 10 fingers. If no local guidance is used, the forces between these fingers therefore accumulate. This accumulation of forces has no effect on the vertical sliding motion of the fingers. However, these do have an effect on the individual horizontal motions of the fingers. The friction

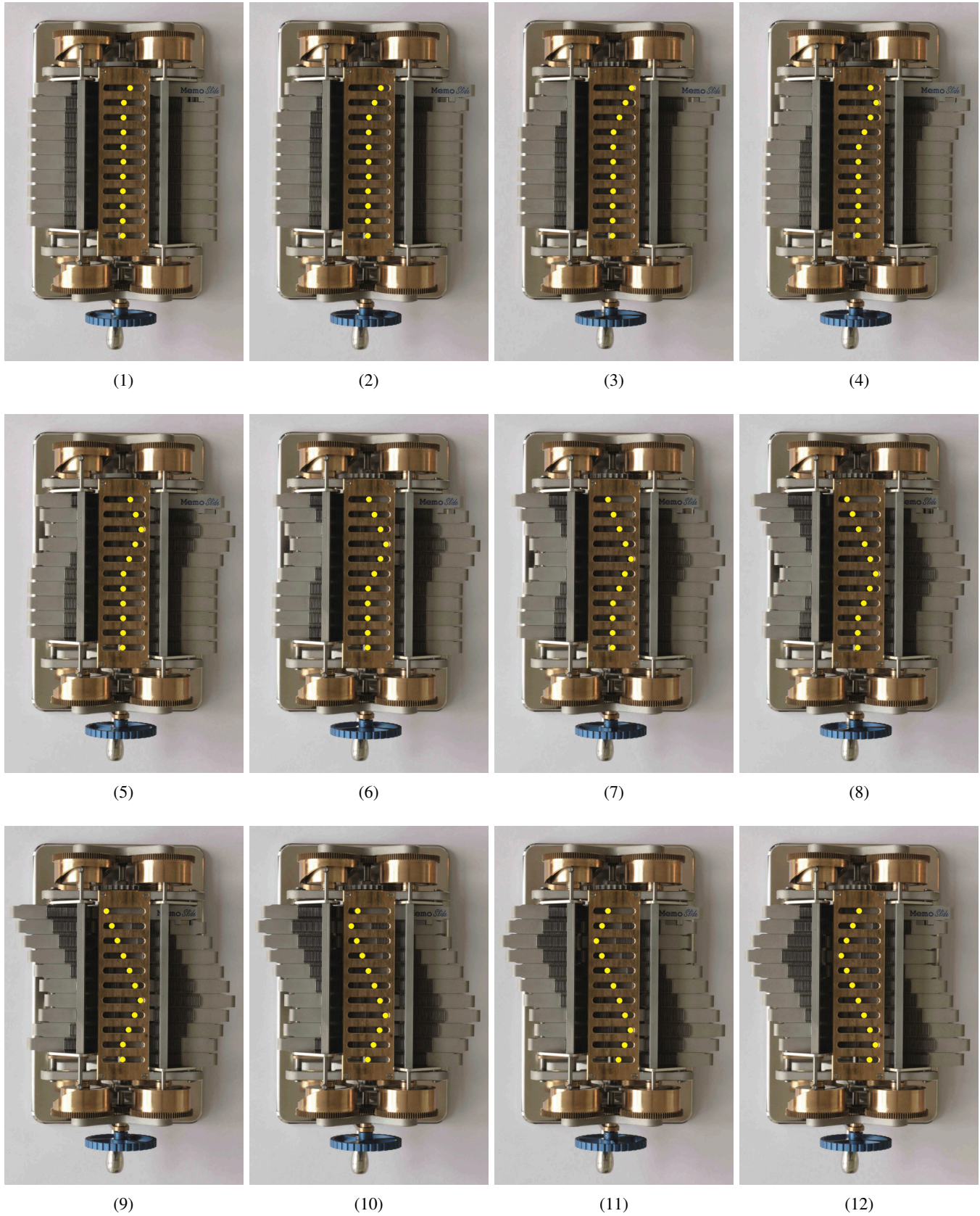


Fig. 21: Complex shape transfer
 A complex shape is input and transferred throughout the PoC demonstrator.

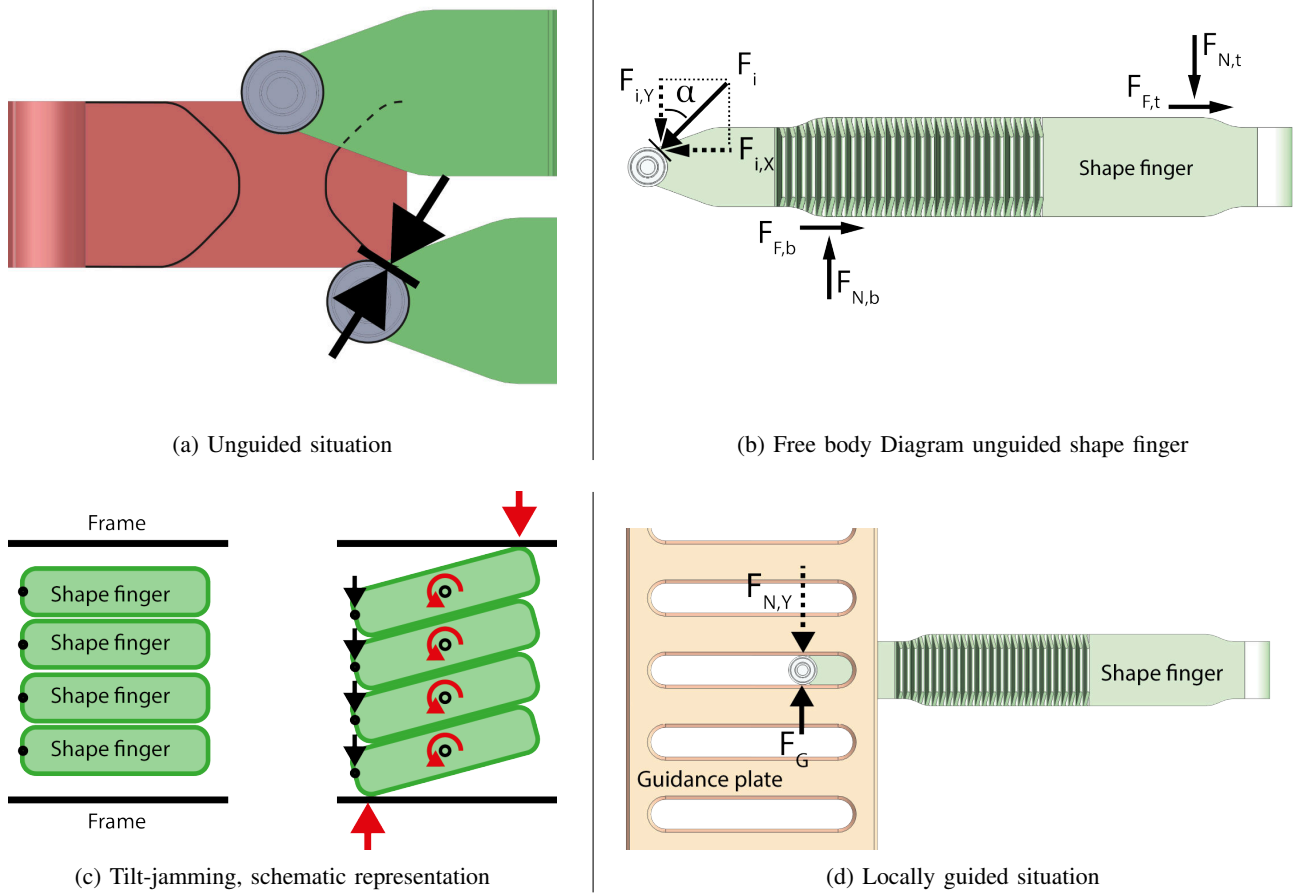


Fig. 22: Tilt-jamming, problem and solution

The force situation and its effect on the fingers is seen. Local guidance solves the tilt-jamming problem.

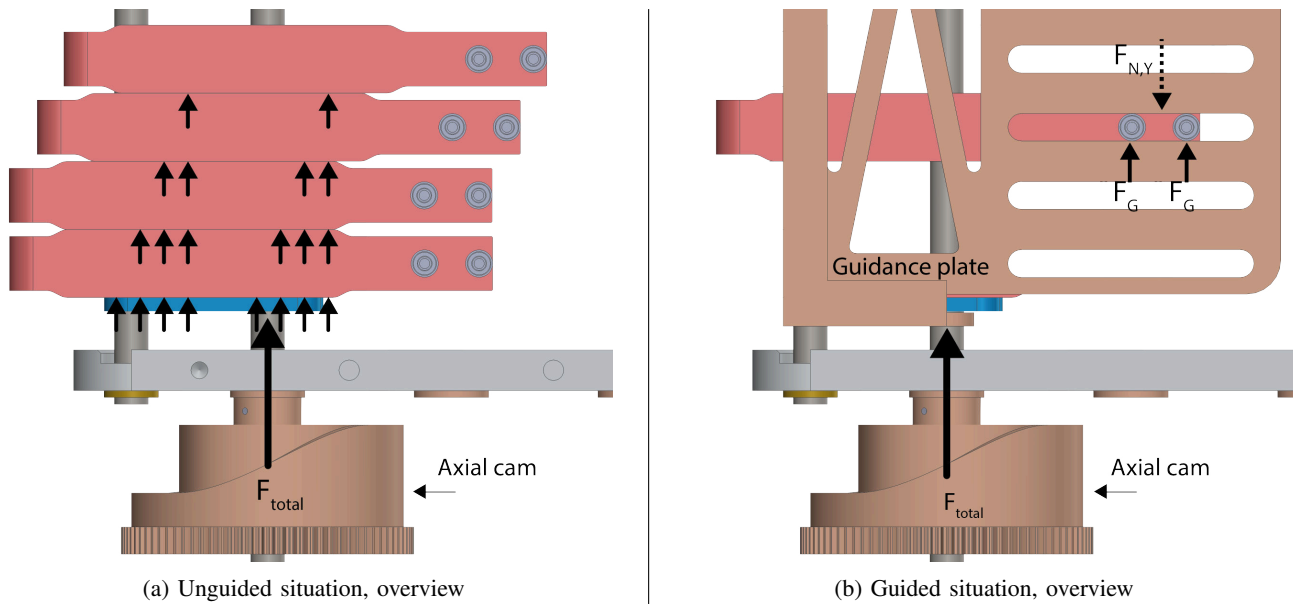


Fig. 23: Friction accumulation, problem and solution

The original situation introduced accumulation of friction forces. Local guidance solves the friction accumulation problem.

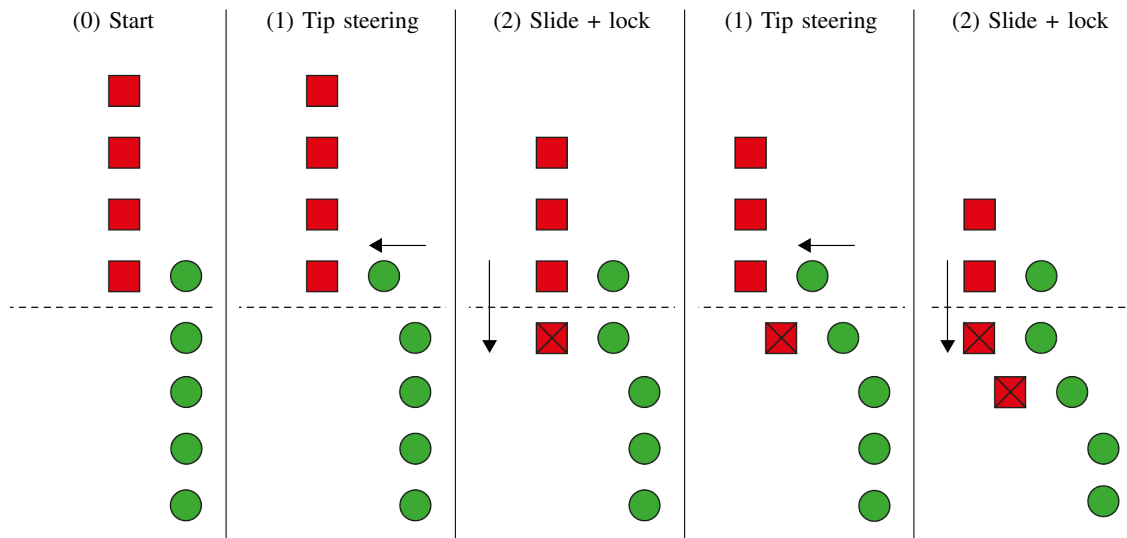


Fig. 24: One-way slide algorithm, D/B representation

The original algorithm can be simplified if the memory bank is introduced one segment at a time instead of reciprocating. Two full algorithm cycles are depicted

forces between fingers depend solely on the friction constant and the normal forces present. Therefore, with higher normal forces between the fingers the friction forces accumulate as well. Fig. 23.b illustrates the effect of locally supporting the forces acting on the fingers. As the normal forces on the fingers are now individually supported by the grooves in the guiding plate, no force accumulation occurs. A more in-depth description of the accumulation of the normal forces is given in appendix A.

The local guidance plates supporting both the shape and memory fingers improved performance greatly. As a result the PoC demonstrator functions extremely fluent. Managing both the tilt jamming and friction accumulation are important design guidelines when designing for a new application.

The discretisation system of the steering input showed smooth performance. The spring loaded rattle enforced the discrete steering input with a clearly felt and audible click.

F. Alterations

A simplification of the algorithm can reduce the complexity of the mechanism. A memory 'magazine', moving along with the steering input, can be introduced from the side instead of a reciprocating rewritable memory. The *Lock memory*, *Memory slide*, *Lock shape* and *Memory reset* steps can now be replaced by a single *Memory slide* in combination with a passive locking system. This reduces the algorithm to a simpler form illustrated in Fig. 24 and Fig. 25.

Algorithm:

Input	
1) Input shape from user:	<i>Steering</i>
Shape transfer	
2) Store & transfer shape:	<i>Memory slide</i>

Fig. 25: Simplified mechanical FTL principle algorithm

IV. CONCEPT DESIGN

A. 2D to 3D translation

To encourage implementation of the MemoSlide principle a plausible concept was designed. The concept is intended to control a steerable cable ring actuated tip, consisting of 10 segments with each 2 DoF. The green and red colours used in the PoC demonstrator correspond to parts with similar functions in the conceptual design.

To implement this principle, the interface between the control module and the steerable tip device must be considered. The PoC demonstrator was constructed to show the reciprocating principle described in section II. However, the simplified algorithm, using sideways introduction of the memory bank, shows another possible configuration in a plane. Both options are illustrated in Fig. 26.a and Fig. 26.b respectively. Until now, the MemoSlide principle has been applied in a single 2D plane. The shape control and memory bank can be positioned out of plane, one moving under the other illustrated in a side view in Fig. 26.c.

Cable guidance can be employed to translate the planar configuration of the demonstrator to the circular set of cables used in remote tip actuation using a cable ring. Alternatively the control module can be formed in a curved plane, to reduce the cable guidance to a reduction in radius of the cable ring. A curved configuration, employing sideways memory introduction and out of plane motion, is illustrated in Fig. 26.d.

B. Design guidelines

The steerable tip to be controlled in the conceptual design introduces a set of practical design guidelines.

1) *Tip*: To control the 20 DoF tip, 40 cables in a cable ring must be controlled, two for each DoF. An artists impression of such a steerable device controlled by a mechanical shape

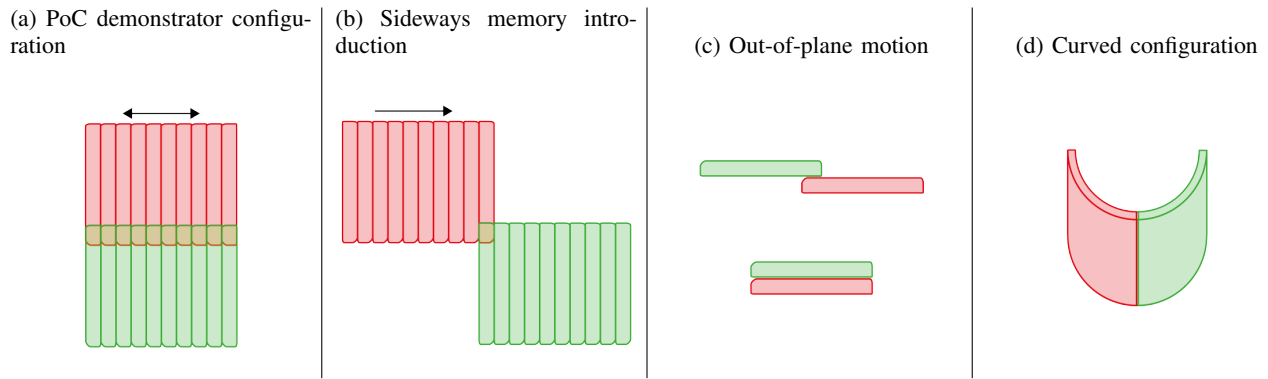


Fig. 26: MemoSlide control module configuration options.

The relative orientation of the shape control (green) and memory bank (red) result in a number of possible configurations.

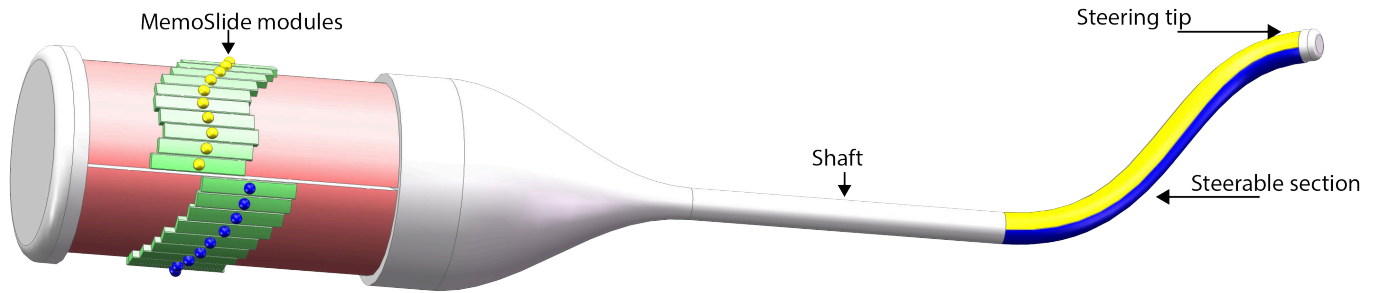


Fig. 27: Artists impression steerable device.

An impression of a remotely actuated steerable device with a physical shape memory control module at its base. 2 DoFs are controlled for each segment, yellow and blue.

memory system is illustrated in Fig. 27.

2) *Stiff tip control*: A stiff steerable tip is obtained if the control cables are pre-tensioned. A stiff tip prevents distortion of the tip shape during use. A straightforward approach to incorporate this cable pre-tension in the design is to connect the two cables controlling 1 DoF of a segment, illustrated in Fig. 6 in section II, by two pulleys and a looped cable. If the pulley mounts are pushed by a spring the pre-tension can be introduced in the steerable tip. The discrete nature of the MemoSlide principle requires the cables controlling 1 DoF of a segment to be connected to prevent shape information or stiffness reduction during the memory slide phase, during which the shape control cable are not held in place by aligned memory grooves.

The evaluation of the PoC demonstrator yielded design guidelines to enable the MemoSlide principle to function properly. The main focus points are the *Friction*, *Jamming* and *Locking* described in more detail.

3) *Friction*: During the validation phase, accumulation of friction between shape and memory fingers was observed during the memory sliding step. Individual linear guidance can prevent such accumulation of friction forces and improve the mechanism performance.

4) *Jamming*: Before addition of the guidance plates, providing local constraint forces, the demonstrator could jam due to tilting of the fingers. Ensuring small force loops by local guidance can prevent tilting and with it jamming of moving parts.

5) *Locking*: An active, reversible locking system was implemented in the demonstrator model. The simplified algorithm detailed at the end of section III does not require a reversible locking system. The memory fingers can be locked and stay locked after the steering moment until the device is retracted. As introduced with the simplified algorithm (Fig. 25) the memory fingers only have to be locked once, namely after the steering input has been given. This can reduce actuation complexity if a passive locking system can be designed that engages at the start of the memory slide phase.

C. Concept design

A concept design is suggested with possible systems complying with the previously identified design guidelines. The concept design is intended to provide a stepping stone in the further research and implementation of the MemoSlide principle in real world applications. The conceptual design is illustrated in Fig. 28. The sub solutions incorporated in the design and their motivations are discussed next.

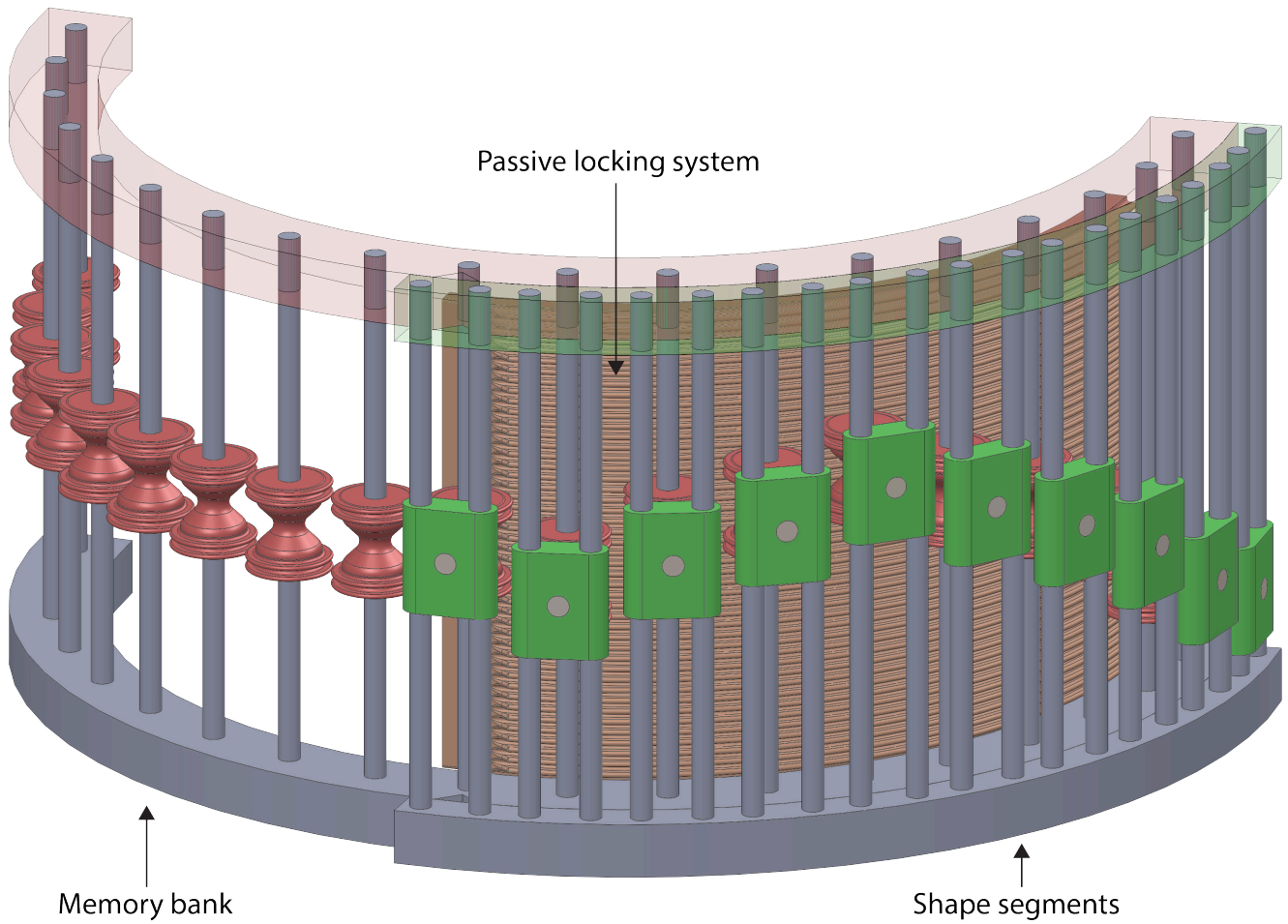


Fig. 28: Concept design tip control module.
A conceptual design of a MemoSlide module in a circular configuration.

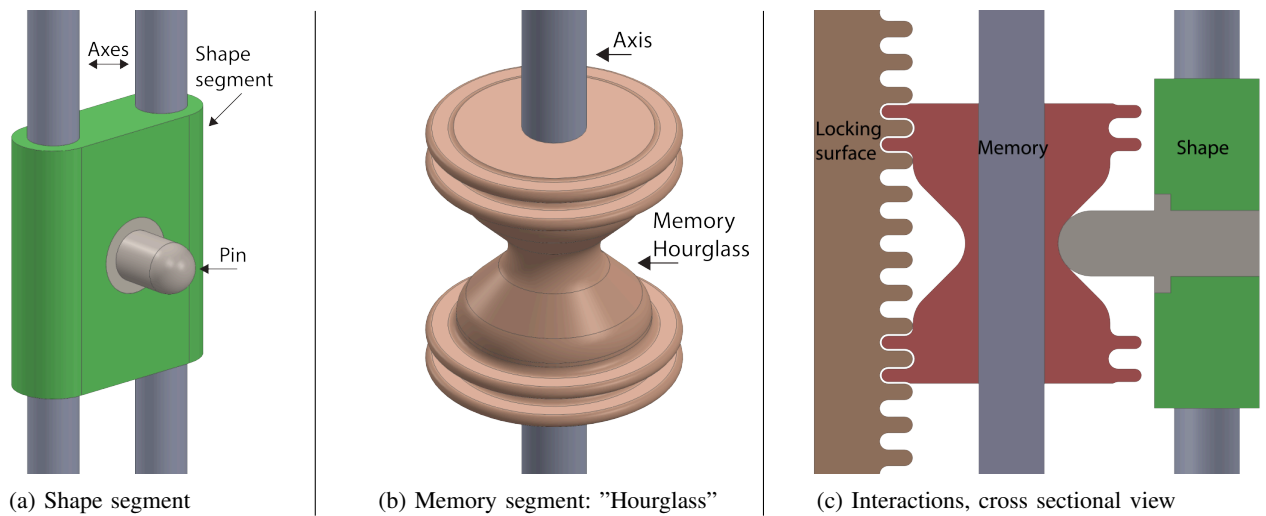


Fig. 29: Basic constraints and interactions of parts

The shape segment slides along 2 axes. The memory hourglasses slide and rotate about a single axis. The cross section illustrates a locked memory hourglass lined up with a shape segment.

1) *Basic constraints/interaction:* Both the shape control and memory segments are individually constrained along axes, illustrated in Fig. 29. Materials are paired to obtain favourable sliding contact interactions to minimise friction forces, for instance steel on bronze has a friction coefficient of $\mu_{SS-B} = 0.16$ [10].

The shape control segments are build of a block guided along two axes to enable sliding motion without rotation, illustrated in Fig. 29.a. A pin in the shape segments is the sole point of interaction with the memory segments.

The memory segments are hourglass shaped, illustrated in Fig. 29.b. This rotation symmetric shape is constrained on a single axis and is therefore free to rotate about its axis.

The shape pin interacts with the hourglass shape analogous to the bearings and grooves described in the PoC demonstrator. A cross section of a shape and memory segment during alignment is illustrated in the cross section in Fig. 29.c. The memory hourglasses are free to rotate about their axis, therefore a rolling contact is achieved between the pin and hourglasses. During the memory slide phase the pin makes contact with the hourglass at either of its 'peaks'. When aligned, the shape pin is positioned in the valley of the memory hourglass.

2) *Locking:* The simplified algorithm requires a system that only locks the memory position after the steering input has been given. Due to the great performance in the MemoSlide prototype, a passive version of the discrete shape closed teeth-teeth locking system was chosen. The memory hourglasses have two teeth integrated on the top and bottom of its alignment valley. These two teeth interlock with a ribbed surface to store the vertical displacement of the hourglass. To allow a free steering input the teeth must interlock after the steering input has been given. The position must be locked during the new memory slide phase. The timing of locking will be discussed later in more detail. Combining the memory-shape interaction with the passive locking system results in the cross section illustrated in Fig. 29.c.

3) *Steering:* The tip of the device can be remotely actuated with a 2 DoF joystick connected to the cables of the first shape control segments. A schematic side view of a 1 DoF joystick is illustrated in straight and steered stance in Fig. 30.a and Fig. 30.b respectively. The curved sides ensure the Dots are displaced along a line. The translation from a 1 DoF set-up to a 2 DoF set-up is illustrated using top views, Fig. 30.c and Fig. 30.d. Each DoF requires 2 cables in a plane to be actuated. Attachment of 4 cables on a disc pivoting around the centre allows control of 2 DoF.

4) *Memory slide:* The required memory slide motion is simplified to a simple rotation of the memory bank containing the hourglasses. The envisioned device consists of 10 steerable segments, actuated by a cable ring consisting of 40 cables. For each step, transferring the steering input to the next follower, the memory hourglasses must rotate by 9° to align with the next shape segment. The axes supporting the memory hourglasses are mounted on a rotating

ring. A full deployment of the device is actuated by a 90° counter-clockwise rotation of the memory ring. Retraction along the stored trajectory requires a 90° clockwise rotation.

5) *Timing:* Before deployment all segments must be locked in the straight configuration. This is achieved using an extra set of 9 memory hourglasses aligned at the centre of the passive locking system. After steering, the memory ring is advanced 9° to store and transfer the latest steering input. The timing of storing and transferring the shape information is now all incorporated in the 9° memory ring rotation. The interactions between the shape segments, memory hourglasses and the passive locking system must therefore be carefully timed. Only 3 phases can now be identified, the *Steering phase*, the *Storing phase* and the *Transfer phase*. These phases are characterised by the interacting segments and illustrated in Fig. 31.

Steering phase: (Fig. 31.a) All shape and memory segments are aligned. Steering input is given to tip, via the joystick that moves the first shape segments.

Storing phase: (Fig. 31.b) Start rotation of the memory ring. All shape and memory segments are still aligned, first memory segment interlocks with passive locking system.

Transfer phase: (Fig. 31.c) Memory ring is rotated further until the locked memory hourglasses make contact with the next shape segments. The locked memory segment starts transferring the shape information. When fully aligned, the shape is successfully transferred and the device is ready for a new steering input.

The validated MemoSlide principle is capable of controlling a steerable tip with a single DoF per segment in a plane. Extending the control to 3D space requires segments with 2 DoFs in planes perpendicular to each other. This means that two MemoSlide modules with 10 control fingers are required for the actuation of the tip.

Implementation of two curved MemoSlide modules can be achieved in a variety of ways: *Radially* spaced, *Axially* spaced or *Integrated* at the same radius and axial location. Sketches of each implementation option are illustrated in Fig. 32.a, Fig. 32.b and Fig. 32.c respectively.

V. DISCUSSION

A. Principle

This paper introduced a fully mechanical shape memory control principle. The shape memory control is envisioned at the base of the device, paired with remote actuation, this allows for tip miniaturisation. A remotely actuated tip does require the control module to move in tandem with the tip. The focus of this paper was put on the storage and transfer of the shape transformation, the paired advancement of the steerable tip was not considered in this paper. Shape information storage and transfer was achieved using the MemoSlide principle.

The MemoSlide captures a control algorithm, similar to software, in its mechanical structure. This approach therefore eliminates the need for large numbers of electric actuators. A

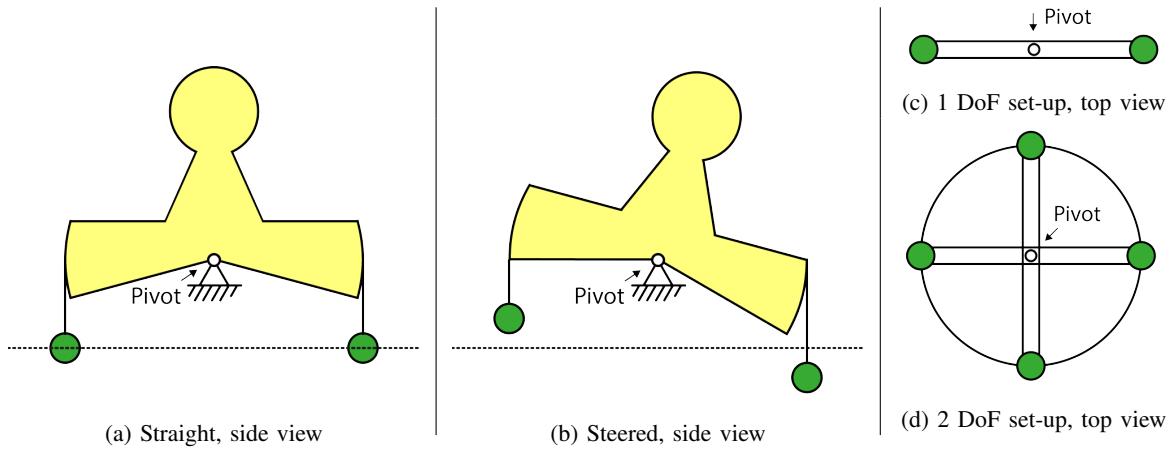


Fig. 30: Joystick, schematic side and top views

A planar joystick with rounded sides ensures straight displacements of the dots in 1 DoF. A crossed configuration of two planar joysticks with a single pivot point in the middle allows control of 2 DoFs simultaneously.

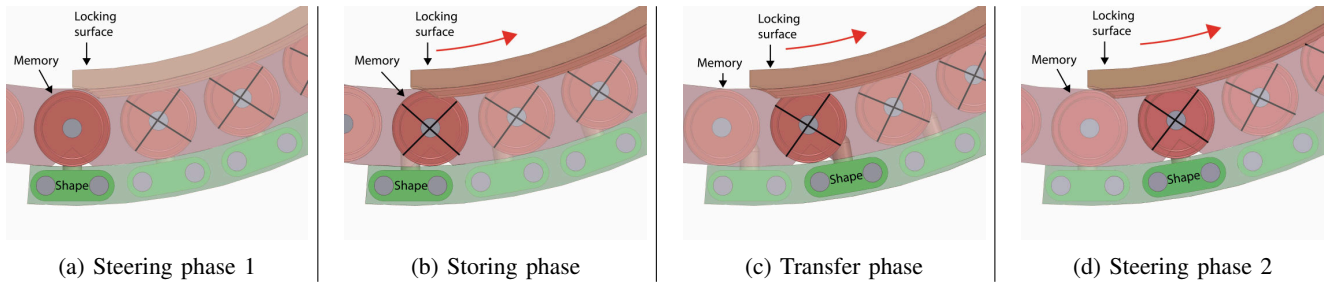


Fig. 31: Timing phase conceptual design, top view.

The parts interacting with each other during the steering and transfer phases are highlighted.

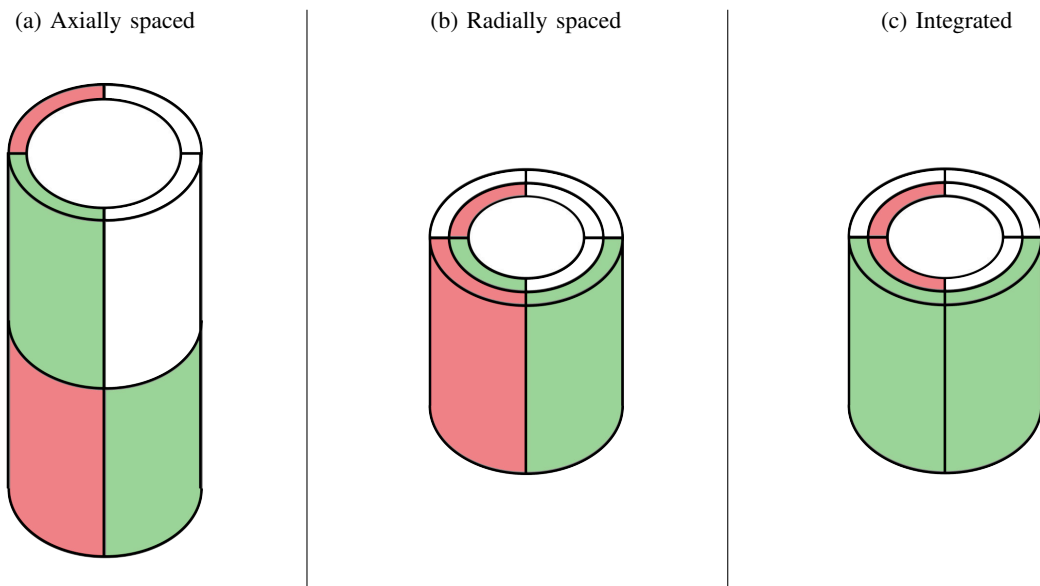


Fig. 32: MemoSlide modules implementation options.

A steerable tip with 2 DoF segments can be controlled by two MemoSlide modules, these modules can be arranged axially spaced, radially spaced or integrated. Shape control is indicated with green, the memory bank with red.

cost reduction can be achieved by exchanging a large number of expensive motors by an increase in fabrication complexity. Additionally no computer control is required since the control algorithm is embedded in the mechanical structure.

A device capable of FTL behaviour without the use of electric actuators opens up the possibility of creating a device compatible with MRI. Enabling surgery on remote targets along complex trajectories with live MRI guidance.

The MemoSlide module can control FTL behaviour, however, no different mode of operation is possible. Whereas computer controlled devices can assume any shape within its RoM from any other configuration, including FTL behaviour. An advantage of computer control is the possibility of interpolation between shape configuration enabling a smoother transition between transfer phases.

Computer-motor controlled devices are limited by the motor force output. Such a force closed system would allow for any shape along the continuous RoM to be stored. However an external force great enough to overcome the internal locking force could corrupt the stored shape information. Potentially causing undesired contact with a fragile environment and possible complications.

The HARP, a physical shape memory system like the MemoSlide module, employs two concentric snakes sliding along each other. To enable the sliding through curves some play was present in the design. This play however, will result in a slight error between the shape of the outer and inner snake. Because each snake shape is locked in a continuous fashion these small errors in shape transfer can accumulate. A system with a discrete locking system can correct such small errors, as long as these errors are smaller than the resolution of the discrete locking system. Moreover, by using a discrete shape information storage, the forces on the tip are not limited by the friction forces of a continuous locking system or the forces of the actuators, but only by the strength of the construction itself. A discrete locking system is therefore capable to maintain its stored information until mechanical failure occurs.

B. PoC validation

The principle introduced was validated using the PoC demonstrator model. The PoC demonstrator was able to receive a steering input, store this shape information and transfer it to the next segment. The cycle of input, storage, transfer and reset introduced in section II was captured successfully in the mechanism created. Rotating the crank in the counter-clockwise direction resulted in the shape being transferred towards the tip of the device, essential for retraction of a deployed device.

Preliminary testing during fabrication revealed issues with the force distribution during the sliding phases of the memory bank. Without individual, local guidance at the bearing/groove interaction the fingers were tilting slightly due to the moment generated by the interaction forces. The tilting of the fingers resulted in jamming of the system. Local guidance proved necessary for the sliding memory bank as well. The normal forces between the moving fingers accumulated without individual guidance. The normal forces are directly responsible

for the friction forces occurring between the fingers. The accumulation of friction between the sliding fingers caused the mechanism to jam as well. Addition of local guidance, by grooved plates in the PoC demonstrator, can solve both these jamming issues. Therefore, local guidance is recommended in further applications of the MemoSlide principle in a working instrument.

The miniaturisation of a MemoSlide control module is limited by the resolution of the discrete locking system. The PoC demonstrator showed that the resolution is directly related to the smallest features of the mechanism, the locking teeth on the fingers. Therefore, the highest resolution obtainable is determined by the limits of fabrication accuracy. The module size is further dependent on the desired step size. The number of steerable segments and the step sizes determines the size of the memory segments, which in turn determine the overall size of the module.

C. Future work

This paper covered a conceptual design of a 1 DoF implementation of the MemoSlide principle. The design featured the simplified algorithm identified as a result of the PoC demonstrator model. The conceptual design presented is a possible structure capable of control using the MemoSlide principle. The concept can be used as inspiration for further research like the PoC demonstrator sparked the idea of the simplified algorithm.

The part geometries in the conceptual design have not yet been optimised. The algorithm simplification reduced the number of actions and also the number of parts required. Furthermore, the sizes of the moving parts were kept small. These reductions in complexity and size are beneficial if dynamic applications are envisioned. Additional research is required to bring the MemoSlide principle to a more mature technology level. The interaction between the surfaces of the pin and hourglass parts could benefit from topological optimisation routines to generate more efficient and reliable interactions.

To achieve control of a device with 2 DoFs per segment, two MemoSlide modules are required. As discussed at the end of section IV the implementation options of two MemoSlide modules must be further investigated. Two MemoSlide modules can be placed on the same axial position and radius to create a compact control module. However, the interaction of memory hourglasses used for both DoFs must be considered in that situation.

The manual steering input is envisioned with a 2 DoF joystick. However, the exact implementation capable of both steering the first segment and moving the memory magazine has not been designed. Further investigation can determine the optimal input strategy. One strategy is a joystick with a direct link between joystick orientation and the steering tip orientation. Another strategy can be a joystick which resets to its starting orientation after each steering input while the tip remains steered.

During the conceptual design phase the assumption is made that the cable attachment points in the tip are all in the same

plane. Cable displacements are therefore assumed to produce a pure bending in that plane. However, in the cable ring design all cables are positioned besides each other in a circle. Therefore, the cable attachment points are not positioned in the same plane. The result is that sequential segments are actuated at a slightly different angle. If the cable displacements are transferred without any change throughout the device, the shape will be rotated over 90° around its longitudinal axis when the device is fully deployed. The shape rotation can potentially be counteracted by rotating the entire device in the opposite direction simultaneously. Another option can be to create the tip with a spiralling cable ring. The attachment points can be lined up in a plane.

VI. CONCLUSION

The workspace in minimal invasive surgery can be extended to currently obstructed locations by instruments capable of Follow-The-Leader behaviour during deployment. From the state of the art it was concluded that a physical memory system could reduce the control complexity. However, the integration of such a physical memory system in the steerable tip of a device can lead to issues concerning accuracy and miniaturisation. Combining a physical memory system with remote actuation using cables could create a system without these issues. This paper introduced a novel, fully mechanical shape memory control principle: the MemoSlide principle. The principle was validated using a Proof of Concept (PoC) demonstrator model. The PoC was designed to be a demonstrator model as well as showcasing the principle and sub-functions captured in its mechanical design.

A discrete steering input can be introduced and transferred mechanically throughout the control module. The shape information created during the steering input is transferred without loss due to the discrete mechanical storage.

Evaluation of the PoC demonstrator led to a simplified control algorithm and identification of practical and principle pitfalls. Design guidelines to handle these pitfalls were suggested and applied to create a feasible conceptual design.

The MemoSlide principle can reduce the amount of DoFs that need active control, reducing the number of actuators required. The MemoSlide module automatically controls the redundant DoFs present in the device tip. With manual steering and actuation the number of actuators could be reduced to zero. The complete removal of actuators from the tip could enable the design to be adapted for MRI compatibility, enabling surgery with live MRI guidance. A reduction in actuators used to actuate a steerable surgical device can reduce the costs and footprint of such devices in the operating room.

ACKNOWLEDGEMENTS

This work has been supported by the Dutch Technology Foundation STW, which is part of the Netherlands Organization for Scientific Research (NWO), and which is partly funded by the Ministry of Economic Affairs.

REFERENCES

- [1] OC Robotics, "OC Robotics X125 series II."
- [2] R. J. Webster, J. M. Romano, S. Member, and N. J. Cowan, "Mechanics of Precurved-Tube Continuum Robots," *IEEE Transactions on Robotics*, vol. 25, no. 1, pp. 67–78, 2009.
- [3] A. Degani, H. Choset, A. Wolf, and M. a. Zenati, "Highly articulated robotic probe for minimally invasive surgery," *Proceedings - IEEE International Conference on Robotics and Automation*, vol. 2006, no. May, pp. 4167–4172, 2006.
- [4] P. Breedveld, J. S. SCHELDES, E. M. BLOM, and J. E. VERHEIJ, "A New, Easily Miniaturized Steerable Endoscope," *IEEE ENGINEERING IN MEDICINE AND BIOLOGY MAGAZINE*, no. December, pp. 40–47, 2005.
- [5] S. Gottenbos, "Follow-The-Leader Surgical Instrument Propagation in Complex Workspaces," tech. rep., TU Delft, 2016.
- [6] A. Loeve, *Shaft-Guidance for Flexible Endoscopes*. PhD thesis, TU Delft, 2012.
- [7] C. Bergeles and P. E. Dupont, "Planning stable paths for concentric tube robots," *IEEE International Conference on Intelligent Robots and Systems*, pp. 3077–3082, 2013.
- [8] H. B. Gilbert and R. J. Webster, "Can concentric tube robots follow the leader?," *Proceedings - IEEE International Conference on Robotics and Automation*, pp. 4881–4887, 2013.
- [9] H. Gilbert, J. Neimat, and R. Webster, "Concentric Tube Robots as Steerable Needles: Achieving Follow-the-Leader Deployment," *IEEE Transactions on Robotics*, vol. PP, no. 99, pp. 1–13, 2015.
- [10] EngineeringToolbox.com, "Friction coefficients - common material combinations."

APPENDIX A
FRICTION ACCUMULATION

The bearing/groove interaction during the memory reset is illustrated in Fig. 33.a. The FBD details the force situation on the memory fingers illustrated in Fig. 33.b. The interaction force (F_i) can again be decomposed into a X ($F_{i,X}$) and Y ($F_{i,Y}$) component dependent of the groove angle α . $F_{i,X}$ is effective and pushes the finger in the desired direction. $F_{i,Y}$ however is not effective and induces normal forces ($F_{N,t}$, $F_{N,b}$) on the top and bottom side of the finger. $F_{N,t}$ contributes to tilt-jamming of the memory fingers. The magnitude of the normal forces determine the friction forces ($F_{F,t}$, $F_{F,b}$) opposing the effective $F_{N,X}$.

Since the memory bank was originally pushed as a whole the force required to move the first finger must be transmitted through the second finger, accumulating the normal forces between the fingers as illustrated in Fig. 33.c. Therefore, the forces F_i must increase in magnitude for every subsequent finger. To explore the force accumulation, the forces acting on the first, second and i th finger are represented in algebraic notation.

The groove angle $\alpha = 45^\circ$, the friction coefficient between the fingers is theoretically $\mu = 0.3$ based on the lubricated aluminium on aluminium sliding contact. The forces in the X direction must be unbalanced to move the finger.

$$\begin{aligned}\alpha &= 45^\circ \\ F_{i,Y} &= F_i \cdot \cos(45^\circ) \\ F_{i,X} &= F_i \cdot \sin(45^\circ) \\ F_{i,Y} &= F_{i,X} \\ F_{F,t} &= \mu \cdot F_{N,t} \\ F_{F,b} &= \mu \cdot F_{N,b} \\ \Sigma F_X \neq 0 &: F_{F,t} + F_{F,b} \neq F_{i,X}\end{aligned}$$

The first finger has no contact with the restricting frame on the top, so no normal or friction forces.

$$\begin{aligned}F_{N1,t} &= F_{F1,t} = 0 \\ \Sigma F_{Y1} &= 0: F_{1,Y} = F_{N1,b} \\ F_{F1,b} &= \mu \cdot F_{1,Y} \\ \Sigma F_{X1} \neq 0 &: F_{F1,b} \neq F_{1,X} \\ \mu \cdot F_1 \cdot \cos(45^\circ) &\neq F_1 \cdot \sin(45^\circ) \\ \mu \cdot F_1 &< F_1\end{aligned}$$

The second finger does have a normal force from the top, this is the reaction force from the first finger.

$$\begin{aligned}F_{N2,t} &= F_{N1,b} = F_{1,Y} \\ F_{F2,t} &= \mu \cdot F_{1,Y} \\ \Sigma F_Y &= 0: F_{N2,b} = F_{1,Y} + F_{2,Y} \\ F_{F2,b} &= \mu \cdot (F_{1,Y} + F_{2,Y}) \\ \Sigma F_X \neq 0 &: (F_{F2,t} + F_{F2,b}) \neq F_{2,X} \\ \mu \cdot (2 \cdot F_1 + F_2) \cdot \cos(45^\circ) &< F_2 \cdot \sin(45^\circ) \\ \mu \cdot (2 \cdot F_1 + F_2) &< F_2\end{aligned}$$

The force imbalance in the X direction can be described in general terms for the i th finger for a maximum of M fingers as a function of the μ and α :

$$\begin{aligned}\mu \cdot \left(\sum_{i=1}^{M-1} (2 \cdot F_i) + F_M \right) \cdot \cos(\alpha) &< F_M \cdot \sin(\alpha) \\ \sum_{i=1}^{M-1} (F_i) + F_M &< F_M \cdot \frac{\tan(\alpha)}{2\mu}\end{aligned}$$

As a simplification the increasing forces F_i can be taken as a constant: F . This simplification reduces the previous formula to a function of the number of controlled segments, μ and the groove angle α .

$$\begin{aligned}M \cdot F &< F \cdot \frac{\tan(\alpha)}{2\mu} \\ M &< \frac{\tan(\alpha)}{2\mu}\end{aligned}$$

Inserting the parameters of the PoC demonstrator will prove if the unguided situation is viable. The friction coefficient of aluminium on aluminium in a lubricated state $\mu = 0.3$. The groove angle $\alpha = 45^\circ$. The number of memory fingers $M = 10$.

$$\begin{aligned}\mu &= 0.3 \\ \alpha &= 45^\circ \\ M &= 10 \\ 10 &\not< \frac{\tan(45^\circ)}{2 \cdot 0.3} = 1.66\end{aligned}$$

The unguided situation is proven not to be viable. Even with a favourable simplification the requirement is not met with a set of just two fingers. Therefore, we can conclude another approach is necessary. Local support of the memory fingers using a grooved guidance plate prevents accumulation of friction forces. The grooves supply guidance forces (F_G) to two bearings mounted on the underside of the memory fingers, illustrated in Fig. 33.d. The guidance plate with bearings reduces the force situation of each finger to one analogous to the first finger. The only requirement is now $\mu \cdot F_1 < F_1$, with a $\mu = 0.3$ this requirement is always satisfied and increasing the number of fingers has no effect on this force situation.

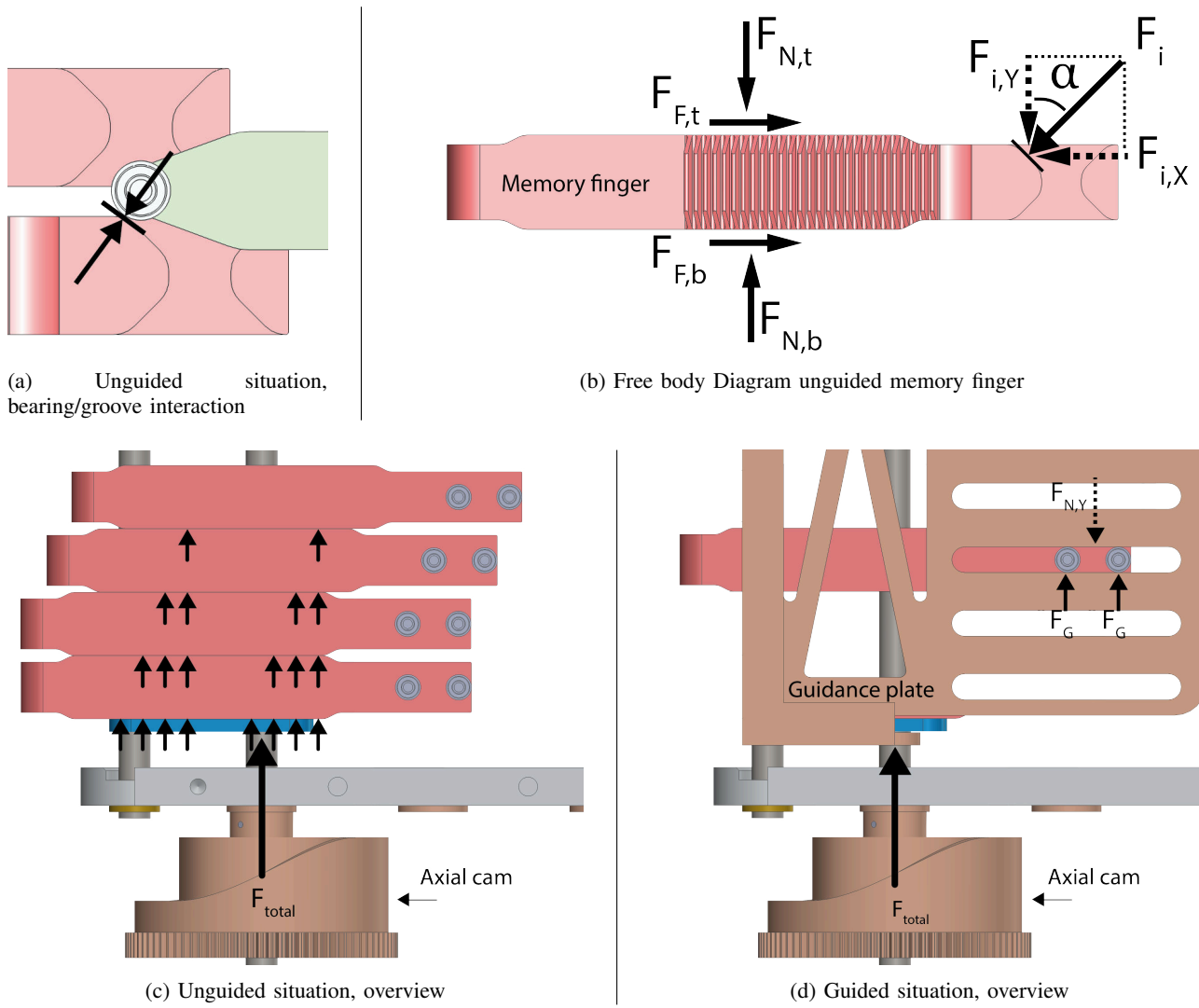


Fig. 33: Friction accumulation, problem and solution

APPENDIX B
LITERATURE PAPER

In preparation for this Thesis a literature research was performed. The literature research investigated the current state of the art of devices capable of Follow-The-Leader behaviour. The paper documenting the literature survey is included in this appendix.

Follow-The-Leader surgical instrument propagation in complex workspaces

Stefan Gottenbos, *MSc student, TU Delft*

Abstract—Surgical procedures are shifting towards Minimal Invasive Surgery (MIS). Surgeons are currently limited in their actions by the straight instruments available to them. Devices capable of navigating along complex trajectories increase a surgeon’s workspace. This paper investigates the state of the art of Highly Redundant Devices (HRD) capable of Follow-The-Leader (FTL) behaviour. A categorisation was made, based on the level of interaction of the devices with the environment, ranging from fully dependent to fully independent of the environment. The differences in interaction with the environment will lead to different methods of FTL behaviour. Combinations of environments call for hybrid solutions. Devices capable of complex movements have been developed, however more research and development is necessary to find optimal solutions for practical applications.

Index Terms—Follow-The-Leader, FTL, highly redundant devices, HRD, shape memory transfer, minimal invasive surgery, MIS.

I. INTRODUCTION

In recent years, many surgical procedures have shifted from open to Minimal Invasive Surgery (MIS). In MIS surgical instruments are inserted through small incisions into the body. Current surgical instruments are straight, which limits the surgical workspace to locations reachable via a straight path from incision to target. The instruments pivot at the incision location. Insertion angle, depth and tip orientation are the only methods to control the tool at the tip. To enable a surgeon to operate on an obscured target an instrument requires additional Degrees of Freedom (DoF) used to work around an obstacle. The human elbow for example provides us with such an extra DoF to enable picking up an object behind an obstacle. In more complex tasks, the available workspace can be restricted further by more and closer boundaries. When more DoF are added, more obstacle or boundaries can be avoided. Surgery on remote locations requires the instruments to be able to propagate along complex trajectories containing multiple curves. Highly Redundant Devices (HRD) have numerous redundant DoF for a simple positioning task of the tip. However, these extra DoF enable the device to conform to, and follow tortuous trajectories.

The numerous extra DoF of HRD increase control complexity. The design of HRD is inspired by snakes to control many DoF to enable devices to insert along tortuous trajectories to obscured surgical targets. A snake can navigate cluttered environments by employing Follow-The-Leader (FTL) behaviour. The snake body follows the snake head around obstacles, illustrated in Fig. 1. The shape of the body is shifted backwards through its body, propelling the snake forwards since the obstacles are stationary.



Fig. 1: Follow-The-Leader (FTL) locomotion modes of snakes. The body follows the path of the head.

Hirose et al. applied the modes of snake locomotion to HRD for the first time in 1993. [1] Since this pioneering work many research groups have dedicated their efforts to understanding the modes of snake locomotion and applying them to HRD. This field focusses on planar guided motion, i.e. using a planar surface for traction and support. Even though these devices are the first to include FTL behaviour, planar guided motion is not encountered in surgery, which is why these devices are not included in this paper.

There are several methods to realize FTL behaviour which can be categorized based on the interaction of the device with the environment. A biopsy of lung tissue at a remote location functions as a clear example exhibiting varying degrees of interaction with the surrounding tissue. First the bronchoscope is inserted through the trachea and bronchi. After this, the device must transition from following an existing lumen to navigating through tissue. Navigating such different situations result in other sets of requirements on the FTL method used. These requirements vary from full contact allowed with the environment to no interaction with the surrounding tissue in fragile environments.

Each category of devices described in this paper will have its Follow-The-Leader methods evaluated according to the following definition:

Follow-The-Leader method: *The method used by a device to obtain, store and transfer the shape information from the leading segment throughout its body.*

TABLE I: Search query construction

Device		OR	AND	Device type		OR	AND	Control behaviour		OR
robot*								snake*		
scope				flex AND steer*						track*
probe				continu*						planning
catheter				hyperredundant				path	AND	follow*
				highly*articulated						track*
				serpentine						planning
				actuation*redundancy				trajectory	AND	follow*
				multi*link						track*
				hyper*mobile						planning
								obstacle avoidance		

The search query is constructed using one term of each of the 'Device', 'Type' & 'Control behaviour' columns. The terms used to describe the 'Control behaviour' is either *obstacle avoidance* or a composite of the words *leader*, *path* or *trajectory* with *follow*, *track* or *planning*.

Goal

The goal of this paper is to create an overview of the current state of the art of HRD capable of FTL behaviour suited for the medical field. The focus of this paper lies on the method of reaching remote locations through complex trajectories, with an extra focus on devices independent of their environments. This is realised via a literature survey. The results of this survey will be categorised to create a systematic overview of FTL methods based on the level of device-environment interaction. This overview will help in identifying the current challenges and potential improvements in FTL instruments. Industrial HRD applications are included in the study to enable cross-pollination.

Structure

In section II the methodology of the literature search is described. Section III introduces the categorisation used to create a systematic overview of FTL methods. The identified categories and their hybrids are highlighted in sections IV to VII. Finally, the current state of the art devices and challenges for future devices are discussed in section VIII. The paper is concluded in section IX.

II. METHODS

Terminology & search query

To explore the state of the art in HRD capable of FTL behaviour in the medical and industrial fields a literature survey was performed using Scopus.com. The search query, shown in Table I, is composed of three parts. These parts are the device, device type and control behaviour. The sets of search terms are combined to construct the final search query. The terminology is discussed below, followed by the used methods of further selection.

To obtain relevant articles concerning HRD showing FTL behaviour the devices within focus consist of robots and a set of medical devices capable of FTL behaviour. There is no consensus in nomenclature concerning HRD. Therefore, a set of search terms is chosen to complement the device search terms in order to limit the amount of devices found on HRD. To describe the desired FTL and related behaviour, another

set of search terms is constructed. Again, there is no real consensus on the use of Follow-The-Leader or related terms. The composition of these sets of search terms are further explained in Table I.

The final search query is derived from the aforementioned terminology. To create a more potent search string wildcards (*) are used to allow Scopus to search for plural forms and variations of a word. An example search query is: (robot* AND snake* AND (trajectory AND track*))

Selection

The defined search query matrix yielded 1897 papers (last update 16/03/2016). The amount of hits due to the expansive search query is reduced by manual title selection on potential relevance. Further manual selection on availability and reading the abstracts resulted in 44 relevant papers. Relevant references from these papers and commercial applications resulted in 9 additional papers. Including the commercial applications the total of 53 papers span the intended FTL capable HRD research field.

III. CATEGORISATION

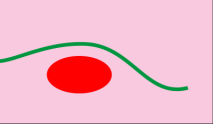
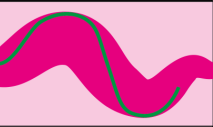
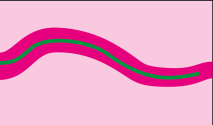
Reaching deep targets inside the body often require complex trajectories, as described in the first section. The focus of this paper lies on the method of reaching these remote locations through complex trajectories. Current instruments used to reach unobstructed surgical targets along straight trajectories are included in the categorisation to provide context. However, these are not relevant for this research and therefore only mentioned and not further explored.

In the devices capable of navigating tortuous trajectories to reach a remote target, different degrees of environment interaction are observed. The categorisation focuses on sorting the existing devices based on these levels of device-environment interaction (Table II).

Environmental interaction

Three discrete levels of device-interaction are introduced: Trajectory *fully dependent*, *partially dependent* and *fully independent* of the environment. Each of these levels of environmental interaction introduce a different set of requirements to obtain FTL behaviour.

TABLE II: Categorisation results

		Environment complexity			
		Straight, unobstructed trajectory	Complex trajectory	Situation sketch	Minimal FTL requirements
Environment interaction	Fully dependent	<i>Needles</i>	Tissue guided motion <i>Steerable needles</i>		Surrounding tissue fully supports the shape memory transfer of the device. No self-guidance is required.
			Stiff lumen guided motion <i>Catheters</i>		
	Partially dependent	<i>Snake robots</i>	Compliant lumen guided motion <i>Colonoscopes</i>		Surrounding tissue can not fully support the shape memory transfer of the device. Some degree of self-guidance is required.
	Fully independent	<i>DaVinci surgical platform</i>	Self-guided motion <i>Concentric Tube Robots</i>		Surrounding tissue can not support the shape memory transfer of the device. Complete self-guidance and support is required.

The discrete levels of environmental interaction are spaced vertically. Next, each category of devices working along tortuous trajectories is clarified with a situation sketch and the minimal FTL constraints accompanied by their situations.

The fully dependent category describes instruments that use the surrounding tissue and structures to enable FTL behaviour. A division can be seen in devices creating their own path through a (uniform) tissue volume, such as needles: *Tissue guided motion*, and devices following an existing stiff lumen, such as catheters: *Stiff lumen guided motion*.

The partially dependent category consists of devices able to use surrounding structures to some extent to enable FTL behaviour. The used structures are not stiff enough, relative to the device used, to support the device completely. These devices, such as a colonoscope, perform: *Compliant lumen guided motion*.

The fully independent category contains devices not relying on environment interaction for support. The instrument must contain its own mechanism to enable FTL behaviour. These devices perform: *Self-guided motion*.

In practice, procedures encounter combinations of these previously described situations. For example, a biopsy of remote lung tissue requires both stiff lumen and tissue guided motion. *Hybrid* systems are being developed to facilitate combined situations.

For each category, the working principles for achieving FTL behaviour will now be discussed. There is no standard set of performance metrics in literature. If available, metrics will be given as they are presented in the literature.

IV. PATH FULLY DEPENDENT OF ENVIRONMENT

Devices which are fully dependent of their environment are steered by the user by manipulating a handle to control the tip section. The interaction of the tip section with the surrounding environment determines its direction. The shape of the trajectory is therefore *obtained* by steering the tip. The shape information of the trajectory is *stored* in the environment

due to the relative stiffness of the environment with respect to the flexible device. When propagated, the rest of the device follows the tips' trajectory due to the device-environment interaction. The shape of the trajectory is therefore *transferred* via the environment to the remainder of the device. Two types can be identified: *Tissue guided motion* & *Stiff lumen guided motion*.

Tissue guided motion

Tissue guided motion is performed by steerable needles. Steering of the needles can be used by surgeons to avoid obstacles like veins, nerve bundles or bones. The FTL method is the same for all steerable needles; by cutting a tunnel through the tissue the desired trajectory is obtained and the created path is stored in the tissue. The shape is automatically transferred to the rest of the needle when pushed forward. All steerable needles found in this study use this FTL method, the difference between them lies in the steering strategy used.

When assessing the performance of steerable needles three main metrics are used. The *size*, *radius of curvature* and *accuracy*. The relevant sizes of steerable needles is the diameter of the device. The diameter influences the device-environment interaction. The device length limits the minimal diameter due to buckling issues. The radius of curvature quantifies the sharpest bend the needle can perform. It is the radius of the circular arc which best estimates the trajectory followed by the needle. The accuracy states the positioning error of the needle tip with respect to the target.

A needle with a lumen cannot be symmetrically tipped with a cone shape, instead it has a bevelled tip. The distribution of the forces acting at the tip is asymmetric due to the tip geometry, this causes the needle to bend in the direction of the bevel angle (Fig. 2) [2]. Combination of translation and

rotation around the needle axis can control the direction of steering to follow tortuous trajectories. [3], [4] The force imbalance, and therefore the amount of steering, of the tip depends on the bevel angle [5] and can be amplified by introducing a pre-bent, curved tip section in addition to the bevelled tip seen in Fig. 2(c). This extra curved tip section can increase the damage to the surrounding tissue when the needle is rotated [6].

The needle-tissue interaction is of great importance to the performance of steerable needles. Modelling of these interactions [7], [8] is crucial to creating path planning [9]–[12] and control [13]–[18] algorithms. Guided steering algorithms are created using different sensing modalities such as MRI, CT-scanning, ultrasound or any other medical imaging [19]–[23].



Fig. 2: The force balance and imbalance on a needle with (a) a symmetrical, (b) a bevelled tip and (c) a bevelled and curved tip [24]

Frasson *et al.* designed a steerable needle with a so-called 'programmable' bevel [25]–[28]. This device can control the curvature of its path allowing greater freedom in following tortuous trajectories. The 'programmable' bevel is constructed using relative sliding needle sections (Fig. 3a). Creating an offset between the sliding segments results in different curvatures while inserted, as illustrated in Fig. 3b. The device illustrated in Fig. 3b has a diameter of 12 mm and can obtain a minimal radius of curvature of 178.6 mm. The tip can be positioned with a mean positioning error of 0.68 mm with a standard deviation 1.45 mm and a maximal error of 5.44 mm.

A bevelled tip with a flexible hinge behind the tip is illustrated in Fig. 4. The force imbalance caused by the bevelled tip bends the hinge creating a bend in the tip allowing a sharper steering radius. However if the tip is rotated the hinge is not allowed to bend and the needle can move in a straight trajectory. Needles with a pre-bent, curved tip section cannot move with a perfect straight trajectory. The curved tip carves a spiral through the tissue it is propagated through [6]. The needle illustrated in Fig. 4 has an outer diameter of 0.91 mm and can obtain a minimal radius of curvature of 121 mm in gelatin and 176 mm in ex-vivo pork loin. The average error of the tip target positioning is 0.72 mm.

An alternate method to steer a needle through tissue and reach a target uses the flexible interactions between the tissue and a relatively stiff needle. Due to the inverted relative stiffness repositioning the insertion point deforms the tissue which allows a new insertion direction for the needle. A test procedure avoiding an obstacle to reach a target below is illustrated in Fig. 5 [29]–[31]. The needle used in Fig. 5 is a standard 22 gauge needle, with an outer diameter of 0.7176 mm. Using this steering technique the tip can be positioned within a 1 mm error margin.

Using the steering techniques - as seen in literature - planning algorithms are developed to reach targets behind a

number of obstacles. Two discrete control algorithms were found: the stop-and-turn, and the helical strategy. In the former the needle is pushed forward, stopped, rotated and pushed forward again. With this cycle a set of connecting planar arcs form a 3D trajectory through the tissue. The latter pushes the needle forward with a constant speed while controlling the rotation speed step-wise. This produces a set of connected helical trajectories as the name implies. These algorithms use discrete control inputs to reduce the computational cost of trajectory planning. Both strategies showed great versatility by being able to reach the test targets [4].

Although the steering methods and path planning strategies differ among the devices seen in literature, the shape memory transfer methods are the same for all steerable needles. The trajectory is obtained by steering of the tip whereas the shape information is stored and transferred solely by the tissue surrounding the needle.

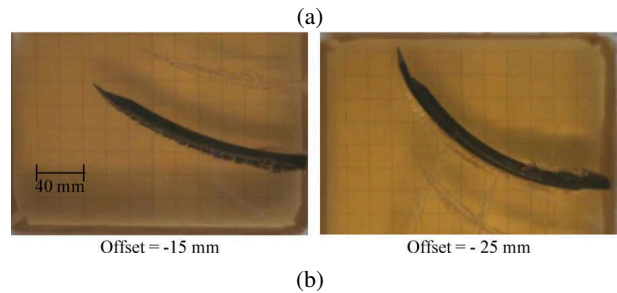
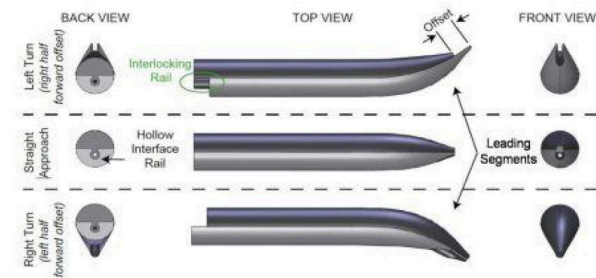


Fig. 3: The STING, a steerable needle with a 'programmable bevel'. (a) Design image of the programmable bevel concept. (b) An offset of two parts of the flexible probe determines the amount of steering and direction of the tip [25] *Stiff lumen guided motion*

A device can be guided by a stiff lumen in a similar way as steerable needles. The difference lies in the fact that the path is not cut by the tip but the device follows an existing lumen. These devices are catheters, flexible probes following the windings of a blood vessel. These devices are relatively flexible with respect to the existing stiff blood vessel. Navigating the many complex trajectories requires control of not only the direction of the tip of the device but the actual shape of the tip section.

It is difficult to quantify the performance of catheters based on accuracy. Due to the fact that the catheter always stays within the confines of the lumen its following accuracy is irrelevant. The size of the state of the art catheters is, however a suitable metric as it determines the maximal reach of the catheter.

In current procedures with catheters a large range of catheters are used subsequently. Each of them having their

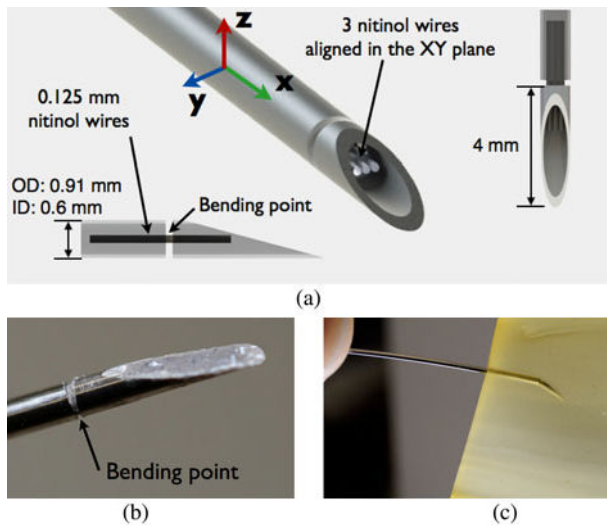


Fig. 4: Flexure-tip needle design. (a) CAD drawing of the flexure-tip needle concept with dimensions shown. (b) Close-up of the flexure-tip prototype. (c) The flexure-tip bends in the direction of the bevel when inserted into tissue, thus kinking the tip of the needle. [6]

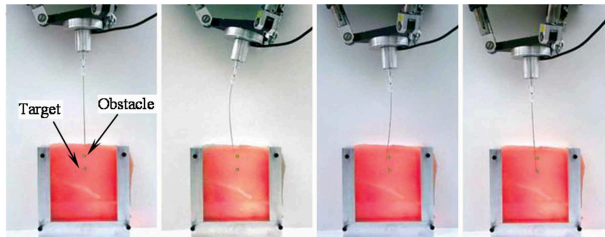


Fig. 5: Process of steering a flexible needle by manipulating the insertion location and direction. [29]

own specific control shape for a specific bend or bifurcation in the vein to be followed, a selection of catheters available are shown in Fig. 6 [32]. Catheters are inserted together with a guide wire, a stiff wire which straightens the catheter tip shape when inserted. When the guide wire is retracted or the catheter advanced without the guide wire the tip control shape can be used. Once the control shape has navigated the bend, the guide wire can slide along the catheter continuing the procedure. When the next complex bend is reached the first catheter must be fully retracted to leave space for the next catheter with the appropriate control shape. Such switches of catheter are required for each complex structure to be navigated in the procedure.

Steerable catheters can overcome the need of multiple insertion of differently bent catheters for each complex structure. The literature search of this study included no steerable catheters, yet *Ali et al.* reviewed the complete scope of, currently used and under development, steerable catheters [33]. The main division in steering principles was identified between 'Force generation in tip' and Force transmission to tip'. Force can be generated by electric, thermal or magnetic actuation. Force can be transmitted using hydraulics to actuators in the tip or mechanically by using cables. The sizes of currently used

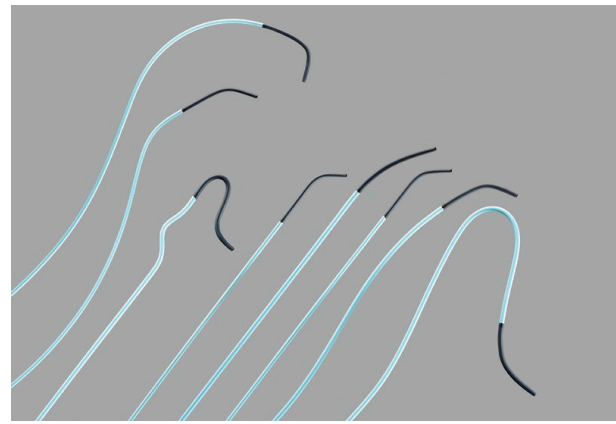


Fig. 6: Selection of commercially available passive catheters by COOK medical [32].

and catheters under development range from 0.2 - 5 mm.

Like the steerable needles the difference between devices lies in the steering methods. The trajectory information is obtained by the control shape of the tip, choosing a path through the existing lumen. The devices follow the geometry of the existing lumen, the trajectory is stored in the existing lumen. The trajectory is transferred to the remainder of the device via the environment.

V. PATH PARTIALLY DEPENDENT OF ENVIRONMENT

Devices inserted into a compliant lumen can only partially depend on the environment for guidance. This category is therefore named *Compliant lumen guided motion*. Due to the relative stiff device with respect to the environment the device shape cannot be controlled solely by the environment. To navigate a compliant lumen not only the device tip, but the entire device shape must be controlled to some extent.

Compliant lumen guided motion

The situation of a device guided by a compliant lumen can be seen in endoscopic procedures such as colonoscopies. In these procedures a relatively stiff scope is inserted into the flexible colon. This unfavourable, relative stiffness is necessary to prevent buckling during axial loading, which is required during insertion of the endoscope. However, this relative stiffness increases the difficulty of navigating the convoluted path of the colon [34].

Devices employing compliant lumen guided motion can be quantified by their size and the forces acting on the colonic wall. These forces are a measure for the patient's comfort during the procedure.

This stiffness can produce loops of the colon preventing the advance of the scope. Special manoeuvres are required to enable continuation of the procedure. Externally applied pressure by the physician can help position the scope. Alternatively, manoeuvres involving twisting the scope and lifting up the colon with it can be performed. Moreover, retraction of the scope can straighten the colon as illustrated in Fig. 7. The device will follow the outer shape of the lumen. However due to the relative stiffness of the device with

respect to the colon the colon wall is stretched. The resulting elastic forces will bend the colonoscope until a balance is found. The scope bends as soon as the restoring elastic forces of the stretched colon are greater than the scope stiffness. Colonoscopes capable of FTL behaviour could improve patient comfort and procedure time.

Chen *et al.* designed a modular continuum robotic endoscope containing seven bending segments, illustrated in Fig. 8. Each segment contains a set of actuators that drive short cables that enable bending of the segments. These segments are continuum segments, are 15 mm in diameter and can turn 180 degrees. The bending segments communicate with each other and are independently controlled to enable FTL behaviour. The complete robot has 14 DOF, is 0.91 m long, weighs 157 grams.

The robotic endoscope is shown to be able to perform an automatic uncoiling motion into the colon. (Fig. 9) This FTL mode can be used to navigate the inside of the colon by following a defined set of bends dictated by the lead bending segment. These bends are then followed by all the subsequent segments when they reach the same position. Using the FTL mode it can reach the end of the large colon while causing less stress in the colonic walls compared to conventional colonoscopes. The modular design requires the shape of each segment to be controlled independently. The shape information is obtained by steering the first segment. The shape memory information is stored externally by a computer, the transfer of this shape information to the next segments is controlled by the control algorithm.

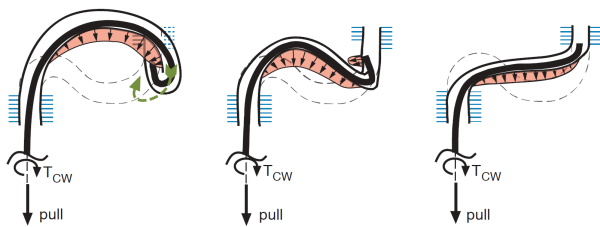


Fig. 7: Straightening an N-loop. The relatively high stiffness of the scope shaft is used to lift and pull back the distal part of the scope and straighten the colon by applying clockwise twist (T_{CW}) to the scope shaft and pulling it back [34].

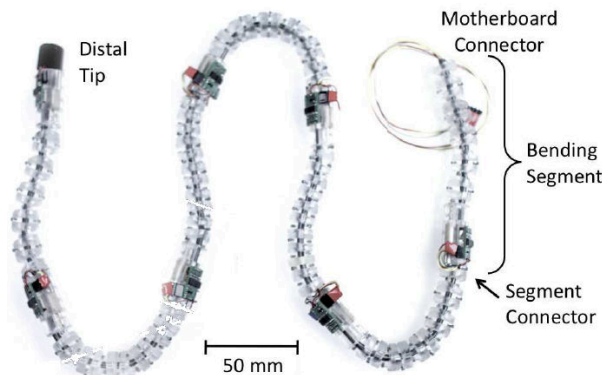


Fig. 8: The robotic colonoscope without the outer sheath [35].

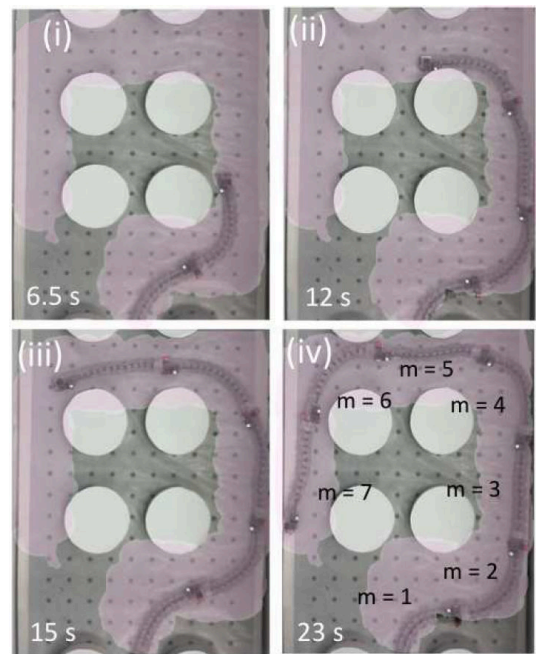
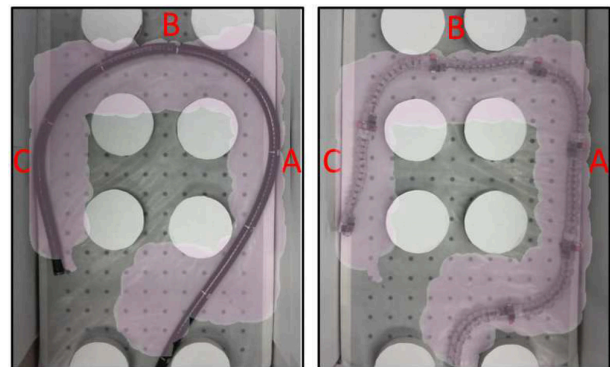


Fig. 9: Robotic endoscope automatic colonic insertion, experimental result [35].



(a) Conformation of a Olympus CF-IBW endoscope (left) and the continuum robotic endoscope to a colonic phantom. The normal forces exerted by the endoscopes on the walls are measured at three points A, B and C [35].

(b) Forces measured on points A, B and C.

Endoscope	Maximum Force (N) Exerted on Wall		
	A	B	C
Conventional	1.72 ± 0.14	1.69 ± 0.24	1.06 ± 0.38
Robotic	0.34 ± 0.08	0.20 ± 0.04	0.09 ± 0.03

Fig. 10: Force measurement setup in a colonic phantom.

To evaluate the performance of the robotic colonoscope compared to conventional colonoscopes the contact forces were measured within a phantom of the colonic track. The forces were measured in the three locations: A, B & C illustrated in Fig. 10a. The resulting forces are listed in table 10b [35].

A compliant lumen can provide some steering and support

when a device is inserted. However not sufficient steering can be provided to insert passive instruments. A colonoscope capable of steering and controlling its entire shape can potentially improve success of the procedures.

VI. PATH FULLY INDEPENDENT OF ENVIRONMENT

Neuro-surgery is an example where a surgical target can be obscured by many delicate and vital structures. Contact with this delicate environment should therefore be avoided, which implies the need for *self-guided* motion that is fully independent from the environment.

Self-guided motion

Following spatial trajectories with every segment of a device is the focus of an increasing number of research groups. Two different types of devices that are capable of this level of FTL behaviour were found, *serial* and *parallel* devices. Serial devices are build up from segments connected to each other in series, with a specified orientation towards their neighbouring segments. The final shape and orientation is the sum of its segment orientations. Parallel devices rely on the balance found between the interactions of its segments, finding a force balance between elastic segments. The final shape is a (non-linear) function of its segment orientations.

Serial

Tappe et al. developed an active shaft concept. The active shaft system is based on 1 DOF binary electromagnetic actuators. Segments incorporate a hinge and two electromagnetic actuators with a diameter of 45 mm and heights ranging from 4 to 16 mm, Fig. 11a. Every segment is bistable and can only reach two discrete states: tilted to the left or tilted to the right, again within a range of 6 to 25° per segment. With this segment height and angular tilt ranges, the minimal obtainable radius of curvatures can vary between 30 to 350 mm. To allow spatial motion these 1 DOF actuators must be stacked with a rotation about the longitudinal axis. The electromagnetic actuators provide high stiffness and potential for miniaturisation. For a given trajectory the actuator parameters, height and tilt angle, can be found using optimisation algorithms. After such an optimisation procedure the active shaft can deploy along a trajectory with FTL behaviour. The tracking errors for a planar S-shape, helical and a trajectory through a colon are respectively below 6.8, 9 and 11.87 mm [36].

The *Highly Articulated Robotic Probe* (HARP) is a device without an active shaft while maintaining FTL capabilities. It is controlled with a joystick coupled with the steerable tip and a button to move forward or backward. The *CardioArm* is the latest iteration of the HARP, a deployed CardioArm is illustrated next to a model of a heart in Fig. 11c. Its outer diameter is 12 mm to be compatible with existing trocars. It is composed of 50 rigid cylindrical links serially connected by three cables. In the lumen of these cylindrical links an inner snake resides, serially connected by a single cable. Due to its resemblance these linked segments are called 'snakes', the outer and inner snake. The link interfaces resemble a spherical

surface, therefore two adjacent links can rotate 15° relative to each other. Tension on the inner cable makes the inner snake stiff, releasing tension makes it flexible again. The outer snake rigidity is controlled by tensioning and relaxing the 3 outer cables.

The shape memory transfer is incorporated into the mechanical design. This limits the need for complex computer control of each segment orientation. The gait sequence performed is illustrated in Fig. 11d. Step 1 shows the outer snake is advanced a single segment forward, while the inner snake is rigid. In step 2 this tip segment obtains the new trajectory by steering using the 3 control cables the outer snake is then made rigid, storing the new trajectory information. Next, in step 3 the inner snake is advanced to catch up with the outer snake. Once the inner snake is caught up it is made rigid copying the trajectory information. The outer snake can now be advanced again to obtain the next trajectory section. Using the alternating stiff and flexible inner and outer snakes produces the desired FTL behaviour. This gait sequence can be seen as a mechanical equivalent of the control algorithm. This type of control is intuitive to an operator since only the tip needs to be controlled. This design is a passive shaft with an active tip. In contrast with the previously described active shaft concept.

A disadvantage, due to the discrete nature of the device links sliding relatively, is the interplay between the outer and inner links. This play is necessary to allow the relative sliding when the device is curved. However, this play acts as a damper on the shape information stored in the snakes. With each step a small portion of the shape information is lost [37]–[39].

The first interlaced continuum robot by *Kang et al.* employs a similar alternating track building method [40]. It features two interlaced continuum robots (CRs) that are identical, illustrated in Fig. 11e(1). They are concentrically located, angularly shifted and can slide on each other, illustrated in the cross section in Fig. 11e(2). An outer diameter of 30 mm is chosen to prevent fabrication issues in the prototyping phase. The CRs are devised to alternately guide each other, with the exception of the distal section of the distal CR, which is free to incrementally obtain the deployment trajectory. The gait cycle is illustrated in 11e(3). This new trajectory information is stored in the differential translations of the deployment rods. The trajectory information is transferred to the proximal CR from the distal CR during deployment: there is a leader CR (LCR) and a follower CR (FCR); the CRs reverse their role during retraction.

FTL deployment performance was assessed using experiments. The interlaced continuum robot was deployed over planar trajectories, with single and double curvatures. The continuum robot was deployed manually to obtain the tightest single curvature, achieving track-building with a radius of curvature as low as twice the probe diameter. Track-building was more challenging when pursuing double curvature trajectories. The second curve influenced the previously taken trajectory, reducing the first curve to a straight section. *Kang et al.* indicate further research is required to counteract this behaviour.

An industrial application of a serial, active shaft device is

the *Series II, X125 system* build by OC Robotics. It has an manipulator arm of 3.1 metres capable of performing tasks in areas beyond human reach. 12 links with a diameter of 125–140 mm and 2 DOFs of up to 27.5° bends are placed in series, Fig. 11f. Resulting in a radius of curvature range of 160–950 mm. Each segment of the X125 system is controlled and supported by cables running the length of the snake arm. These cables are actuated by electro motors placed at the base of the instrument. The shape memory transfer used to reach remote targets is controlled electronically [41].

Based on the same principle and patent US 4494417 A: 'Flexible arm, particularly a robot arm' [42], a 24 DoF snake arm has been designed by *Palmer et al.* [43]. Details of the snake arm construction are not shared in the paper. Implementing their FTL control algorithm enabled the snake arm to perform FTL behaviour, illustrated in Fig. 11g. A tip deployment speed of 4.5 mm s⁻¹ was reached. For most configurations the deviations in the path can be kept below 15 mm with a tip accuracy of ± 0.75 mm.

Obtaining the shape information at the tip is fairly straightforward in serial devices. However storing and transferring the obtained shape information requires control. The computer controlled active shaft devices, [36], [41], rely on kinematic models. Differences between the device and its model introduces uncertainty in the shape control. The mechanical shape storage and transfer of the HARP is dampened by the play necessary for the mechanism to function [37].

Parallel

To enable application of steerable devices to areas such as neurosurgery, the device size must be reduced. *Webster et al.* developed a 2.4 mm device consisting of a set of concentric tubes that slide into each other illustrated in Fig. 12a. Each of the concentric tubes each have a pre-bend state and can be considered to be springs. When slid into each other it is just like two different springs coupled in parallel. This results in a combined curvature which is a combination of the two start states, as illustrated in Fig. 12b. These devices were called *Active cannulas* and more recently *Concentric Tube Robots* or CTRs [44]. The CTR's have diameters ranging from 0.8-2.4 mm. In theory, the minimal radius of curvature is limited by plastic deformation and can be as low as 6.25 mm. However, when considering practical limitation of tubes required to rotate inside each other a minimal radius of curvature of 26 mm was measured. To facilitate acceptance in the operating theatre an MRI compatible CTR is developed [45].

When using CTRs to reach a remote surgical location, for instance in the brain, the path stability must be considered. During the insertion procedure stability issues can arise. Unstable configurations can be passed while working towards the final configuration. At unstable configurations, small perturbations in relative rotation anywhere along a tubes length can produce large displacements at the distant end. A deployment planner takes the intermediate configurations into account and avoids unstable paths [46]. New control strategies are developed to enable interactive rate shaft control [47], [48].

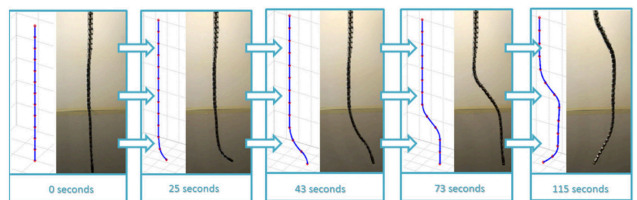
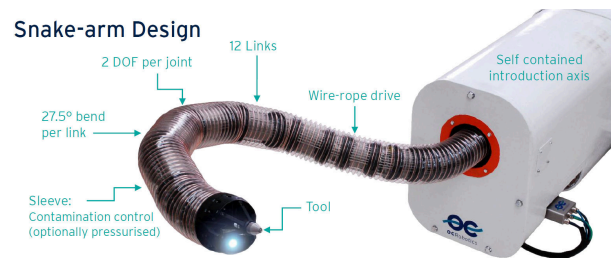
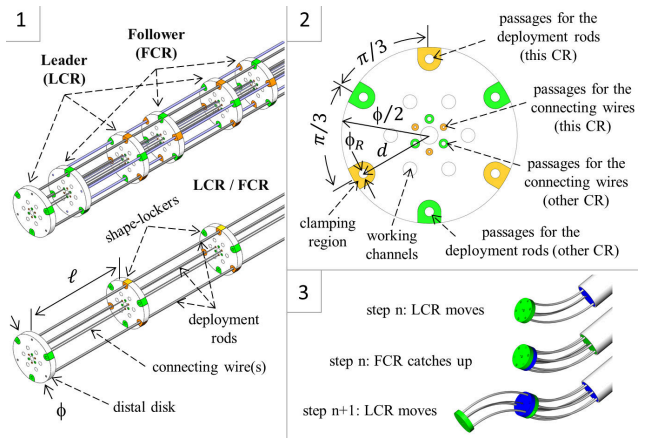
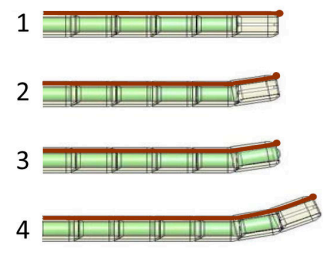
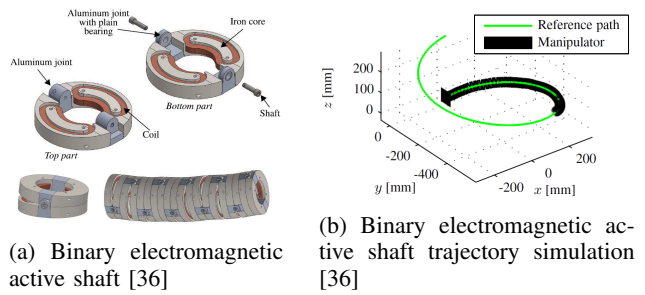


Fig. 11: Serial self-guided devices: in literature and commercially available

A manual deployment device was developed. Supported by a planning program which outputs a step-by-step guide for a surgeon to follow [49].

FTL behaviour is only obtainable by CTRs when specifically designed for this purpose [50]. When properly designed, FTL behaviour is possible in several special cases: One but not both of the tubes has zero precurvature, both tubes are circular in precurvature or both tubes are helical in precurvature with the same helical torsion. The last two options require the tubes to have a constant angular displacement with respect to each other of $n\pi$. Experiments prove CTRs are capable of FTL behaviour with small tracking errors of under 3 mm [51]. FTL enables CTRs to act like steerable needles that do not depend on tissue interaction to steer.

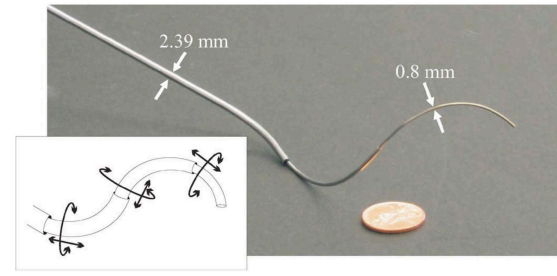
Obtaining the shape information for FTL behaviour in the parallel system of the CTR must be planned. Storing the shape information is straightforward due to the low number of input variables, being the translation and rotation of each concentric tube. However, during transfer of the shape stability issues can cause large displacements of the tip with small changes in input variables.

VII. HYBRIDS

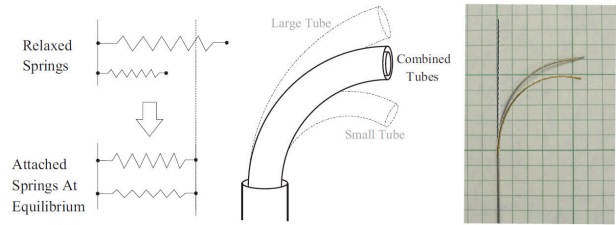
In previous sections we have seen that each environment requires and allows different methods of FTL behaviour. Since, in practice, not all procedures are limited to a single type of environment we can find hybrid solutions. One approach combines characteristics of two devices described in the previous section in a unique device. Another hybrid is created with a specific procedure in mind, a remote lung biopsy. This hybrid combines two situations, an tackles the transition between two different categories of guided motion: Stiff lumen to tissue guided motion.

Combination of characteristics

Each type of device in the categories has its strengths and weaknesses. *Mahvash et al.* attempts to combine the best of both world from the HARP and CTR. The small dimensions of the CTR is desired together with the higher stiffness of the HARP system. A CTR is inserted in the working channel of a HARP-like device. The HARP functions as a remote and stiff deployment base for the CTR. The CTR can work from there, decreasing its deployed length and thus increasing the tip stiffness. [53] The bottleneck of this approach lies in the stiffness of the CTR applying a moment to the HARP, which limits the radius of curvature obtainable by the combined device. When surpassing this limitation, the CTR movement can corrupt the shape stored in the HARP mechanism. The relation between the force required for locking the HARP and the minimal radius of curvature has been investigated. Higher tension in the cable enables a smaller radius of curvature. The found relations for a single and a double CTR is depicted in Fig. 13. The obtained radii of curvature range from 21 mm with a single CTR tube and a cable force of 9.61 N to 80 mm with a double tubed CTR and a cable force of 73.28 N.



(a) Concentric Tube Robot



(b) Concentric Tube Robot principle

Fig. 12: Parallel self-guided devices: (a) Concentric Tube Robot (CTR) by Webster (b) Working principle of Concentric Tube Robots [52]

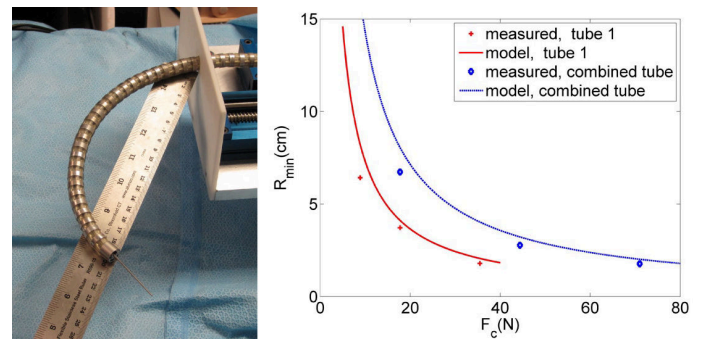
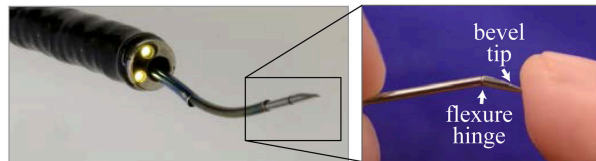


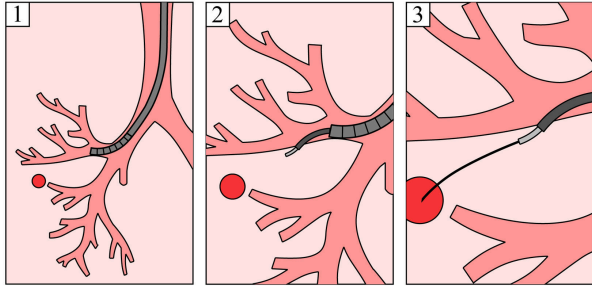
Fig. 13: CTR/HARP hybrid by *Mahvash et al.*, combining characteristics of two self-guided devices [53].

Combination of situations

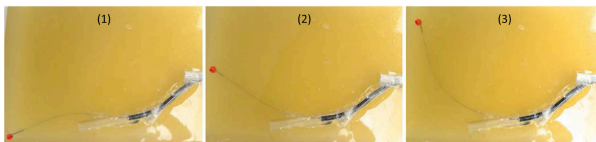
In practice, procedures do not encounter just one type of device-environment interaction. *Swaney et al.* therefore focuses on a device designed for a lung biopsy procedure, illustrated in Fig. 14a, of a remote piece of lung tissue. In such procedure a bronchoscope is used for the first stage of the path, following through the trachea and bronchi. Next a CTR is employed to make the transition from stiff lumen guided motion to tissue guided motion. The CTR is further used to bring the biopsy target into the workspace of a steerable needle. A steerable needle can then be used to take a biopsy or deliver localised medicine. [54] The size of the device varies along its deployed length. The bronchoscope has a diameter of 6 mm, whereas the CTR and steerable needle deployed from the bronchoscope tip are respectively 1.38 mm and 1.16 mm. In targeting experiments performed with the CTR and steerable needle stage, illustrated in Fig. 14b, an average error of 0.72 mm was measured.



Lung targeting using the three-stage steering system above



(a) Layout and deployment phases



(b) steering system deployed to three separate targets in the phantom. The tip error for each of the three runs was (1) 1.3 mm, (2) 0.5 mm, and (3) 0.2 mm.

Fig. 14: Bronchoscope/CTR/Steerable needle hybrid by Swaney *et al.*, combining a stiff lumen, self and tissue guided device to navigate situations encountered in a practical application [54].

VIII. DISCUSSION

This paper focused on the state of the art of HRD performing FTL behaviour. The FTL methods varied along with the levels of device-environment interaction described. Each category employs FTL methods to *obtain*, *store* and *transfer* shape information to accomplish FTL behaviour. Each method is suitable for the levels of allowed environment interaction: *Fully dependent*, *Partially dependent* and *Fully independent*.

Follow-The-Leader methods

In the category *Fully dependent* of the environment, there is a division between *Tissue guided* and *Stiff lumen guided* motion. Steerable needles performing tissue guided motion showed only a rotation of the bevelled tip is sufficient to fully control the needle trajectory and therefore obtain the shape information. The shape is stored in the tunnel cut into the tissue by the tip, by propagating the needle, this shape is subsequently transferred to the rest of the needle. Catheters performing stiff lumen guided motion require a larger control shape at the distal tip of the device in order to obtain the shape information required to navigate complex structures. The shape is further stored and transferred by the confines of the stiff lumen.

Devices *Partially dependent* of the environment cannot rely solely on a compliant lumen for steering, due to the higher relative stiffness of the device versus environment. The higher relative stiffness requires the entire shape of the device

to be controlled to some degree. Conventional colonoscopes are deployed along the same principle as *Stiff lumen guided* devices, however the stiff colonoscope influences the lumen geometry. Therefore they require the application of external forces on the body to obtain the desired trajectory and transfer it through the colon. The force balance between the device and the stretched colon stores the obtained shape. An active colonoscope controlling its entire body shape in discrete steps reduces stress on the colon during insertion and does not require externally applied forces for deployment.

At the moment that a device operates where environment interaction is not permitted *Self-guided* motion is required. Self-guided devices are the focus of an active field of study and an existing commercial application. To achieve the self-supported FTL behaviour, able to navigate the delicate environments encountered in the medical field, full shape control is required: to obtain, store and transfer shape information.

These devices can be constructed out of *serial* or *parallel* connected segments. The serial devices obtain the shape information from the control input of the user, while the parallel setup of the CTR requires careful planning before the procedure to determine the possible shapes. Storing the shape information in both the active shaft and parallel devices is done outside the device by control algorithms. The HARP, however, stores the shape information obtained in its mechanical structure itself. Storing the shape information outside the device in the software allows for the shape to be measured and known. In the case of the HARP, the device shape must be approximated by a model in order to know its shape. The HARP's mechanical structure allows for transfer of this shape information to the next segments as well.

Control complexity

Control complexity of devices exhibiting FTL behaviour varies across the identified categories. A decrease of interaction with the environment is paired with an increase in control required of the device. For the fully dependant motion, the shape is stored and transferred by the environment itself, resulting in a low level of control complexity. Obtaining of the shape differs between tissue guided motion and stiff lumen motion. With tissue guided motion the trajectory is made by the instrument itself, while in stiff lumen guided motion, the trajectory is already in place. With partially guided motion, the trajectory is only partially stored and transferred by a relatively flexible lumen, meaning that the shape of the instrument should be partially controlled. In self-guided motion, the trajectory must be fully stored and transferred by instrument, resulting in highest level of control complexity. The level of control complexity for self-guide devices does however differ per device. An active shaft requires a control signal for each actuator in its body, while the HARP stores and transfers its trajectory mechanically resulting in a much lower level of control. However the shape information loss due to damping prevents the HARP from achieving accurate FTL behaviour. The parallel segmented nature of CTR's require the trajectory to be planned before the actual deployment of the device, as the parallel segments influence each other during propagation.

Research focus in time

When investigating the publishing dates of the self-guided literature found in this study a trend can be seen. The field FTL HRD (as focused on in this paper) has produced significantly more papers in recent years. Two-thirds of the papers were published in the period 2011-2015 while one-third was published in the period of 2006-2010. A clear trend can be seen: research into FTL HRD has increased significantly in recent years.

Future challenges

The state of the art of FTL HRD in the medical field focus on increasing the workspace and capabilities of surgeons. Self-guided devices enable working on remote and obstructed surgical targets while leaving the environment intact. Full shape control is required to reach remote targets obscured by delicate structures. The damping of shape information and the approximate FTL performance of respectively the HARP and the CTR should be improved upon. The active shaft devices show great promises due to the active full control of the shape. However there is still room for improvement when considering the current sizes, accuracy and control complexity.

IX. CONCLUSION

HRD devices capable of FTL behaviour were categorised based on the level of environmental interaction. Three distinct levels were identified: *Fully dependent*, *Partially dependent* and *Fully independent* of the environment. Each level of interaction allowed for a different shape memory transfer strategy to be deployed. To obtain FTL behaviour, a decrease in environmental interaction requires greater control of device shape. State of the art devices deploy various methods of *obtaining*, *storing* and *transferring* shape information. Hybrids were designed for procedures that encounter multiple levels of device-environment interaction. They combine characteristics of different categories to find an optimal solution for practical applications. Different surgical procedures require a unique combination of multiple levels of device-environment interaction, suggesting an equal variety of optimal solutions.

Remote surgical targets can be reached with FTL HRD while avoiding delicate structures en route. Self-guided devices and hybrids tailored for a procedure can improve procedure time and performance. This wide, still partly unexplored, field of study is an interesting, active field with a large potential to improve Minimal Invasive Surgery.

ACKNOWLEDGEMENTS

This work has been supported by the Dutch Technology Foundation STW, which is part of the Netherlands Organization for Scientific Research (NWO), that is partly funded by the Ministry of Economic Affairs.

REFERENCES

- [1] S. Hirose, *Biologically inspired robots : snake-like locomotors and manipulators TT -*. Oxford ;: Oxford University Press,.
- [2] W. Park, Y. Wang, and G. S. Chirikjian, "Path Planning for Flexible Needles Using Second Order Error Propagation," pp. 583-595.
- [3] R. J. Webster, N. J. Cowan, G. S. Chirikjian, and A. M. Okamura, "Nonholonomic Modeling of Needle Steering,"
- [4] V. Duindam, R. Alterovitz, S. Sastry, and K. Goldberg, "Screw-Based Motion Planning for Bevel-Tip Flexible Needles in 3D Environments with Obstacles," pp. 2483-2488, 2008.
- [5] R. J. Webster, J. Memisevic, and A. M. Okamura, "Design Considerations for Robotic Needle Steering," no. April, 2005.
- [6] P. J. Swaney, J. Burgner, H. B. Gilbert, and R. J. Webster Iii, "A Flexure-Based Steerable Needle : High Curvature With Reduced Tissue Damage," vol. 60, no. 4, pp. 906-909, 2013.
- [7] C. Chui, S. Teoh, C. Ong, and I. Sakuma, "Integrative Modeling of Liver Organ for Simulation of Flexible Needle Insertion," 2006.
- [8] N. Sadati, M. Torabi, and R. Vaziri, "Soft-Tissue Modeling and Image-Guided Control of Steerable Needles," pp. 5122-5125, 2009.
- [9] C. Caborni, S. Y. Ko, E. D. Momi, G. Ferrigno, F. Rodriguez, and A. B.-i. F. Probe, "Risk-Based Path Planning for a Steerable Flexible Probe for Neurosurgical Intervention," no. 0, pp. 866-871, 2012.
- [10] J. Lee and W. Park, "Insertion planning for steerable flexible needles reaching multiple planar targets," pp. 2377-2383, 2013.
- [11] X. Li, C. A. Lehocny, and C. N. Riviere, "Efficient 3D Control for Needle Steering using Duty-cycled Rotation," pp. 192-199, 2013.
- [12] J. Wang, X. Li, J. Zheng, and D. Sun, "Dynamic Path Planning for Inserting a Steerable Needle into Soft Tissue," vol. 2012, no. December, pp. 5-7, 2012.
- [13] R. Alterovitz, A. Lim, G. S. Chirikjian, and A. M. Okamura, "Steering Flexible Needles Under Markov Motion Uncertainty," pp. 2-7, 2005.
- [14] O. A. Bobrenkov, J. Lee, W. Park, O. A. Bobrenkov, and J. Lee, "A new geometry-based plan for inserting flexible needles to reach multiple targets Oleg A . Bobrenkov , Jaeyeon Lee and Wooram Park ," no. December 2013, pp. 985-1004, 2014.
- [15] S. Misra, K. B. Reed, and B. W. Schafer, *Mechanics of Flexible Needles Robotically Steered through Soft Tissue*, vol. 29. 2010.
- [16] C. D. Rucker, "Sliding Mode Control of Steerable Needles," vol. 29, no. 5, pp. 1289-1299, 2013.
- [17] A. Krupa, "A new duty-cycling approach for 3D needle steering allowing the use of the classical visual servoing framework for targeting tasks," pp. 301-307, 2014.
- [18] N. Hamzavi and C.-K. Chui, "Flexible Liver-Needle Navigation using Fish-Like Robotic Elements," pp. 3491-3496, 2008.
- [19] M. Abayazid, G. J. Vrooijink, S. Patil, R. Alterovitz, and S. Misra, "Experimental evaluation of ultrasound-guided 3D needle steering in biological tissue," pp. 931-939, 2014.
- [20] M. C. Bernardes, B. V. Adorno, P. Poignet, and G. A. Borges, "Mechatronics Robot-assisted automatic insertion of steerable needles with closed-loop imaging feedback and intraoperative trajectory replanning," *Mechatronics*, vol. 23, no. 6, pp. 630-645, 2013.
- [21] Z. Neubach and M. Shoham, "Ultrasound-Guided Robot for Flexible," vol. 57, no. 4, pp. 799-805, 2010.
- [22] N. A. Patel, T. V. Katwijk, G. Li, P. Moreira, W. Shang, S. Misra, and G. S. Fischer, "Closed-loop Asymmetric-tip Needle Steering Under Continuous Intraoperative MRI Guidance," pp. 4869-4874, 2015.
- [23] N. Shahriari, E. Hekman, M. Oudkerk, and S. Misra, "Design and evaluation of a computed tomography (CT)-compatible needle insertion device using an electromagnetic tracking system and CT images," *International Journal of Computer Assisted Radiology and Surgery*, pp. 1845-1852, 2015.
- [24] N. J. Cowan, K. Goldberg, G. S. Chirikjian, G. Fichtinger, R. Alterovitz, K. B. Reed, V. Kallem, W. Park, S. Misra, and A. M. Okamura, "Robotic Needle Steering : Design , Modeling , Planning , and Image Guidance," pp. 557-582.
- [25] L. Frasson, S. Y. Ko, A. Turner, T. Parittotokkaporn, J. F. Vincent, and F. R. Baena, "STING : a soft-tissue intervention and neurosurgical guide to access deep brain lesions through curved trajectories," vol. 224, pp. 775-788, 2009.
- [26] S. Y. Ko, L. Frasson, and F. Rodriguez Y Baena, "Closed-loop planar motion control of a steerable probe with a programmable bevel inspired by nature," *IEEE Transactions on Robotics*, vol. 27, no. 5, pp. 970-983, 2011.

- [27] S. Young and F. Rodriguez, "Trajectory following for a flexible probe with state / input constraints : An approach based on model predictive control," *Robotics and Autonomous Systems*, vol. 60, no. 4, pp. 509–521, 2012.
- [28] S. Bano, S. Y. Ko, F. Rodriguez, and F. Rodriguez Y Baena, "Smooth path planning for a biologically-inspired neurosurgical probe," *Proceedings of the Annual International Conference of the IEEE Engineering in Medicine and Biology Society, EMBS*, pp. 920–923, 2012.
- [29] S. P. Dimaio and S. E. Salcudean, "Needle Steering and Motion Planning in Soft Tissues," pp. 965–974, 2005.
- [30] D. Glozman, M. Shoham, D. Glozman, and M. Shoham, "Flexible needle steering for percutaneous therapies Flexible needle steering for percutaneous therapies," vol. 9088, no. December, 2006.
- [31] D. Glozman, M. Shoham, and A. Member, "Image-Guided Robotic Flexible Needle Steering," vol. 23, no. 3, pp. 459–467, 2007.
- [32] C. Medical, "COOK medical catheters."
- [33] A. Ali, D. H. Plettenburg, and P. Breedveld, "Steerable Catheters in Cardiology : Classifying Steerability and Assessing Future Challenges," vol. 63, no. 4, pp. 679–693, 2016.
- [34] A. Loeve, "Shaft-Guidance for Flexible Endoscopes," 2012.
- [35] Y. Chen, J. Liang, and I. W. Hunter, "Modular continuum robotic endoscope design and path planning," *2014 IEEE International Conference on Robotics and Automation (ICRA)*, pp. 5393–5400, 2014.
- [36] S. Tappe, J. Kotlarski, T. Ortmaier, M. Dörbaum, A. Mertens, and B. Ponick, "The Kinematic Synthesis of a Spatial, Hyper-Redundant System based on Binary Electromagnetic Actuators,"
- [37] A. Degani, H. Choset, A. Wolf, and M. a. Zenati, "Highly articulated robotic probe for minimally invasive surgery," *Proceedings - IEEE International Conference on Robotics and Automation*, vol. 2006, no. May, pp. 4167–4172, 2006.
- [38] T. Ota, A. Degani, D. Schwartzman, B. Zubiate, J. McGarvey, H. Choset, and M. A. Zenati, "A Highly Articulated Robotic Surgical System for," pp. 3–6, 2009.
- [39] S. Tully, G. Kantor, M. a. Zenati, and H. Choset, "Shape estimation for image-guided surgery with a highly articulated snake robot," *IEEE International Conference on Intelligent Robots and Systems*, pp. 1353–1358, 2011.
- [40] B. Kang, R. Kojcev, and E. Sinibaldi, "The First Interlaced Continuum Robot , Devised to Intrinsically Follow the Leader," pp. 1–16, 2016.
- [41] OC Robotics, "OC Robotics X125 series II."
- [42] O. Larson and C. Davidson, "Flexible arm, particularly a robot arm," 1985.
- [43] D. Palmer, S. Cobos-Guzman, and D. Axinte, "Real-time method for tip following navigation of continuum snake arm robots," *Robotics and Autonomous Systems*, vol. 62, no. 10, pp. 1478–1485, 2014.
- [44] R. J. Webster, A. M. Okamura, and N. J. Cowan, "Toward active cannulas: Miniature snake-like surgical robots," *IEEE International Conference on Intelligent Robots and Systems*, pp. 2857–2863, 2006.
- [45] H. Su, D. C. Cardona, W. Shang, A. Camilo, G. A. Cole, D. C. Rucker, R. J. Webster, and G. S. Fischer, "A MRI-Guided Concentric Tube Continuum Robot with Piezoelectric Actuation: A Feasibility Study," 2012.
- [46] C. Bergeles and P. E. Dupont, "Planning stable paths for concentric tube robots," *IEEE International Conference on Intelligent Robots and Systems*, pp. 3077–3082, 2013.
- [47] R. Xu, A. Asadian, A. S. Naidu, and R. V. Patel, "Position Control of Concentric-Tube Continuum Robots using a Modified Jacobian-Based Approach," 2013.
- [48] L. G. Torres, C. Baykal, and R. Alterovitz, "Interactive-rate Motion Planning for Concentric Tube Robots.," *IEEE International Conference on Robotics and Automation : ICRA : [proceedings] IEEE International Conference on Robotics and Automation*, vol. 2014, pp. 1915–1921, 2014.
- [49] J. Burgner, P. J. Swaney, T. L. Bruns, M. S. Clark, D. C. Rucker, E. C. Burdette, and R. J. Webster, "An Autoclavable Steerable Cannula Manual Deployment Device: Design and Accuracy Analysis," *Journal of Medical Devices*, vol. 6, no. 4, p. 41007, 2012.
- [50] H. B. Gilbert and R. J. Webster, "Can concentric tube robots follow the leader?," *Proceedings - IEEE International Conference on Robotics and Automation*, pp. 4881–4887, 2013.
- [51] H. Gilbert, J. Neimat, and R. Webster, "Concentric Tube Robots as Steerable Needles: Achieving Follow-the-Leader Deployment," *IEEE Transactions on Robotics*, vol. PP, no. 99, pp. 1–13, 2015.
- [52] R. J. Webster, J. M. Romano, S. Member, and N. J. Cowan, "Mechanics of Precurved-Tube Continuum Robots," vol. 25, no. 1, pp. 67–78, 2009.
- [53] M. Mahvash and M. Zenati, "Toward a hybrid snake robot for single-port surgery," *Proceedings of the Annual International Conference of the IEEE Engineering in Medicine and Biology Society, EMBS*, pp. 5372–5375, 2011.
- [54] P. J. Swaney, A. W. Mahoney, A. A. Ramirez, E. Lamers, B. I. Hartley, R. H. Feins, R. Alterovitz, and R. J. W. III, "Tendons, Concentric Tubes, and a Bevel Tip: Three Steerable Robots in One Transoral Lung Access System," pp. 5378–5383, 2015.

APPENDIX C
WORK DRAWINGS

Detailed work drawings of the PoC demonstrator prototype are included in this appendix. The drawings are scaled down in this appendix from A3 to A4 due to practical reasons. Upon request the drawings and CAD files of all parts and the assembly can be provided. An exploded view is illustrated in Fig. 34.

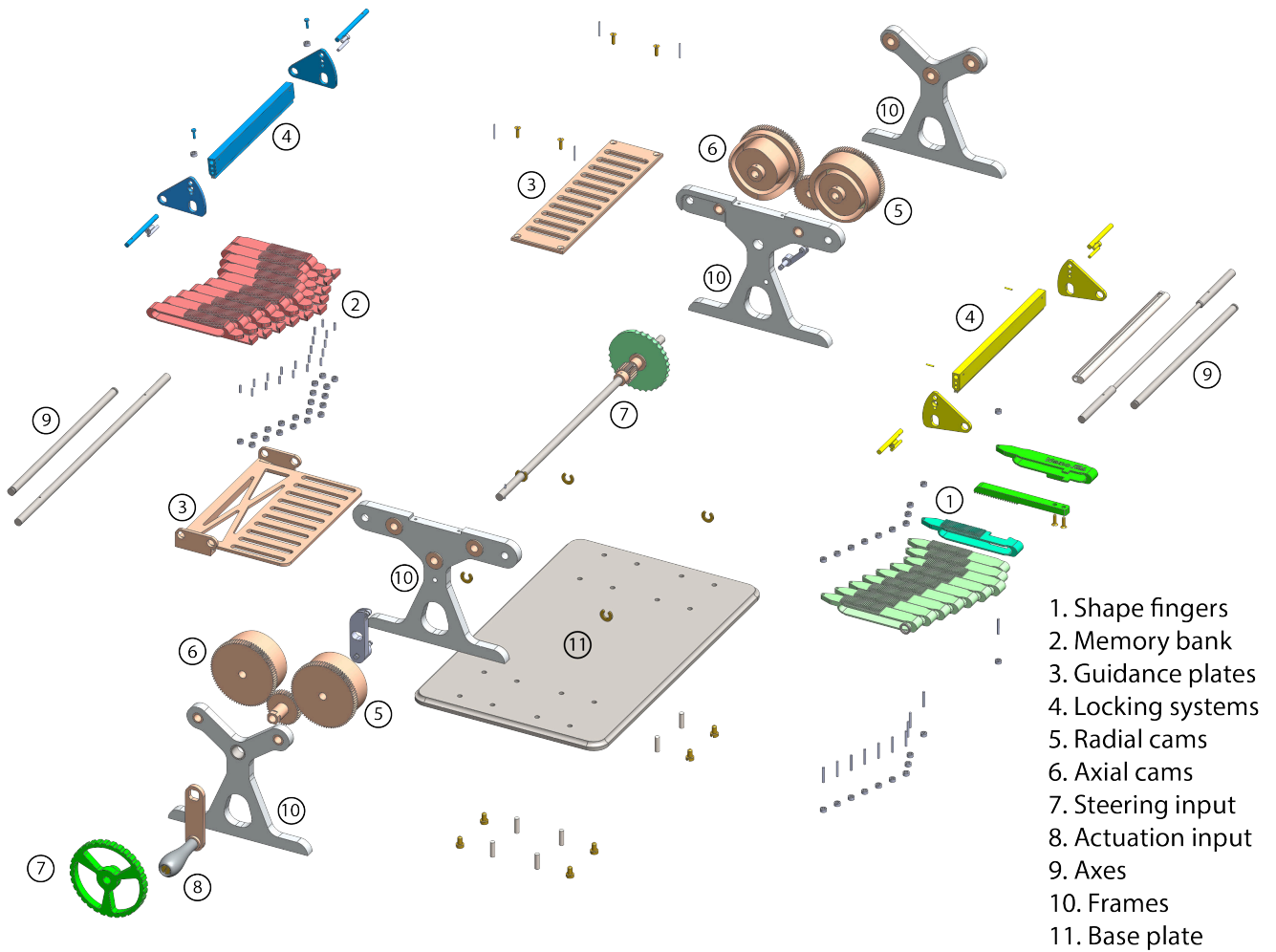
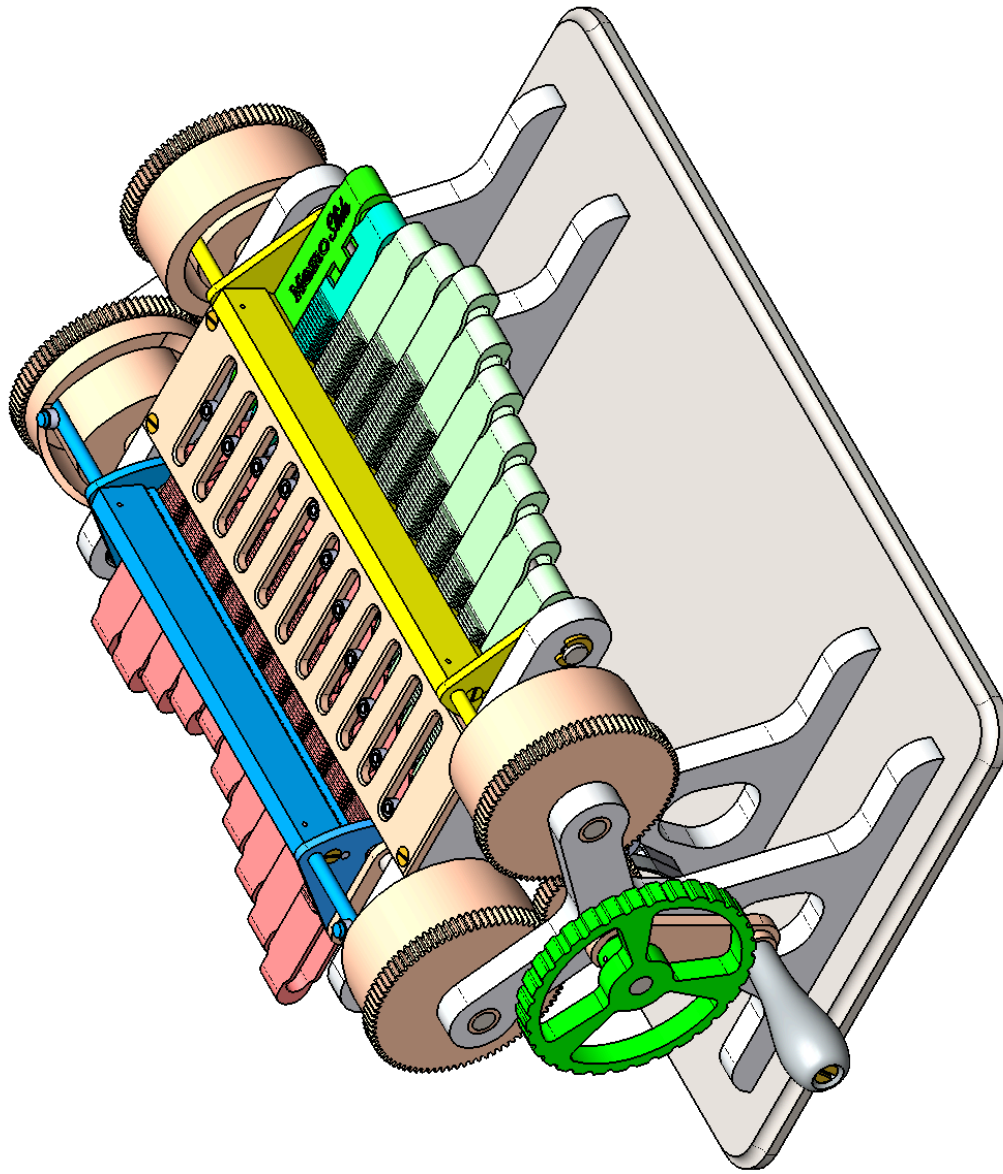


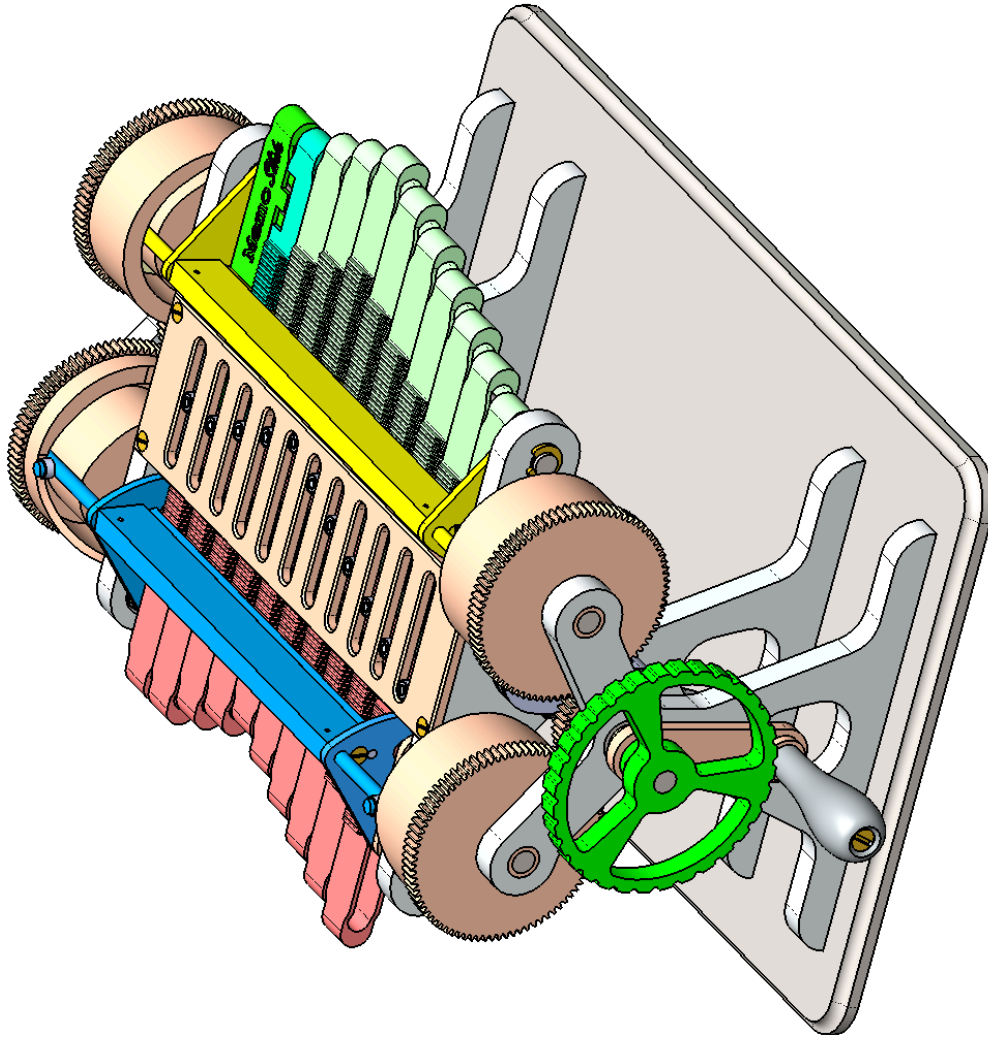
Fig. 34: The 'MemoSlide', exploded view.
An exploded view of the PoC demonstrator gives an impression of the number of parts required.

PART NUMBER	QTY.
1 Base plate	1
2 Frame #1	1
3 Frame #2	1
4 Frame #3	1
5 Frame #4	1
6 Rod 5x132 mm	2
7 Cam Axis - Memory	1
8 Cam Axis - Shape	1
9 Crank	1
10 Steering	1
11 Locking bar - Memory	1
12 Locking bar - Shape	1
13 Memory	10
14 Shape - Active	1
15 Shape - Limiter	1
16 Shape - Passive	9
17 Guide Plate - Top	1
18 Guide Plate - Bottom	1
19 Ring 5x1 mm	2
20 Pin 3x10 mm	8
M3x5 Flat	8
M2x6 Flat	4
C-ring 4 mm	6



UNLESS OTHERWISE SPECIFIED: DIMENSIONS ARE IN MILLIMETERS		FINISH:		DEBUR AND BREAK SHARP EDGES		DO NOT SCALE DRAWING		REVISION	
SURFACE FINISH:		TOLERANCES:		NAME		SIGNATURE		DATE	
LINEAR:		ANGULAR:		DRAWN		CHK'D		APP'D	
				MFG		Q.A.		MATERIAL:	
								WEIGHT:	
								SCALE:1:1	
								SHEET 1 OF 73	
<h1>Overview</h1>								DWG NO. A3	
<h1>MemoSlide</h1>									

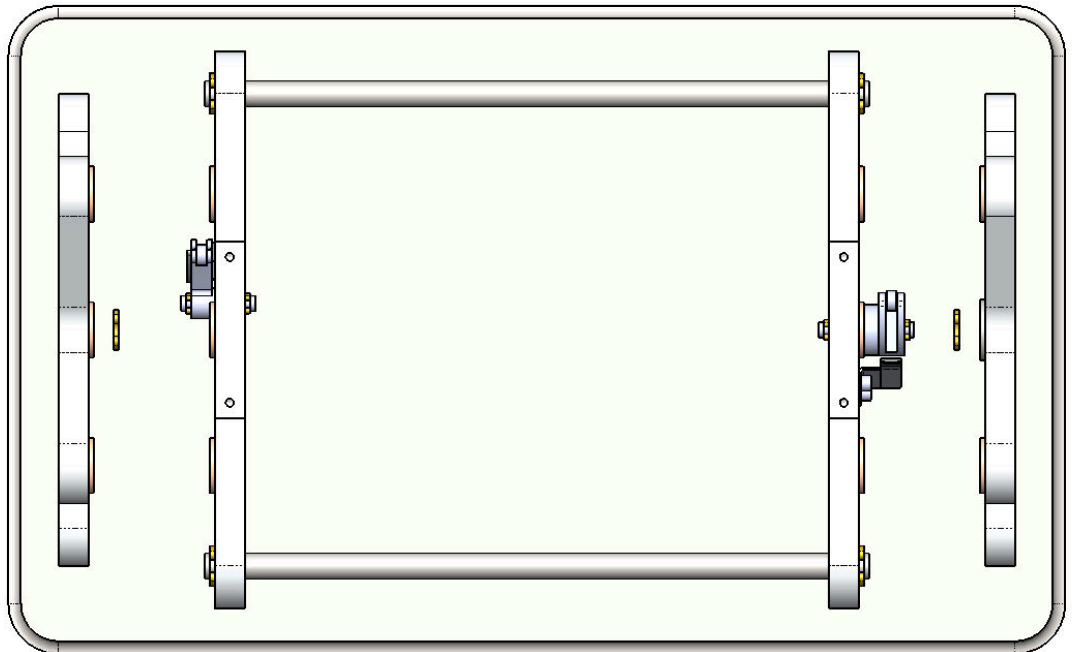
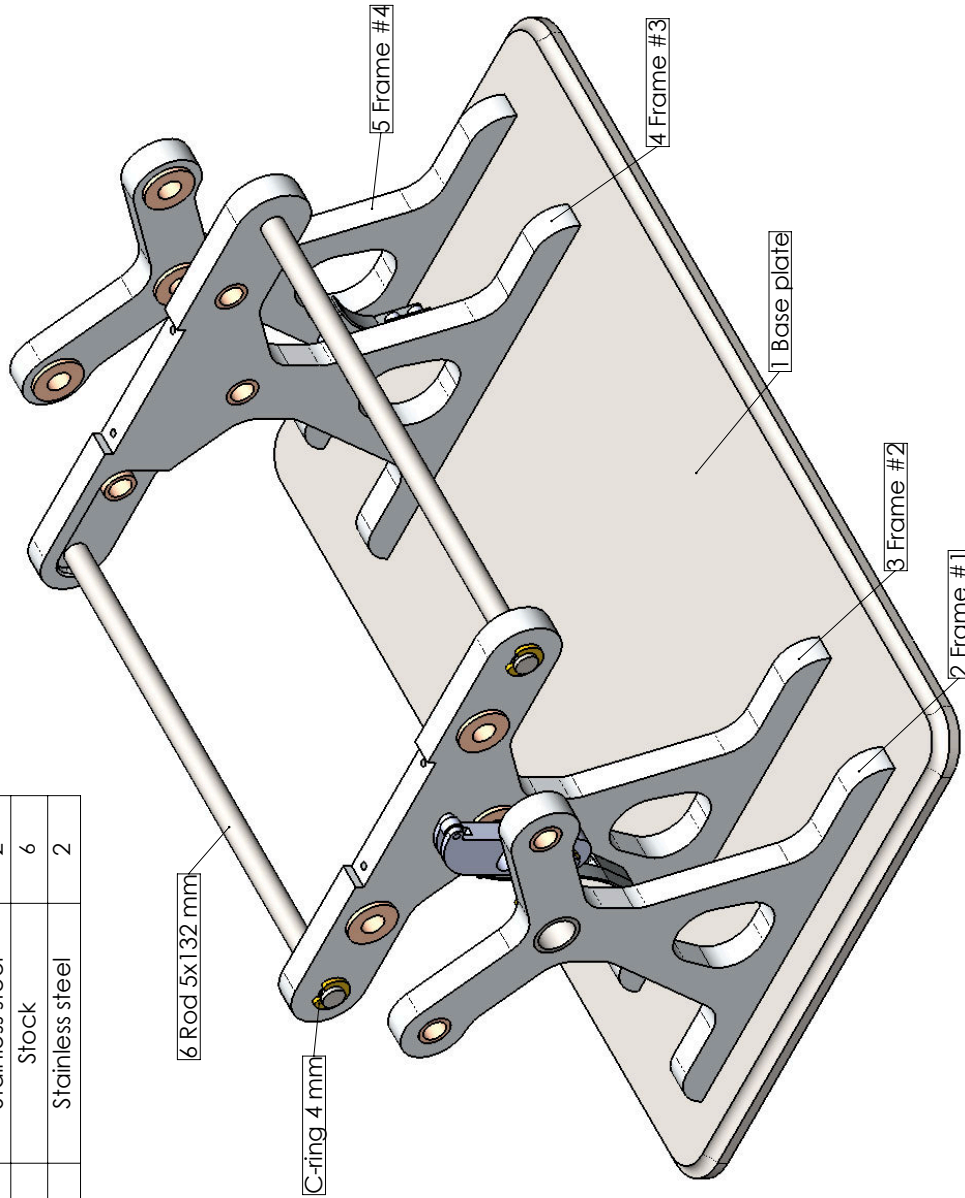
PART NUMBER	MATERIAL	QTY.
M2x3 Hex		4
6 Rod 5x132 mm		2
M3x5 Flat		9
M2x6 Flat		10
11.5 Cam Follower - Memory	Stainless steel	2
11.6 Cam Follower - Bearing Pin	Stainless steel	2
12.1 Teeth Bar - Shape	Aluminium	1
12.2 Cam Follower - Shape	Stainless steel	2
13.1 Finger - Memory	Aluminium	10
13.2 Bearing Pin - Memory	Stainless steel	20
14.1 Finger - Shape - Active	Aluminium	1
14.2 Bearing Pin - Shape	Stainless steel	11
14.3 Steering Rack	Aluminium	1
15.1 Finger - Shape - Limiter	Aluminium	1
16.1 Finger - Shape - Passive	Aluminium	9
17 Guide Plate - Top	Bronze	1
18 Guide Plate - Bottom	Bronze	1
19 Ring 5x1 mm	Stainless steel	2
20 Pin 3x10 mm	Stainless steel	8
C-ring 4 mm	Stock	6



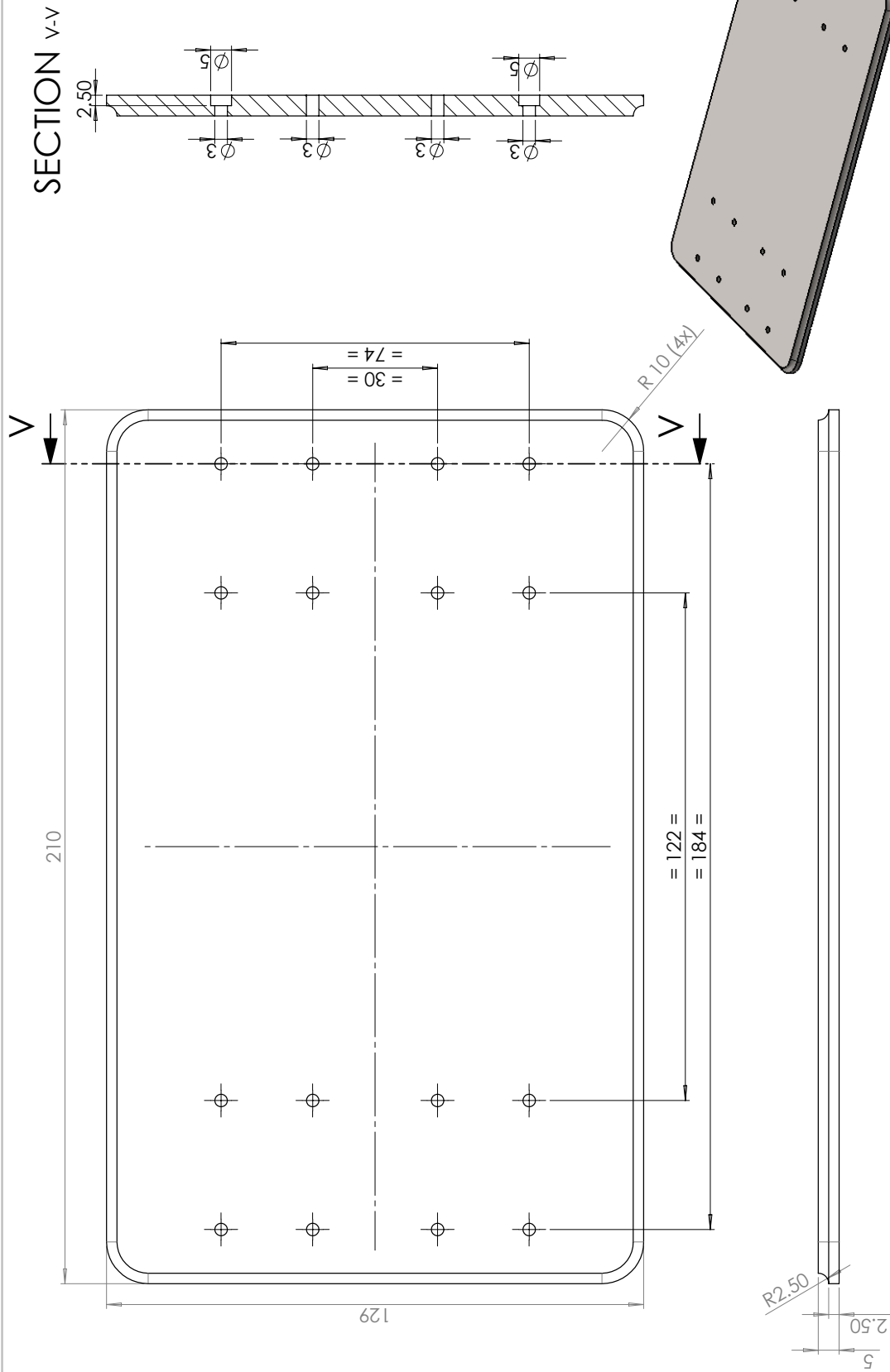
UNLESS OTHERWISE SPECIFIED: DIMENSIONS ARE IN MILLIMETERS		FINISH:		DO NOT SCALE DRAWING		REVISION	
SURFACE FINISH:		TOLERANCES:		DEBUR AND BREAK SHARP EDGES			
DIMENSIONS:		ANGULAR:					
DRAWN	NAME	SIGNATURE	DATE	TITLE			
CHK'D				Material overview 2			
APP'VD							
MEG							
Q.A.							
MATERIAL:		WEIGHT:		DWG NO.		SHEET 3 OF 73	
				MemoSlide		A3	

PART NUMBER	MATERIAL	QTY.
1 Base plate	Stainless steel	1
6 Rod 5x132 mm	Stainless steel	2
7.1 Cam Axis	Stainless steel	2
C-ring	Stock	6
19 Ring 5x1 mm	Stainless steel	2

ITEM NO.	PART NUMBER	QTY.
1	1 Base plate	1
2	2 Frame #1	1
3	3 Frame #2	1
4	4 Frame #3	1
5	5 Frame #4	1
6	6 Rod 5x132 mm	2
7	C-ring 4 mm	6

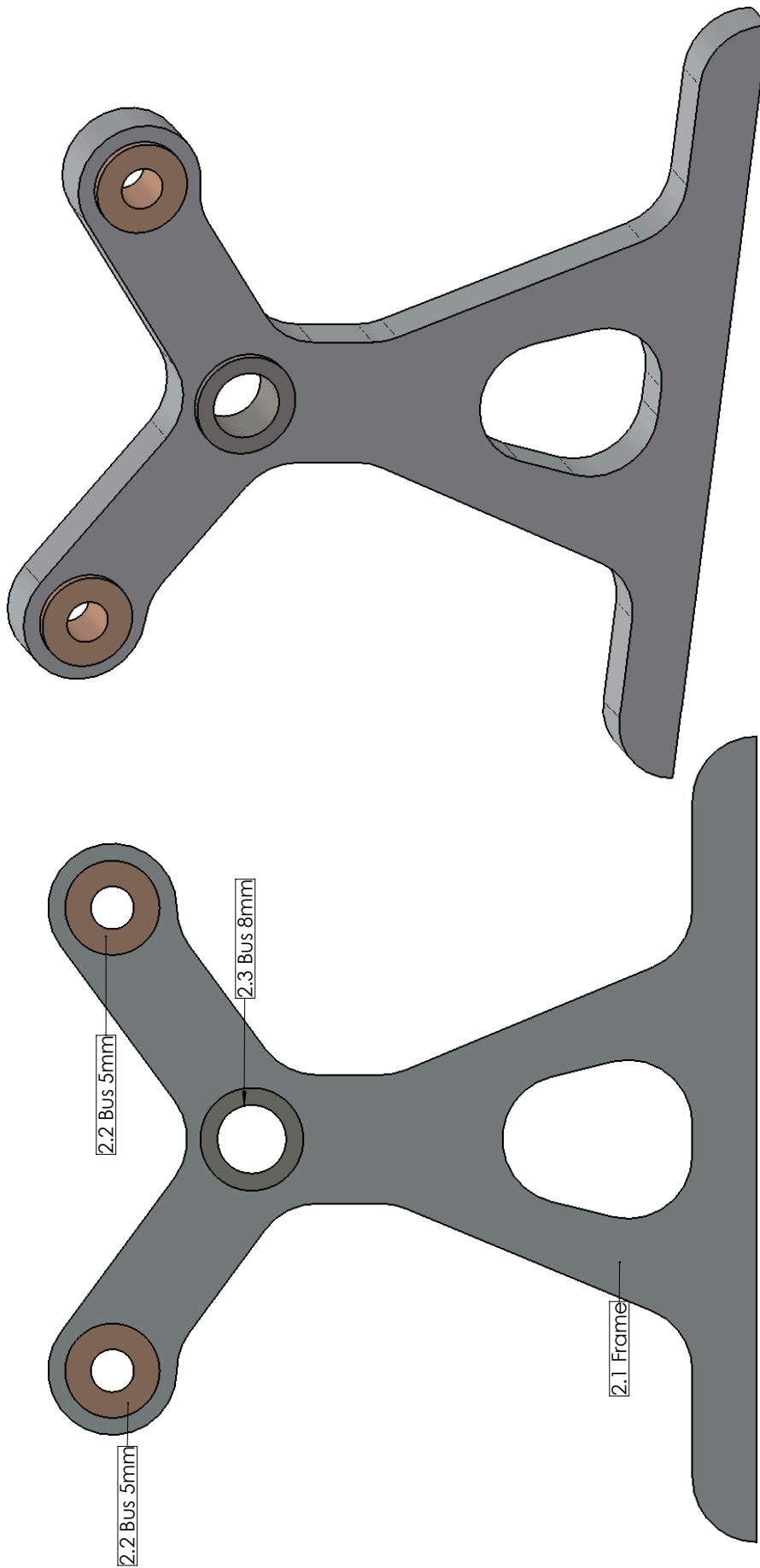


UNLESS OTHERWISE SPECIFIED: DIMENSIONS ARE IN MILLIMETERS		FINISH:	
SURFACE FINISH:		RADIUS:	
TOLERANCES:		ANGULAR:	
NAME	SIGNATURE	DATE	
DRAWN			
CHK'D			
APP'VD			
MFG			
Q.A.			
DEBUR AND BREAK SHARP EDGES		DO NOT SCALE DRAWING	REVISION
TITLE: AS. MK-X, Base/frames/rods		DWG NO. A3	
MATERIAL:		SCALE:1:1	SHEET 4 OF 73
WEIGHT:			



UNLESS OTHERWISE SPECIFIED: DIMENSIONS ARE IN MILLIMETERS		FINISH:		DEBUR AND BREAK SHARP EDGES		DO NOT SCALE DRAWING		REVISION	
SURFACE FINISH:		NAME		SIGNATURE		DATE		1	
TOLERANCES:		DRAWN							
ANGULAR:		CHK'D							
		APP'VD							
		MEG							
		Q.A							
TITLE:		MATERIAL:		DWG NO.		SCALE:1:1		SHEET 5 OF 73	
Base plate		RVS, Hoogglans top							
MemoSlide									
A3									

ITEM NO.	PART NUMBER	MATERIAL	QTY.
1	2.1 Frame	Aluminium	1
2	2.2 Bus 5mm	Bronze	2
3	2.3 Bus 8mm	Stainless steel	1

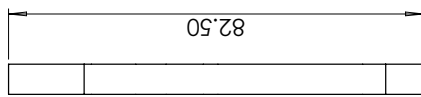
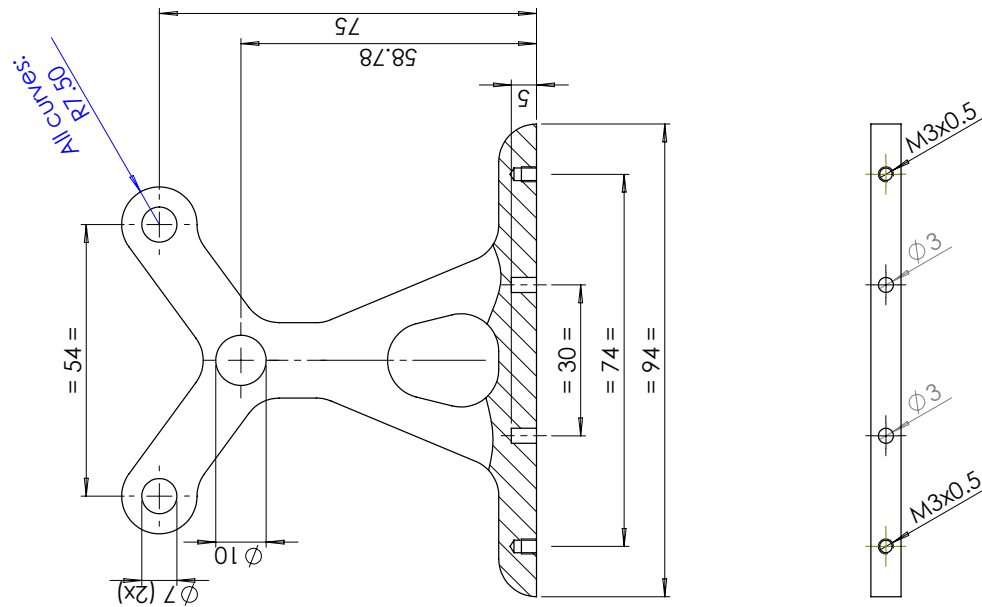


Back view

UNLESS OTHERWISE SPECIFIED: DIMENSIONS ARE IN MILLIMETERS		DO NOT SCALE DRAWING		REVISION	
SURFACE FINISH:		2			
TOLERANCES:					
ANGULAR:					
DRAWN	NAME	SIGNATURE	DATE	TITLE	
CHKD				Frame #1	
APPVD				MemoSlide	
MFG				A3	
Q.A.				DWG NO.	
				SCALE:2:1	
				WEIGHT:	
				SHEET 6 OF 73	

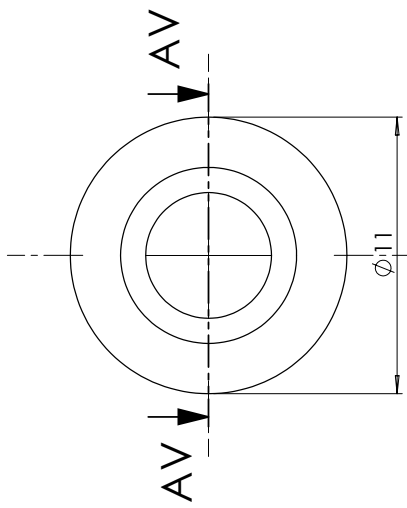
DEBUR AND BREAK SHARP EDGES

MATERIAL:

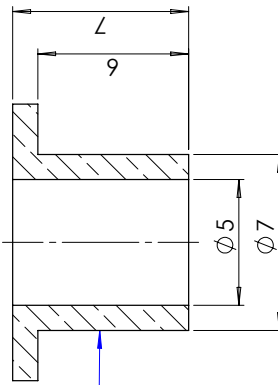


Sketch file is available digitally in part: "2.1 Frame"

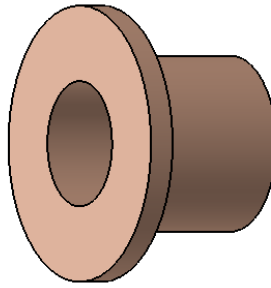
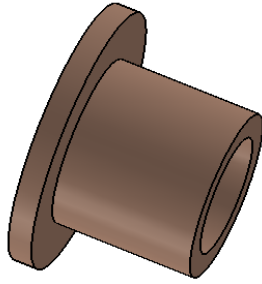
UNLESS OTHERWISE SPECIFIED: DIMENSIONS ARE IN MILLIMETERS		FINISH:	DEBUR AND BREAK SHARP EDGES	DO NOT SCALE DRAWING	REVISION
SURFACE FINISH:				2.1	
TOLERANCES:					
ANGULAR:					
DRAWN	NAME	SIGNATURE	DATE	TITLE	
CHK'D				Frame	
APP'VD				DWG NO.	MemoSlide
MEG				MATERIAL:	Aluminium
Q.A.				WEIGHT:	A3
				SCALE:1:1	SHEET 7 OF 73



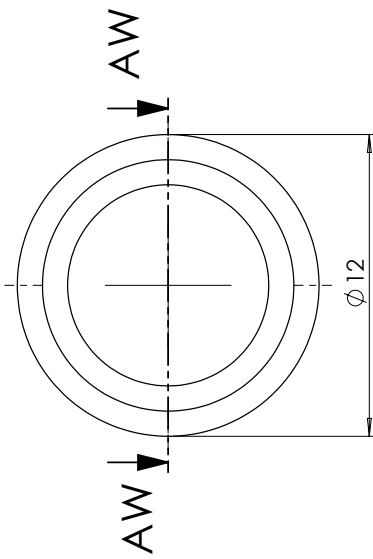
SECTION AV-AV



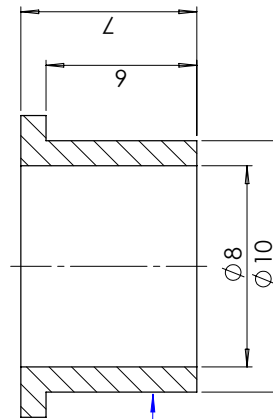
Press fit in 2.1 Frame



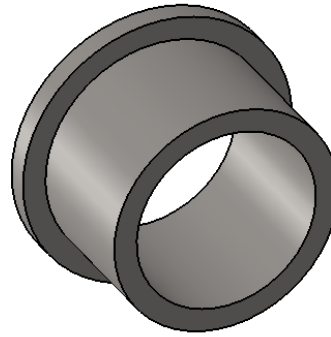
QTY.		11	
UNLESS OTHERWISE SPECIFIED: DIMENSIONS ARE IN MILLIMETERS SURFACE FINISH: TOLERANCES: ANGULAR:		DO NOT SCALE DRAWING	REVISION
FINISH:		2.2	
DEBUR AND BREAK SHARP EDGES		TITLE	
TITLE		Bus 5 mm	
DRAWN		DWG NO.	
CHKD		MemoSlide	
APPRD		A3	
MFG		MATERIAL:	
Q.A		Bronze	
NAME		WEIGHT:	
SIGNATURE		SCALE: 1	
DATE		SHEET 8 OF 73	



SECTION AW-AW

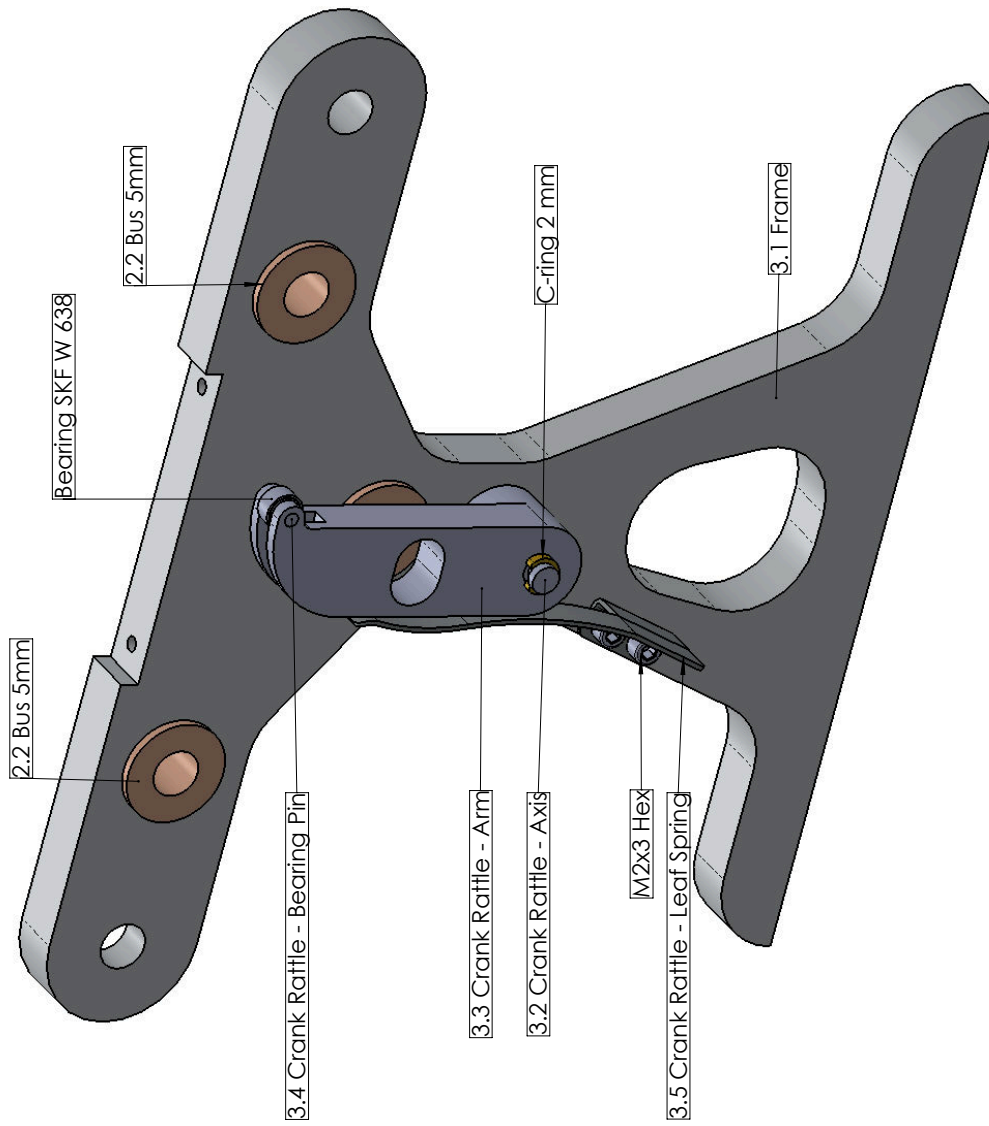


Press fit in 2.1 Frame

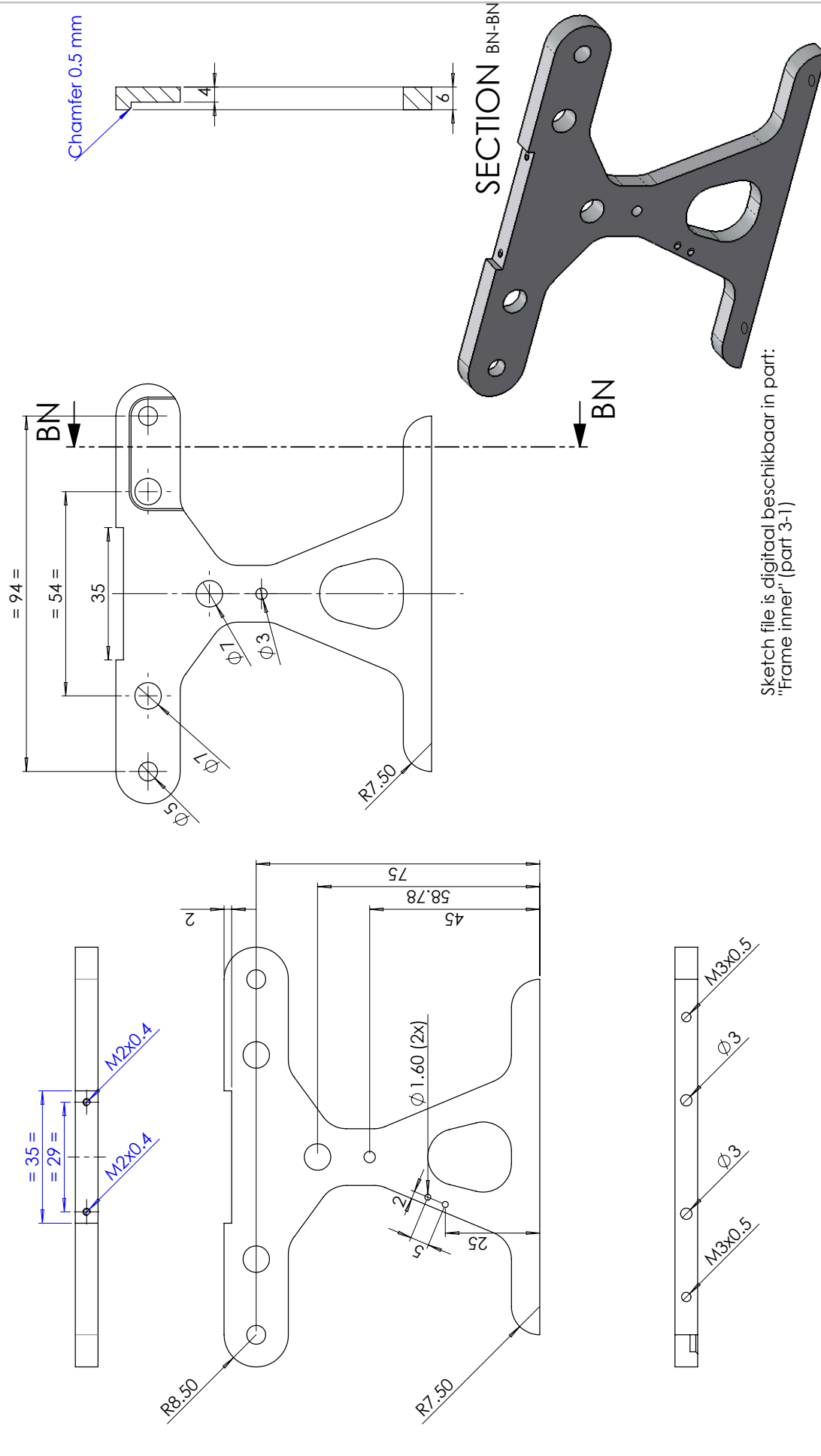


UNLESS OTHERWISE SPECIFIED: DIMENSIONS ARE IN MILLIMETERS		FINISH:		DEBUR AND BREAK SHARP EDGES		DO NOT SCALE DRAWING		REVISION	
SURFACE FINISH:		NAME		SIGNATURE		DATE		TITLE	
TOLERANCES:		DRAWN		CHK'D		APPR'D		MFG	
ANGULAR:		MFG		Q.A.		MATERIAL:		DWGS NO.	
						Stainless steel		MemoSlide	
								A3	
								SCALE: 1	
								SHEET 9 OF 73	
								2.3	
								Bus 8 mm	
								QTY. 1	

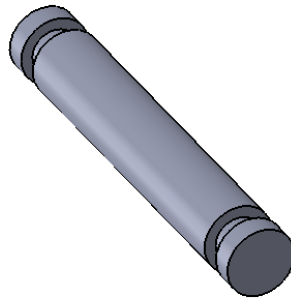
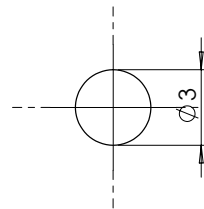
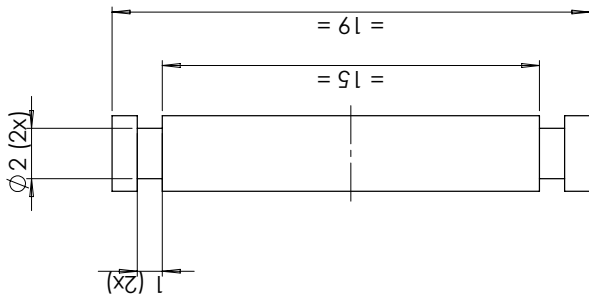
PART NUMBER	MATERIAL	QTY.
3.1 Frame	Aluminium	1
2.2 Bus 5mm	Bronze	3
3.2 Crank Rattle - Axis	Stainless steel	1
3.3 Crank Rattle - Arm	Aluminium	1
C-ring 2 mm	Stock	2
3.4 Crank Rattle - Bearing Pin	Stainless steel	1
Bearing SKF W 638	Stock	1
3.5 Crank Rattle - Leaf Spring	Spring steel	1
M2x3 Hex	Stock	2



UNLESS OTHERWISE SPECIFIED: DIMENSIONS ARE IN MILLIMETERS		FINISH:		DEBUR AND BREAK SHARP EDGES		DO NOT SCALE DRAWING		REVISION	
SURFACE FINISH:		TOLERANCES:						3	
DIMENSIONS:		ANGULAR:						TITLE	
								Frame #2	
								DWG NO.	
								MemoSlide	
								A3	
								SCALE:2:1	
								SHEET 10 OF 73	
								WEIGHT:	
								MATERIAL:	
								NAME	
								SIGNATURE	
								DATE	
								DRAWN	
								CHK'D	
								APP'VD	
								MFG	
								Q.A	

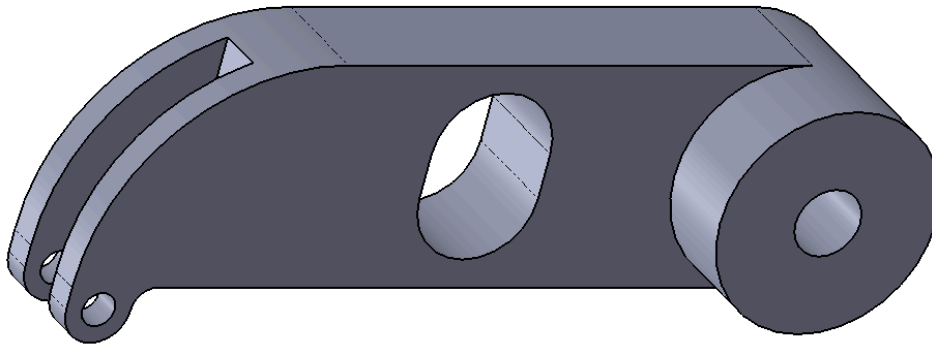
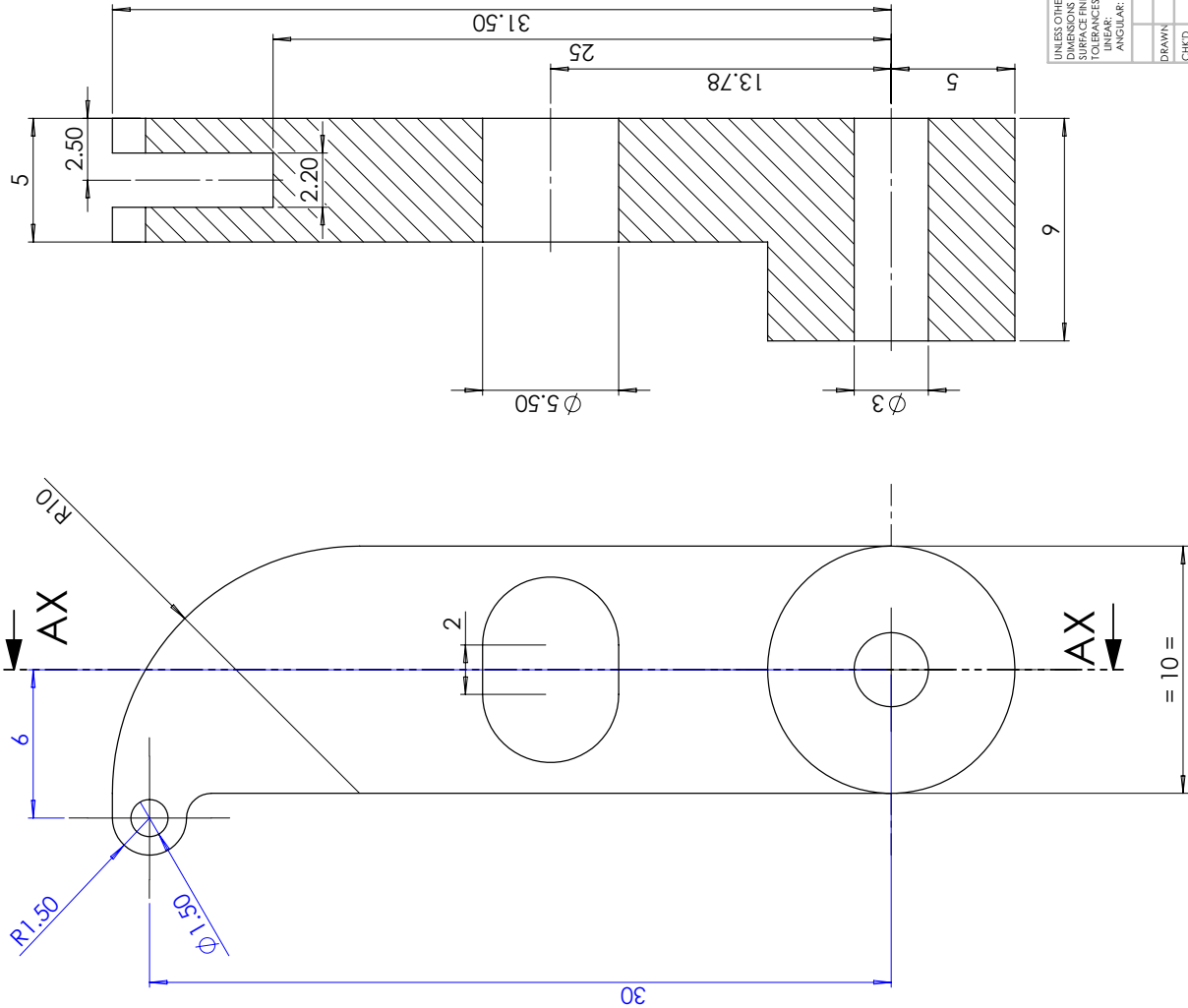


UNLESS OTHERWISE SPECIFIED: DIMENSIONS ARE IN MILLIMETERS		FINISH:		DEBUR AND BREAK SHARP EDGES		DO NOT SCALE DRAWING		REVISION	
SURFACE FINISH:		TOLERANCES:				3-1			
FRACTIONAL:		ANGULAR:				TITLE:		Frame inner	
						NAME:		DWG NO. A3	
						SIGNATURE:		MemoSlide	
						DATE:		SCALE: 1:1	
						MATERIAL:		SHEET 11 OF 73	
						WEIGHT:			

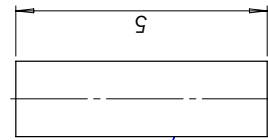
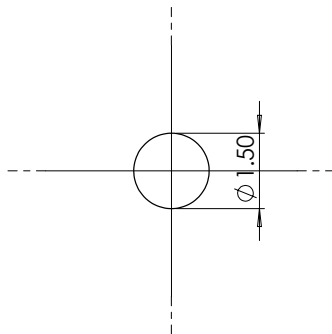


UNLESS OTHERWISE SPECIFIED: DIMENSIONS ARE IN MILLIMETERS SURFACE FINISH: TOLERANCES: ANGULAR:		FINISH:		DEBUR AND BREAK SHARP EDGES		DO NOT SCALE DRAWING	REVISION
						3.2	
DRAWN		NAME	SIGNATURE	DATE	TITLE		
CHKD					Crank Rattle - Axis		
APPVD					MemoSlide		
MFG					DWG NO.	A3	
Q.A					MATERIAL:	Stainless steel	
					WEIGHT:	SHEET 12 OF 73	

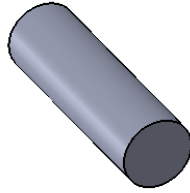
SECTION AX-AX



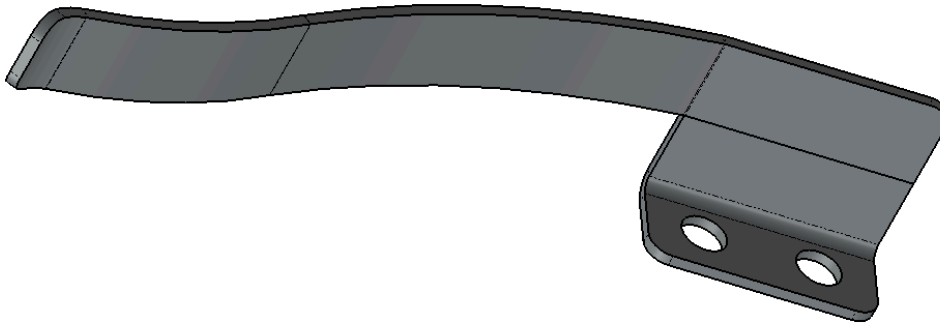
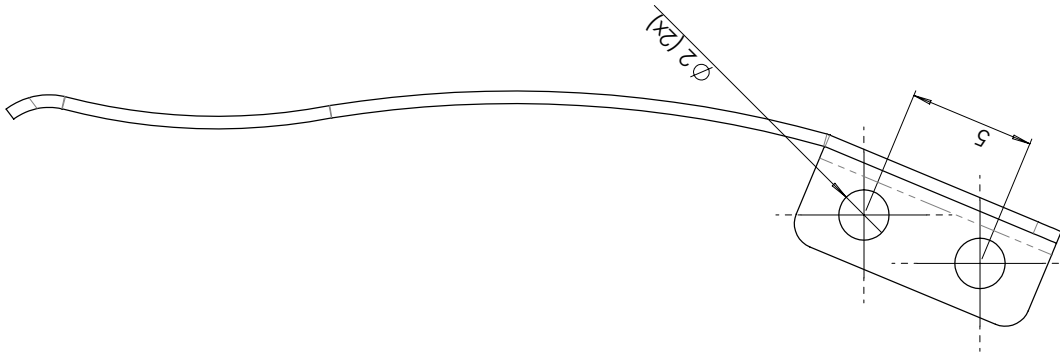
UNLESS OTHERWISE SPECIFIED: DIMENSIONS ARE IN MILLIMETERS		FINISH:		DEBUR AND BREAK SHARP EDGES		DO NOT SCALE DRAWING	REVISION
SURFACE FINISH:		NAME		SIGNATURE		3.3	
TOLERANCES:		DATE		DATE		TITLE	
ANGULAR:		DRAWN		SIGNATURE		Crank Rattle - Arm	
		CHK'D		DATE		DWG NO.	
		APP'VD		DATE		MemoSlide	
		MFG		DATE		MATERIAL:	
		Q.A.		DATE		Aluminium	
				DATE		WEIGHT:	
				DATE		SCALE: 1:1	
				DATE		SHEET 13 OF 73	



Press fit with 3.3 Crank Rattle - Arm & Bearing SKF W 638



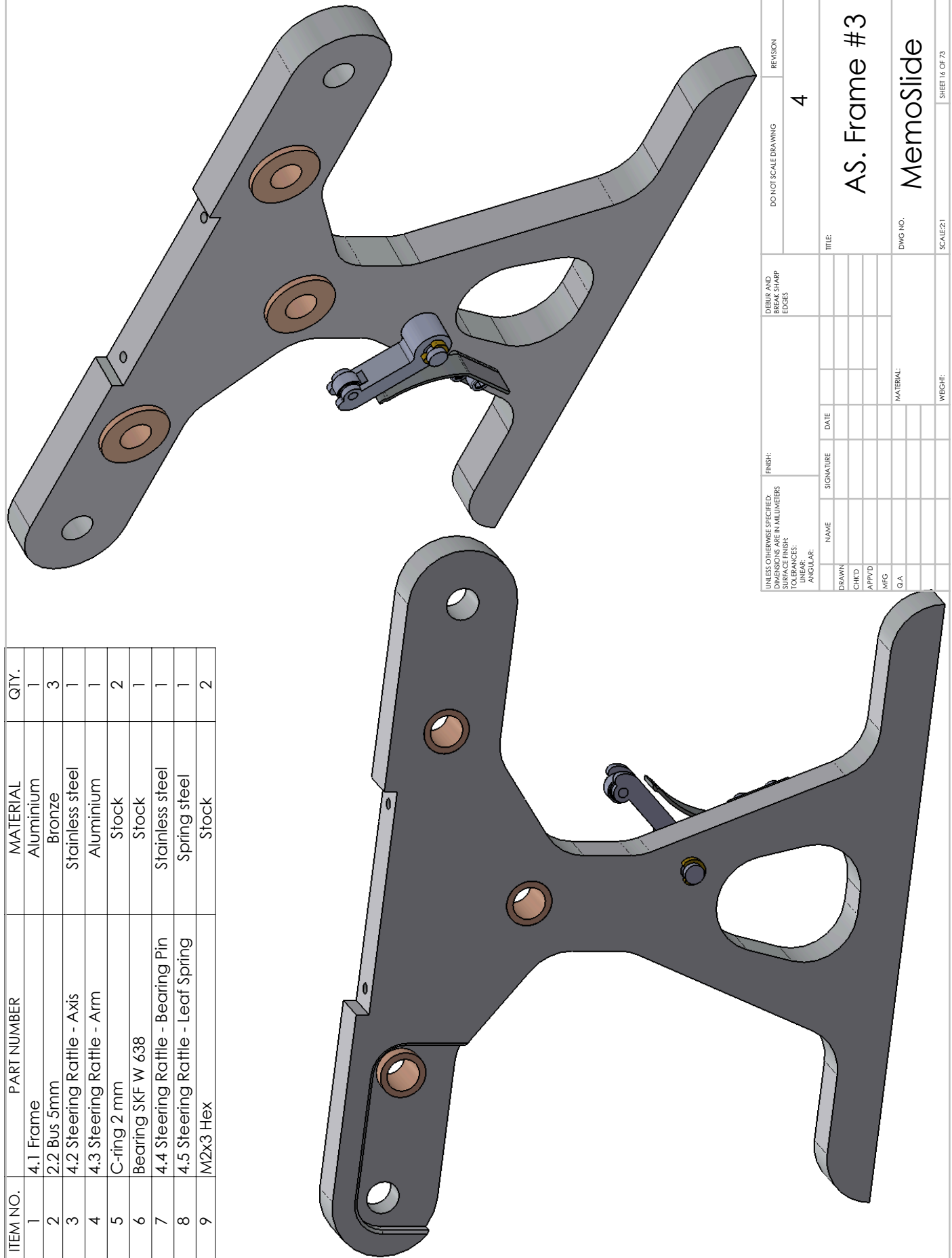
UNLESS OTHERWISE SPECIFIED: DIMENSIONS ARE IN MILLIMETERS		FINISH:		DEBUR AND BREAK SHARP EDGES		DO NOT SCALE DRAWING		REVISION	
SURFACE FINISH:						3.4			
TOLERANCES:									
ANGULAR:									
DRAWN	NAME	SIGNATURE	DATE	TITLE		Bearing pin			
CHK'D				DWG NO.		MemoSlide		A3	
APP'VD				MATERIAL:		Stainless steel			
MFG				WEIGHT:					
Q.A				SCALE:1:01				SHEET 14 OF 73	



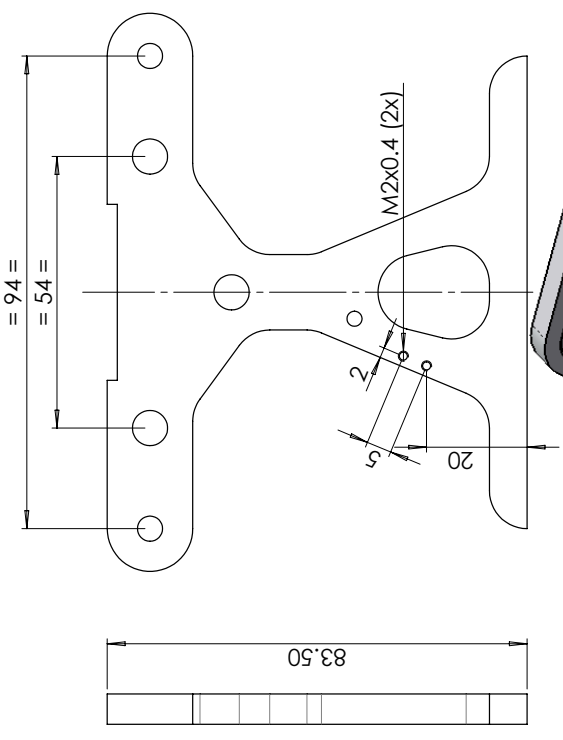
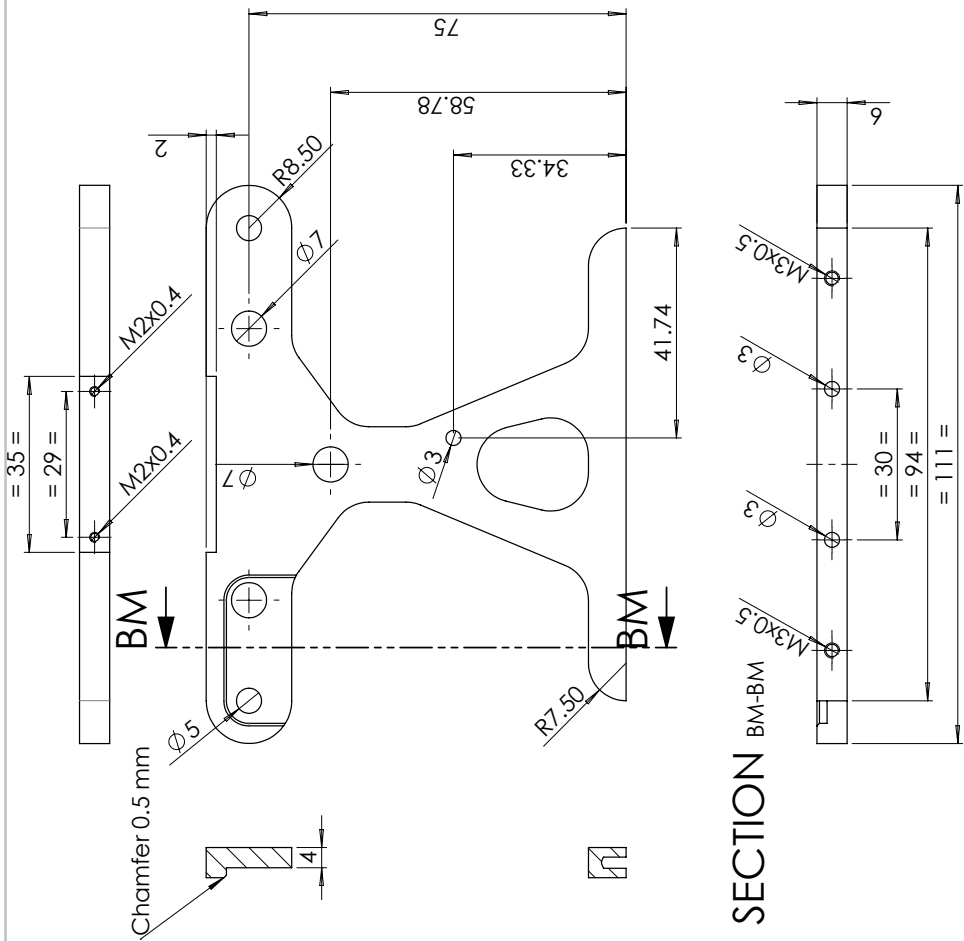
Exact spring shape is made manually by instrument maker

UNLESS OTHERWISE SPECIFIED: DIMENSIONS ARE IN MILLIMETERS		FINISH:	DEBUR AND BREAK SHARP EDGES	DO NOT SCALE DRAWING	REVISION
SURFACE FINISH: TOLERANCES: ANGULAR:				3.5	
DRAWN	NAME	SIGNATURE	DATE	TITLE	
CHK'D				Leaf spring - Crank	
APP'VD				DWG NO.	A3
MFG				MATERIAL:	Spring steel
Q.A				WEIGHT:	SCALE: 1:1
					SHEET 15 OF 73

ITEM NO.	PART NUMBER	MATERIAL	QTY.
1	4.1 Frame	Aluminium	1
2	2.2 Bus 5mm	Bronze	3
3	4.2 Steering Rattle - Axis	Stainless steel	1
4	4.3 Steering Rattle - Arm	Aluminium	1
5	C-ring 2 mm	Stock	2
6	Bearing SKF W 638	Stock	1
7	4.4 Steering Rattle - Bearing Pin	Stainless steel	1
8	4.5 Steering Rattle - Leaf Spring	Spring steel	1
9	M2x3 Hex	Stock	2

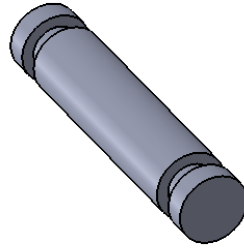
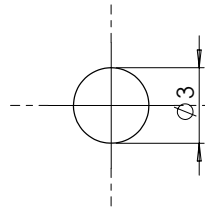
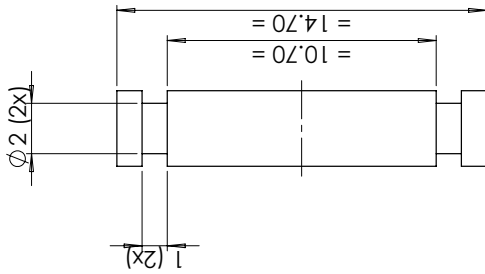


UNLESS OTHERWISE SPECIFIED: DIMENSIONS ARE IN MILLIMETERS		FINISH:		DEBUR AND BREAK SHARP EDGES		DO NOT SCALE DRAWING		REVISION	
SURFACE FINISH:		Rough				4		4	
TOLERANCES:		ANGULAR:							
DRAWN		NAME		SIGNATURE		DATE		TITLE	
CHK'D								AS. Frame #3	
APP'D								MemoSlide	
MFG								DWG NO. A3	
Q.A								SCALE:2:1 SHEET 16 OF 73	
								MATERIAL:	
								WEIGHT:	



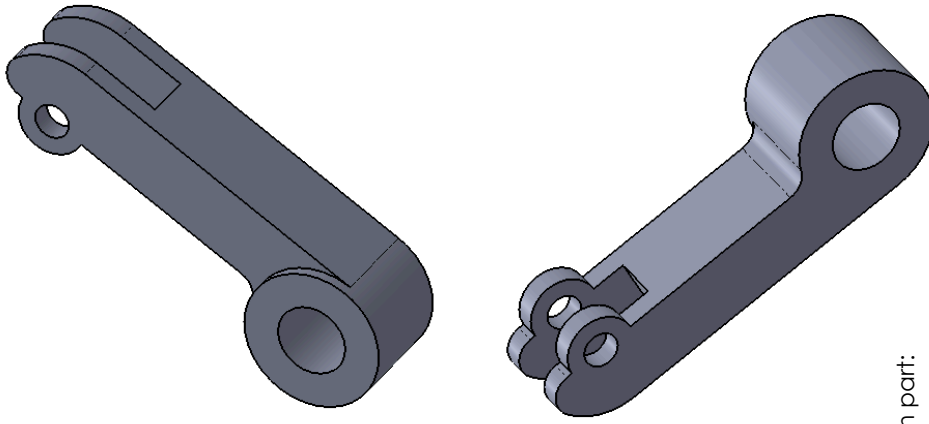
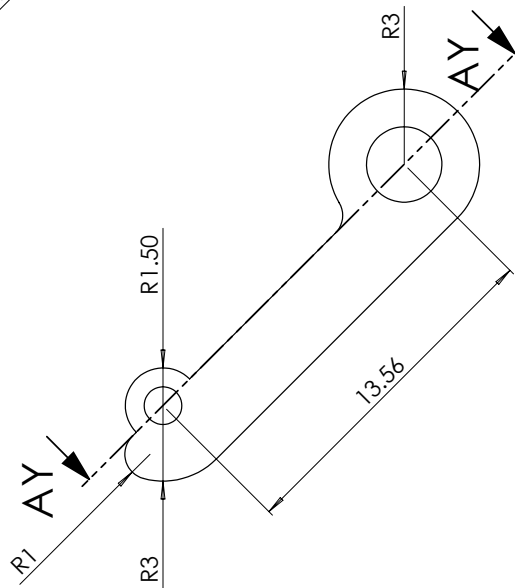
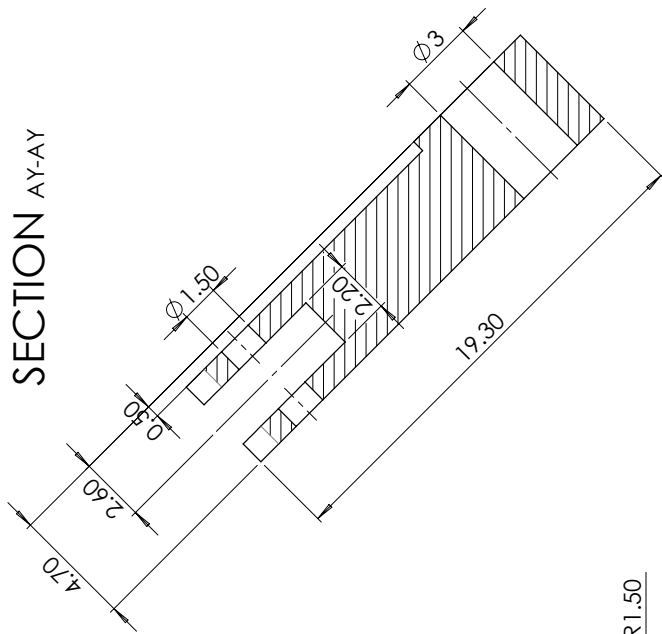
Sketch file is digitaal beschikbaar in part: "Frame inner back" (part 4-1)

UNLESS OTHERWISE SPECIFIED: DIMENSIONS ARE IN MILLIMETERS		FINISH:		DEBUR AND BREAK SHARP EDGES		DO NOT SCALE DRAWING		REVISION	
SURFACE FINISH:		TOLERANCES:						4.1	
DIMENSIONS:		ANGULAR:						TITLE	
								Frame inner back	
DRAWN		NAME		SIGNATURE		DATE		DWG NO.	
CHKD								A3	
APPVD								MemoSlide	
MEG								MATERIAL:	
Q.A								Aluminium	
								SCALE:1:1	
								WEIGHT:	
								SHEET 17 OF 73	



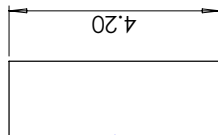
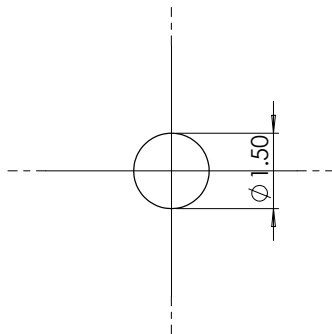
UNLESS OTHERWISE SPECIFIED: DIMENSIONS ARE IN MILLIMETERS SURFACE FINISH: TOLERANCES: ANGULAR:		FINISH:		DEBUR AND BREAK SHARP EDGES		DO NOT SCALE DRAWING	REVISION
						4.2	
						TITLE: Steering Rattle Axis	
						DWG NO. MemoSlide A3	
				MATERIAL: Stainless steel		SCALE: 1:1 SHEET 18 OF 73	
DRAWN	NAME	SIGNATURE	DATE				
CHKD							
APPVD							
MFG							
Q.A							

SECTION AY-AY

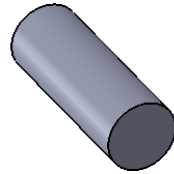


Sketch file is digital beschikbaar in part: "Steering rattle arm" (part 4-3)

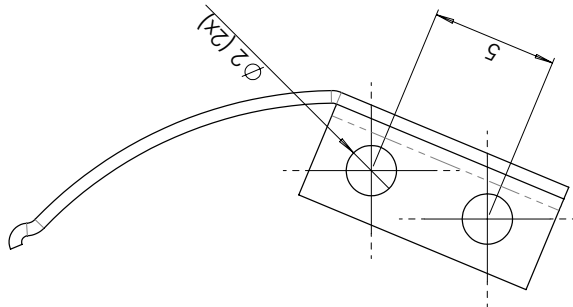
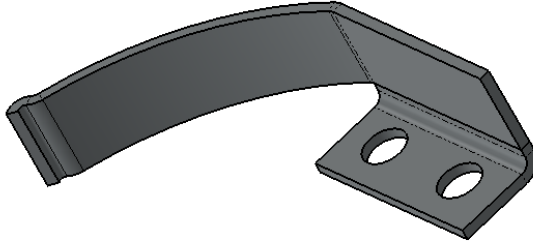
UNLESS OTHERWISE SPECIFIED: DIMENSIONS ARE IN MILLIMETERS		FINISH:		DEBUR AND BREAK SHARP EDGES		DO NOT SCALE DRAWING		REVISION	
SURFACE FINISH:		TOLERANCES:				4.3			
DIMENSIONS:		ANGULAR:							
DRAWN		NAME		SIGNATURE		DATE		TITLE	
CHK'D								Steering Rattle - Arm	
APP'VD								DWG NO. A3	
MFG								MATERIAL: Aluminium	
Q.A								WEIGHT: SCALE: 1:1	
								SHEET 19 OF 73	



Press fit with 4.3 Steering Rattle - Arm
& Bearing SKF W 638



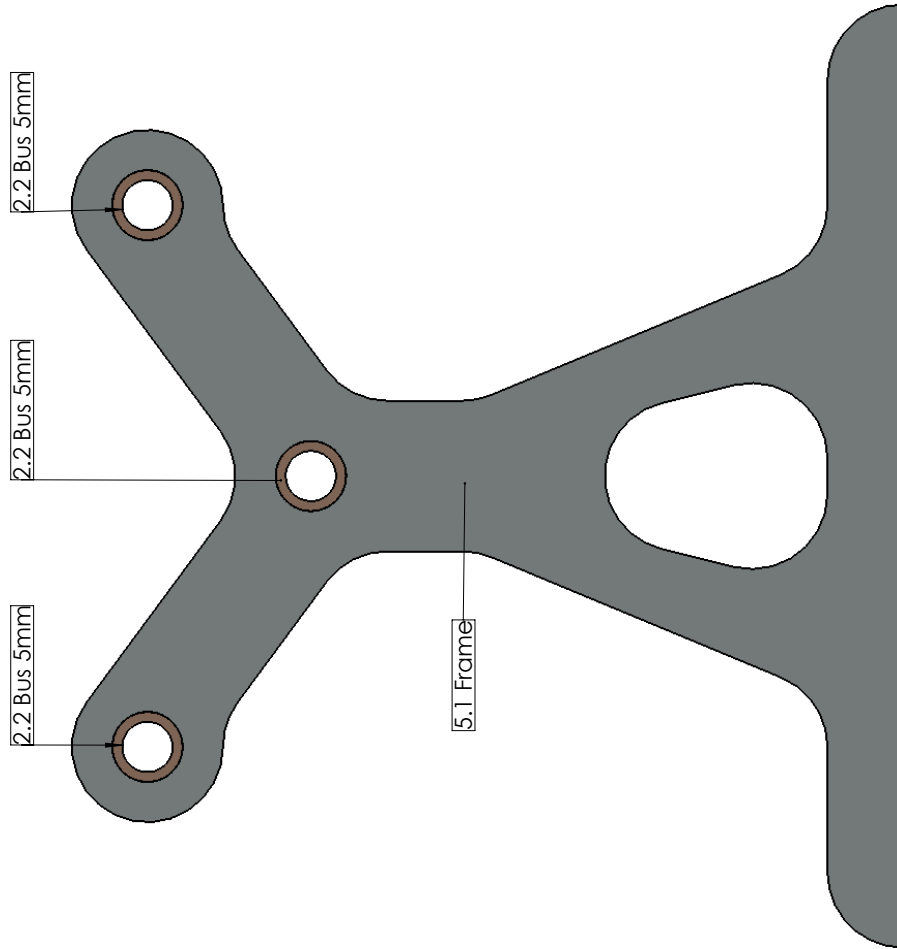
UNLESS OTHERWISE SPECIFIED: DIMENSIONS ARE IN MILLIMETERS		FINISH:	DEBUR AND BREAK SHARP EDGES		DO NOT SCALE DRAWING	REVISION
SURFACE FINISH: TOLERANCES: ANGULAR:					4.4	
NAME	SIGNATURE	DATE	TITLE			
DRAWN			Rattle bearing pin			
CHK'D			DWG NO. A3			
APP'VD			MATERIAL: Stainless steel			
MFG			SCALE: 1:01			
Q.A.			WEIGHT: SHEET 20 OF 73			



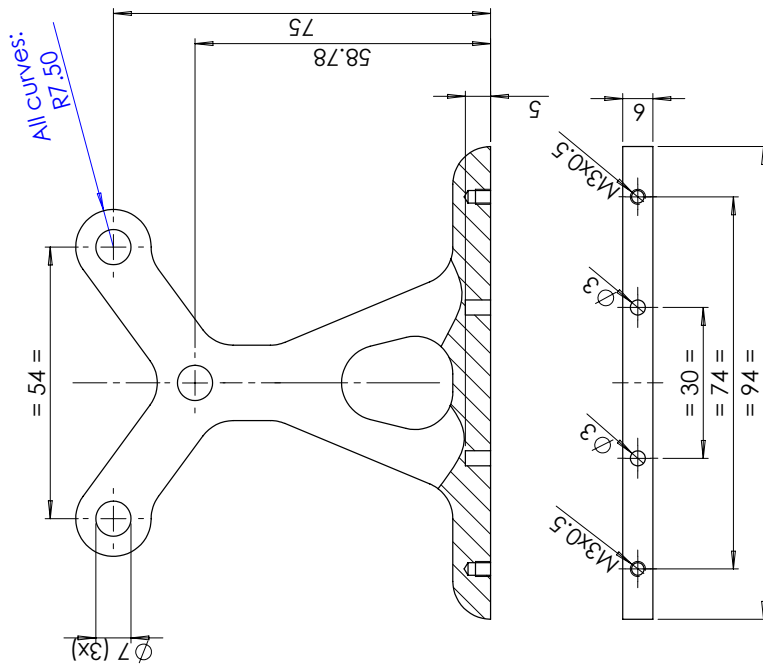
Exact spring shape is made manually by instrument maker

UNLESS OTHERWISE SPECIFIED: DIMENSIONS ARE IN MILLIMETERS		FINISH:	DEBUR AND BREAK SHARP EDGES		DO NOT SCALE DRAWING	REVISION
SURFACE FINISH: TOLERANCES: ANGULAR:					4.5	
DRAWN	NAME	SIGNATURE	DATE	TITLE		
CHK'D				Leaf Spring - Steering		
APP'VD				DWG NO. A3		
MFG				MATERIAL: Spring steel		
Q.A.				WEIGHT: SCALE: 1:1		
				SHEET 21 OF 73		

ITEM NO.	PART NUMBER	MATERIAL	QTY.
1	5.1 Frame	Aluminium	1
2	2.2 Bus 5mm	Bronze	3

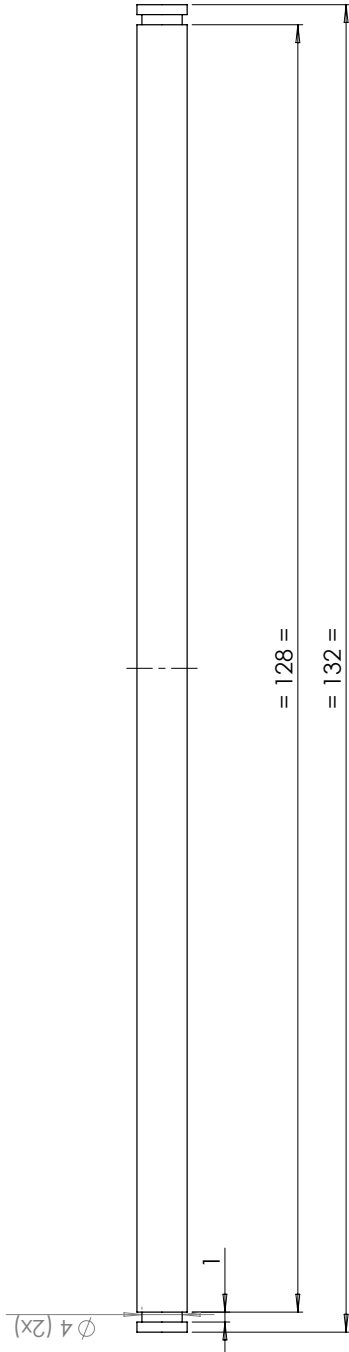


UNLESS OTHERWISE SPECIFIED: DIMENSIONS ARE IN MILLIMETERS		FINISH:	DO NOT SCALE DRAWING	REVISION
SURFACE FINISH:		DEBUR AND BREAK SHARP EDGES	5	
TOLERANCES:				
ANGULAR:				
DRAWN	NAME	SIGNATURE	DATE	TITLE
CHKD				Frame #4
APPVD				MemoSlide
MFG				DWG NO. A3
QA				SCALE:2:1
				SHEET 22 OF 73
				WEIGHT:



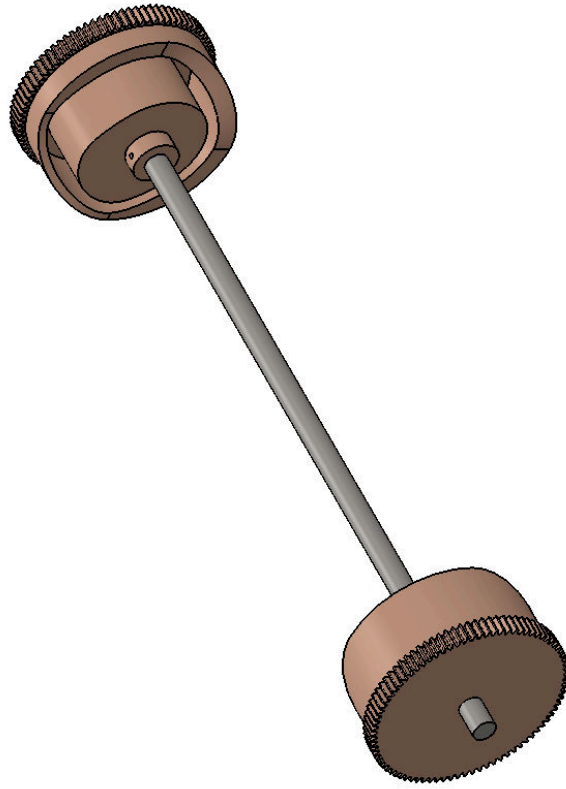
Sketch file is digitaal beschikbaar in part: "5,1 Frame"

UNLESS OTHERWISE SPECIFIED: DIMENSIONS ARE IN MILLIMETERS		FINISH:		DEBUR AND BREAK SHARP EDGES		DO NOT SCALE DRAWING		REVISION	
SURFACE FINISH:		TOLERANCES:						5.1	
LINEAR:		ANGULAR:						TITLE	
								Frame	
								DWG NO. MemoSlide	
								A3	
								SCALE: 1:1	
								SHEET 23 OF 73	
NAME	SIGNATURE	DATE							
DRAWN									
CHK'D									
APP'VD									
MEG									
Q.A.									
				MATERIAL: Aluminium				WEIGHT:	

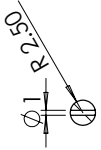


UNLESS OTHERWISE SPECIFIED: DIMENSIONS ARE IN MILLIMETERS		FINISH:		DEBUR AND BREAK SHARP EDGES		DO NOT SCALE DRAWING		REVISION		QTY.	
SURFACE FINISH:		TOLERANCES:		MATERIAL:		6		6		2	
ANGULAR:		NAME		SIGNATURE		DATE		TITLE		Rod 5x132 mm	
DRAWN		CHK'D		APPR'D		MFG		DWG NO.		A3	
Q.A		MATERIAL: Stainless steel		WEIGHT:		SCALE:2:1		SHEET 24 OF 73			

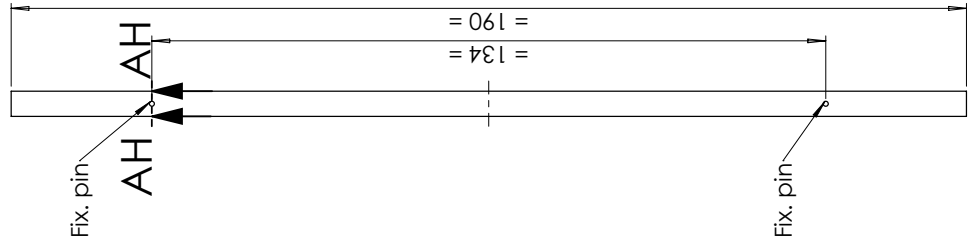
ITEM NO.	PART NUMBER	MATERIAL	QTY.
1	7.1 Cam Axis	Stainless steel	1
2	7.2 Cam - Push+Lock - Front	Bronze	1
3	7.3 Cam - Push+Lock - Back	Bronze	1
4	7.4 Pin 1x10 mm	Stainless steel	2



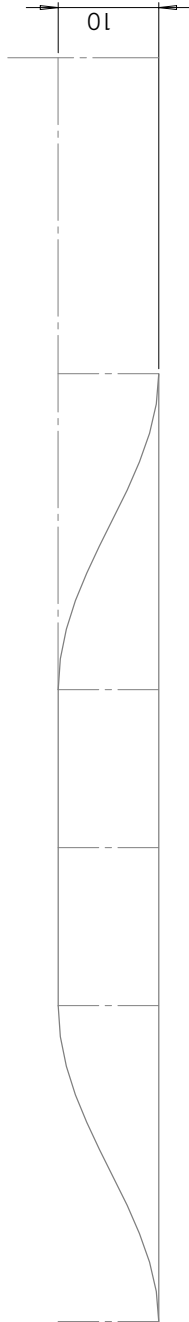
UNLESS OTHERWISE SPECIFIED: DIMENSIONS ARE IN MILLIMETERS		FINISH:		DEBUR AND BREAK SHARP EDGES		DO NOT SCALE DRAWING		REVISION	
SURFACE FINISH:		Roughness:						7	
TOLERANCES:		ANGULAR:							
DRAWN	NAME	SIGNATURE	DATE	TITLE		DWG NO.		SCALE:1:1	
CHK'D				Cam Axis - Memory		MemoSlide		A3	
APP'VD				MATERIAL:		SHEET 25 OF 73			
MEG				WEIGHT:					
Q.A.									



SECTION AH-AH

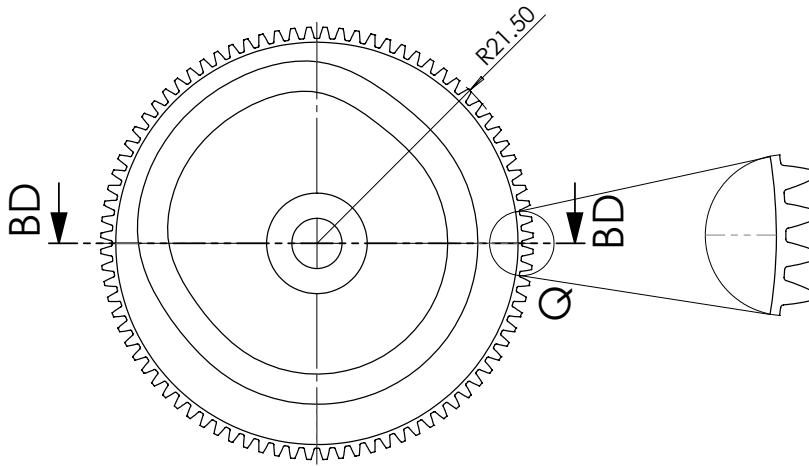
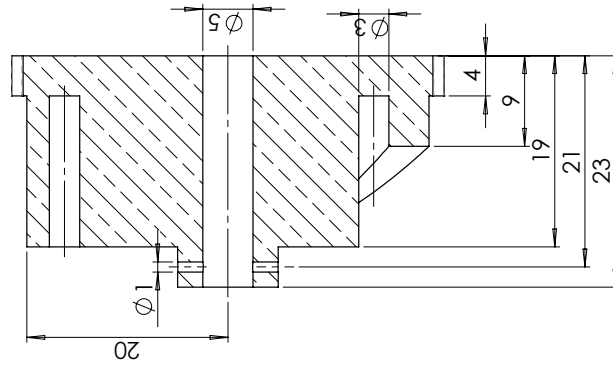


UNLESS OTHERWISE SPECIFIED: DIMENSIONS ARE IN MILLIMETERS		FINISH:		DEBUR AND BREAK SHARP EDGES		DO NOT SCALE DRAWING	REVISION
SURFACE FINISH: TOLERANCES: ANGULAR:						7.1	
NAME	SIGNATURE	DATE	TITLE				
DRAWN			Cam Axis				
CHK'D			MemoSlide				
APP'VD			A3				
MFG			DWG NO.				
Q.A.			MATERIAL: Stainless steel				
			SCALE: 1:1		SHEET 24 OF 73		



The axial cam is defined wrt the front face. This sketch can be wrapped around the cylinder to a depth of 4.5 mm.
The wrap sketch is available digitally in part: "7.2 Cam - Push+Lock - Front"

SECTION BD-BD



The groove radii indicate the groove center line. A groove with a sliding fit wrt: "1.5 Cam Follower - Memory"

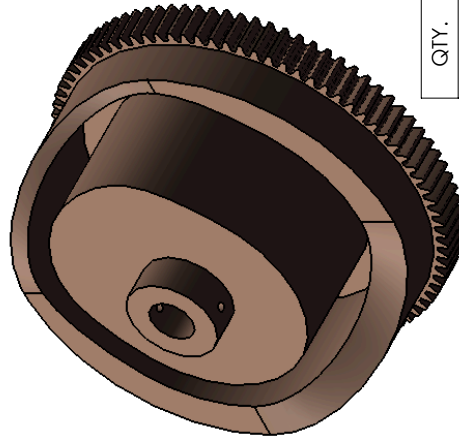
Angle θ [deg] = 0 at top, clockwise positive direction.

Cam groove radii		Axial cam
Angle θ [deg]	R(θ) [mm]	Depth [mm]
0	16.55	0
30	16.7	
60	16.7	
90	16.55	10
120	14.75	
150	14.5	
180	14.5	10
210	14.5	
240	14.5	
270	14.5	0
300	14.5	
330	14.75	

DETAIL Q

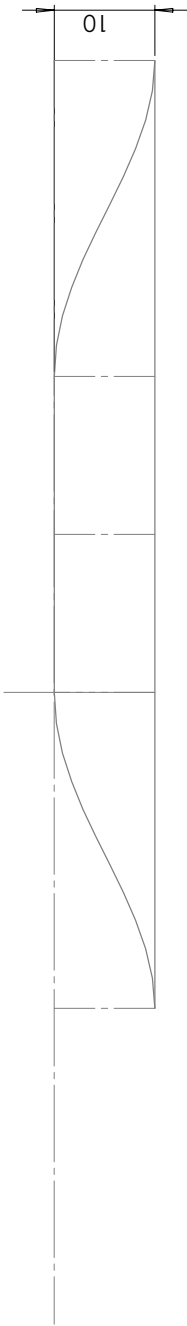
SCALE 5 : 1

Gear teeth sketch is available digitally in part: "7.2 Cam - Push+Lock - Front"



QTY. 1

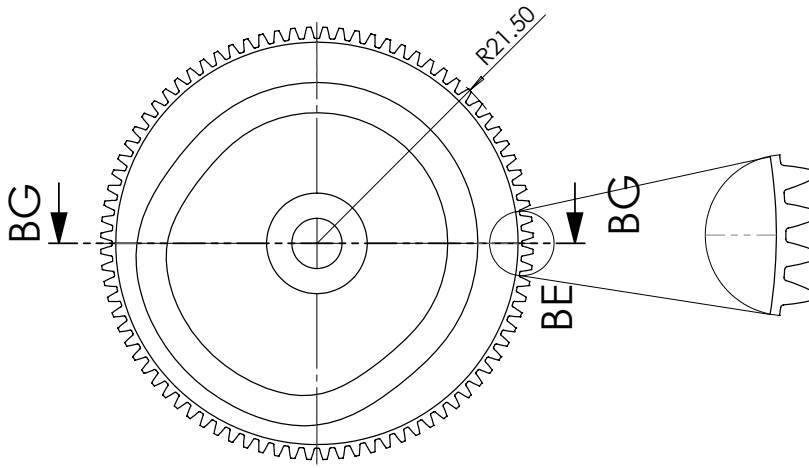
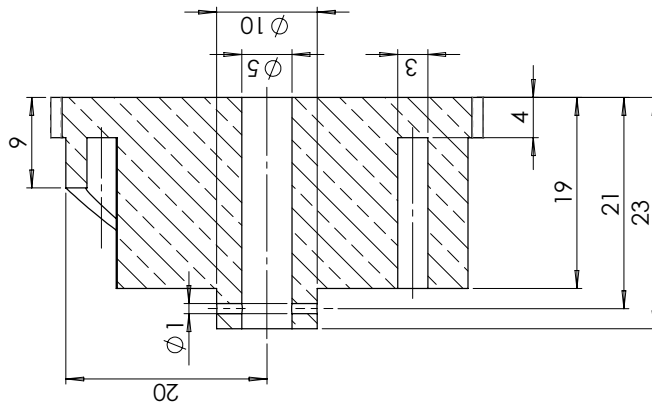
UNLESS OTHERWISE SPECIFIED: DIMENSIONS ARE IN MILLIMETERS		FINISH: SURFACE FINISH: TO SURFACES: ANGULAR:		DEBUR AND BREAK SHARP EDGES		DO NOT SCALE DRAWING		REVISION	
						7.2			
TITLE: Cam - Push+Lock - Front		DRAWN: CHKD: APPVD: MFG: QA:		SIGNATURE: DATE:		DWS NO. A3		SCALE: 2:1	
MATERIAL: Bronze		WEIGHT:		SHEET 27 OF 73					



The axial cam is defined wrt the front face. This sketch can be wrapped around the cylinder to a depth of 4.5 mm.

The wrap sketch is available digitally in part: "7.3 Cam - Push+Lock - Back"

SECTION BG-BG



The groove radii indicate the groove center line. A groove with a sliding fit wrt: "11.5 Cam Follower - Memory"

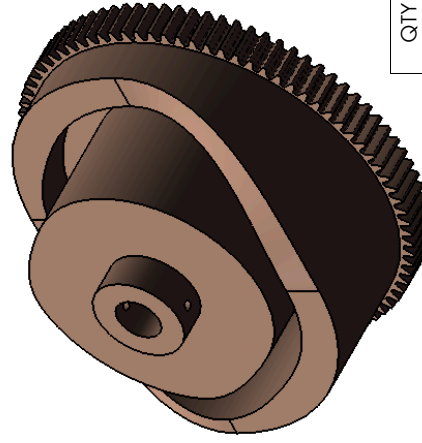
Angle θ [deg] = 0 at top, clockwise positive direction.

Cam groove radii		Axial cam
Angle θ [deg]	R(θ) [mm]	Depth [mm]
0	16.55	10
30	14.75	
60	14.5	
90	14.5	10
120	14.5	
150	14.5	
180	14.5	0
210	14.5	
240	14.75	
270	16.55	0
300	16.7	
330	16.7	

DETAIL BE

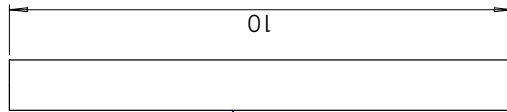
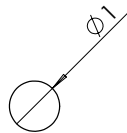
SCALE 5 : 1

Gear teeth sketch is available digitally in part: "7.3 Cam - Push+Lock - Back"



QTY. 1

UNLESS OTHERWISE SPECIFIED: DIMENSIONS ARE IN MILLIMETERS		DO NOT SCALE DRAWING		REVISION	
SURFACE FINISH: TO FINISHES: ANGULAR:		7.3		7.3	
FINISH: DEBUR AND BREAK SHARP EDGES		TITLE: Cam - Push+Lock - Back		DWG NO. A3	
NAME	SIGNATURE	DATE	MATERIAL: Bronze	SCALE:2:1	SHEET 28 OF 73
DRAWN					
CHKD					
APPVD					
MFG					
Q.A					

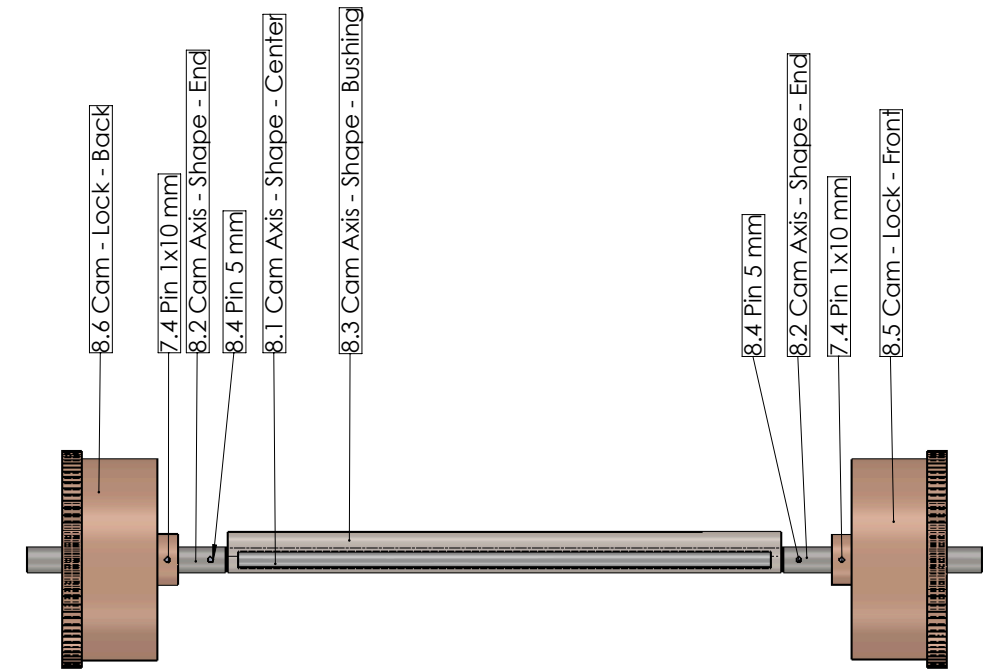


Press fit in 1 mm hole,
to function as locking pin

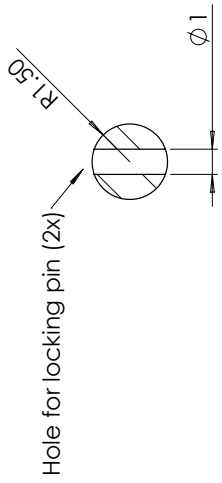


UNLESS OTHERWISE SPECIFIED: DIMENSIONS ARE IN MILLIMETERS		FINISH:		DEBUR AND BREAK SHARP EDGES		DO NOT SCALE DRAWING		REVISION	
SURFACE FINISH:						7.4			
TOLERANCES:									
ANGULAR:									
DRAWN	NAME	SIGNATURE	DATE			TITLE			
CHKD						Pin 1x10 mm			
APPVD									
MFG									
Q.A									
				MATERIAL:		DWGS NO.		A3	
				Stainless steel					
				WEIGHT:		SCALE:1:1		SHEET 29 OF 73	

ITEM NO.	PART NUMBER	MATERIAL	QTY.
1	8.1 Cam Axis - Shape - Center	Stainless steel	1
2	8.2 Cam Axis - Shape - End	Stainless steel	2
3	8.3 Cam Axis - Shape - Bushing	Stainless steel	1
4	8.4 Pin 5 mm	Stainless steel	2
5	8.5 Cam - Lock - Front	Bronze	1
6	8.6 Cam - Lock - Back	Bronze	1
7	7.4 Pin 1x10 mm	Stainless steel	2

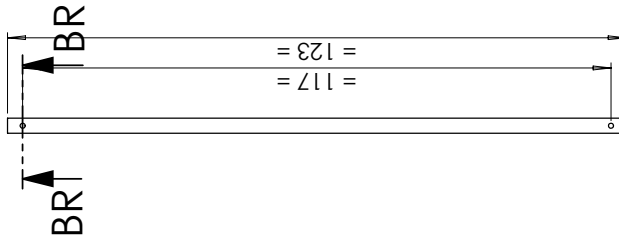


UNLESS OTHERWISE SPECIFIED: DIMENSIONS ARE IN MILLIMETERS		FINISH:		DEBUR AND BREAK SHARP EDGES		DO NOT SCALE DRAWING		REVISION	
SURFACE FINISH:		TOLERANCES:						8	
LINEAR:		ANGULAR:							
DRAWN	NAME	SIGNATURE	DATE	TITLE					
CHK'D				Cam Axis - Shape					
APP'VD				DWG NO. MemoSlide					
MFG				SCALE: 1:1					
Q.A.				SHEET 30 OF 73					
				MATERIAL:					
				WEIGHT:					

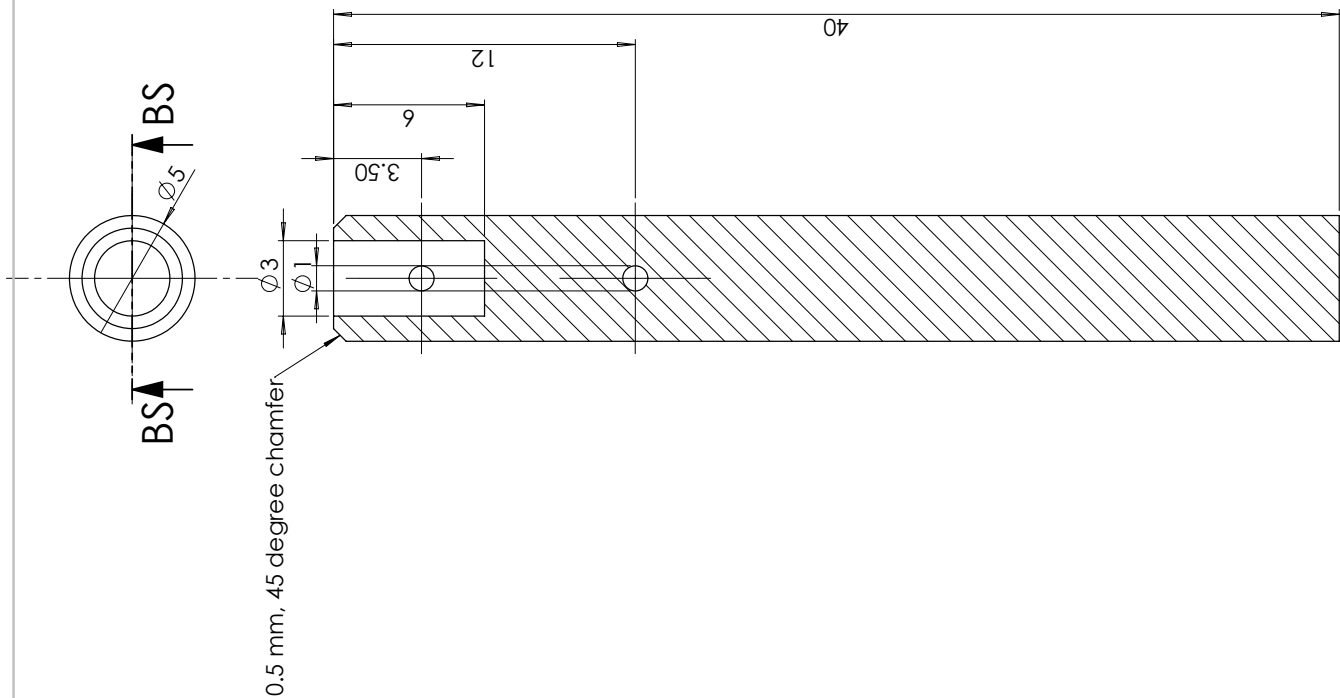


SECTION BR-BR

SCALE 5 : 1

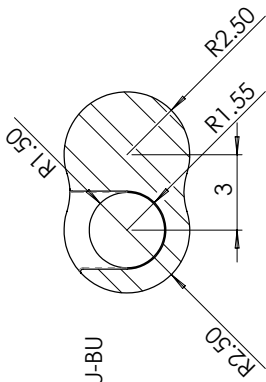


UNLESS OTHERWISE SPECIFIED: DIMENSIONS ARE IN MILLIMETERS		FINISH:		DO NOT SCALE DRAWING		REVISION	
SURFACE FINISH:		DEBUR AND BREAK SHARP EDGES		8.1			
TOLERANCES:				TITLE		Cam Axis - Shape - Center	
ANGULAR:				DWG NO.		MemoSlide	
		MATERIAL: Stainless steel		SCALE: 2:1		A3	
DRAWN	NAME	SIGNATURE	DATE	WEIGHT:		SHEET 31 OF 73	
CHKD							
APPVD							
MFG							
Q.A							

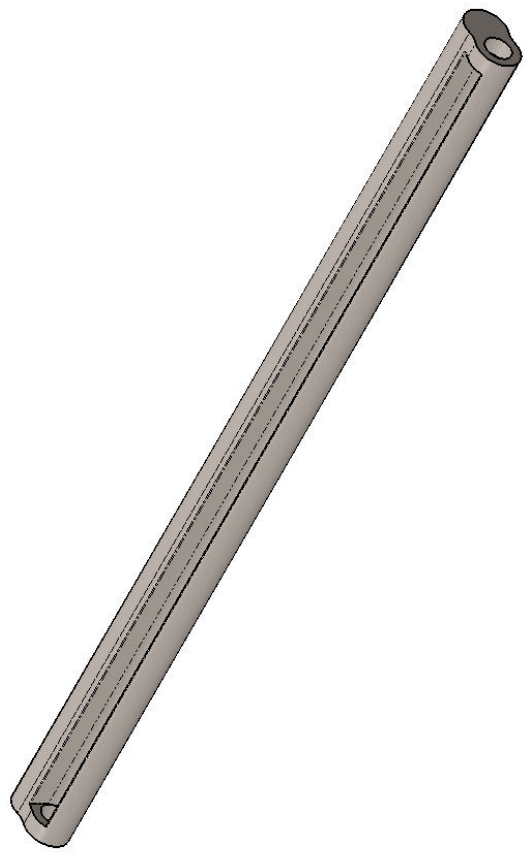
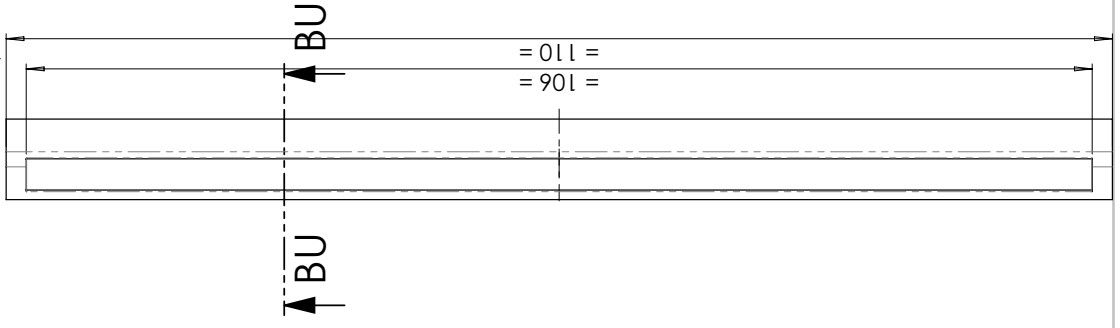


UNLESS OTHERWISE SPECIFIED: DIMENSIONS ARE IN MILLIMETERS		FINISH:		DEBUR AND BREAK SHARP EDGES		DO NOT SCALE DRAWING		REVISION	
SURFACE FINISH:		TOLERANCES:				8.2			
DIMENSIONS:		ANGULAR:							
DRAWN		NAME		SIGNATURE		DATE		TITLE	
CHK'D								Cam Axis - Shape - End	
APP'VD								DWG NO. A3	
MFG								MATERIAL: Stainless steel	
Q.A								SCALE: 1:1	
								WEIGHT: SHEET 32 OF 73	
QTY.								2	

SECTION BS-BS

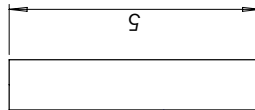
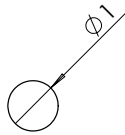


SECTION BU-BU
SCALE 5 : 1



Sketch is available digitally in part:
"8.3 Cam Axis - Shape - Bushing"

UNLESS OTHERWISE SPECIFIED: DIMENSIONS ARE IN MILLIMETERS		FINISH:	DEBUR AND BREAK SHARP EDGES		DO NOT SCALE DRAWING	REVISION
SURFACE FINISH: TOLERANCES: ANGULAR:					8.3	
DRAWN	NAME	SIGNATURE	DATE	TITLE		
CHK'D				Cam Axis - Shape - Bushing		
APP'VD				DWG NO.	A3	
MFG				MATERIAL:	Stainless steel	
Q.A				SCALE:2:1	SHEET 33 OF 73	
				WEIGHT:		

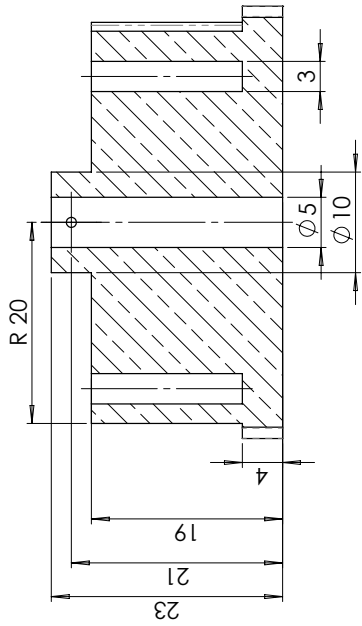


Press fit in 1 mm hole,
to function as locking pin

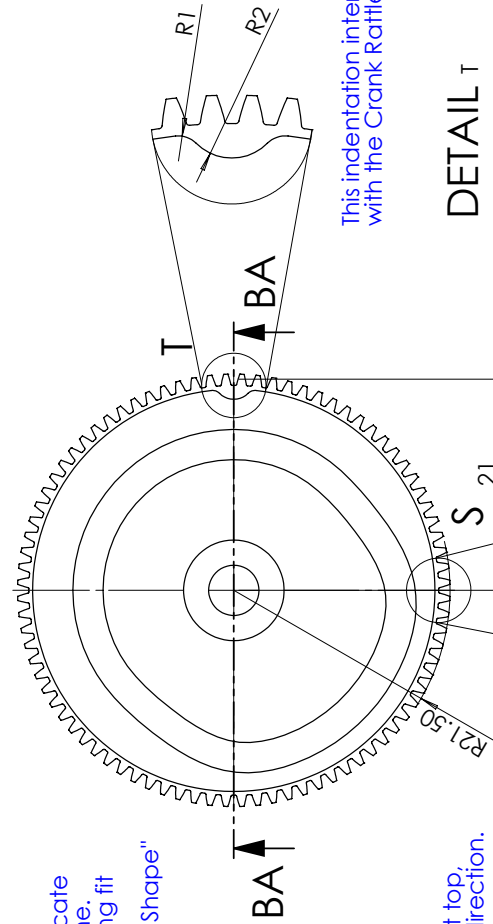


UNLESS OTHERWISE SPECIFIED: DIMENSIONS ARE IN MILLIMETERS		FINISH:		DEBUR AND BREAK SHARP EDGES		DO NOT SCALE DRAWING		REVISION	
SURFACE FINISH:						8.4			
TOLERANCES:									
ANGULAR:									
DRAWN	NAME	SIGNATURE	DATE			TITLE			
CHKD						Pin 1x5 mm			
APPVD									
MFG									
Q.A									
				MATERIAL:		DWG NO.		A3	
				Stainless steel					
				WEIGHT:		SCALE:1:1		SHEET 34 OF 73	

SECTION BA-BA



The groove radii indicate the groove center line. A groove with a sliding fit wrt. "12.2 Cam Follower - Shape"



This indentation interacts with the Crank Rattle

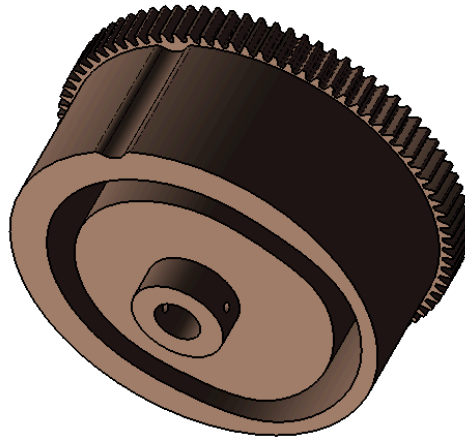
DETAIL T
SCALE 5 : 1

Angle θ [deg] = 0 at top, clockwise positive direction.

Cam groove radii	Angle θ [deg]	R(θ) [mm]
	0	14.5
	30	14.5
	60	14.5
	90	14.5
	120	14.5
	150	14.75
	180	16.55
	210	16.7
	240	16.7
	270	16.55
	300	14.75
	330	14.5

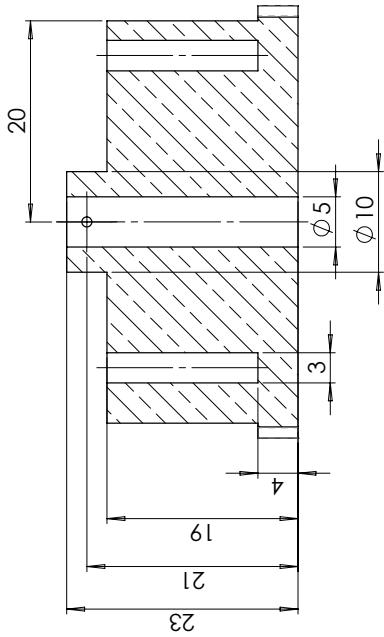
Gear teeth sketch is available digitally in part: "8.5 Cam - Lock - Front"

DETAIL S
SCALE 5 : 1

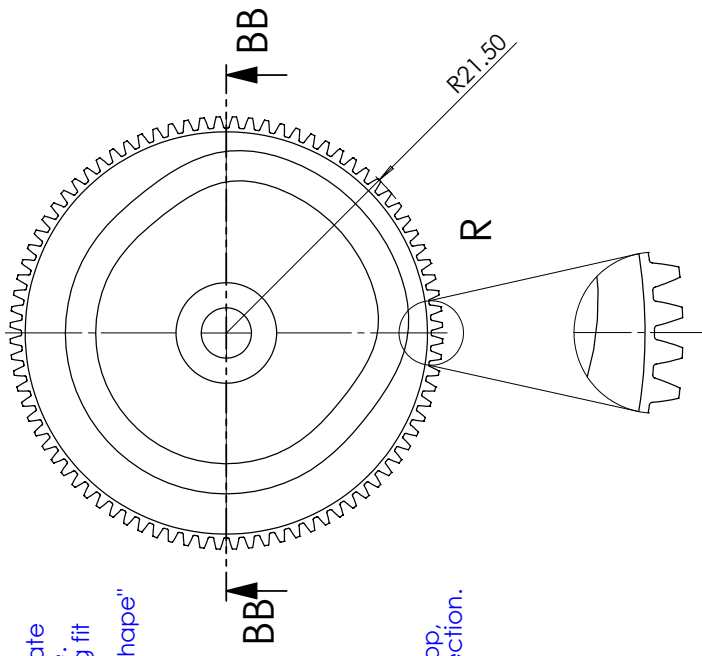


QTY.		DO NOT SCALE DRAWING		REVISION	
1		8.5			
UNLESS OTHERWISE SPECIFIED, DIMENSIONS ARE IN MILLIMETERS		DEBUR AND BREAK SHARP EDGES		TITLE	
SURFACE FINISH TOLERANCES: ANGULAR:				Cam - Lock - Front	
NAME	SIGNATURE	DATE		DWG NO.	A3
				MemoSlide	
DRWN				MATERIAL:	Bronze
CHKD				WEIGHT:	
APPVD					
MEG					
QA					
				SHEET 35 OF 73	

SECTION BB-BB



The groove radii indicate the groove center line. A groove with a sliding fit wrt: "12.2 Cam Follower - Shape"

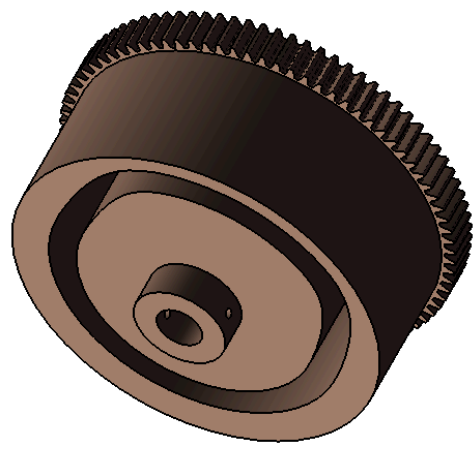


Angle θ [deg] = 0 at top, clockwise positive direction.

Cam groove radii	
Angle θ [deg]	R(θ) [mm]
0	14.5
30	14.5
60	14.75
90	16.55
120	16.7
150	16.7
180	16.55
210	14.75
240	14.5
270	14.5
300	14.5
330	14.5

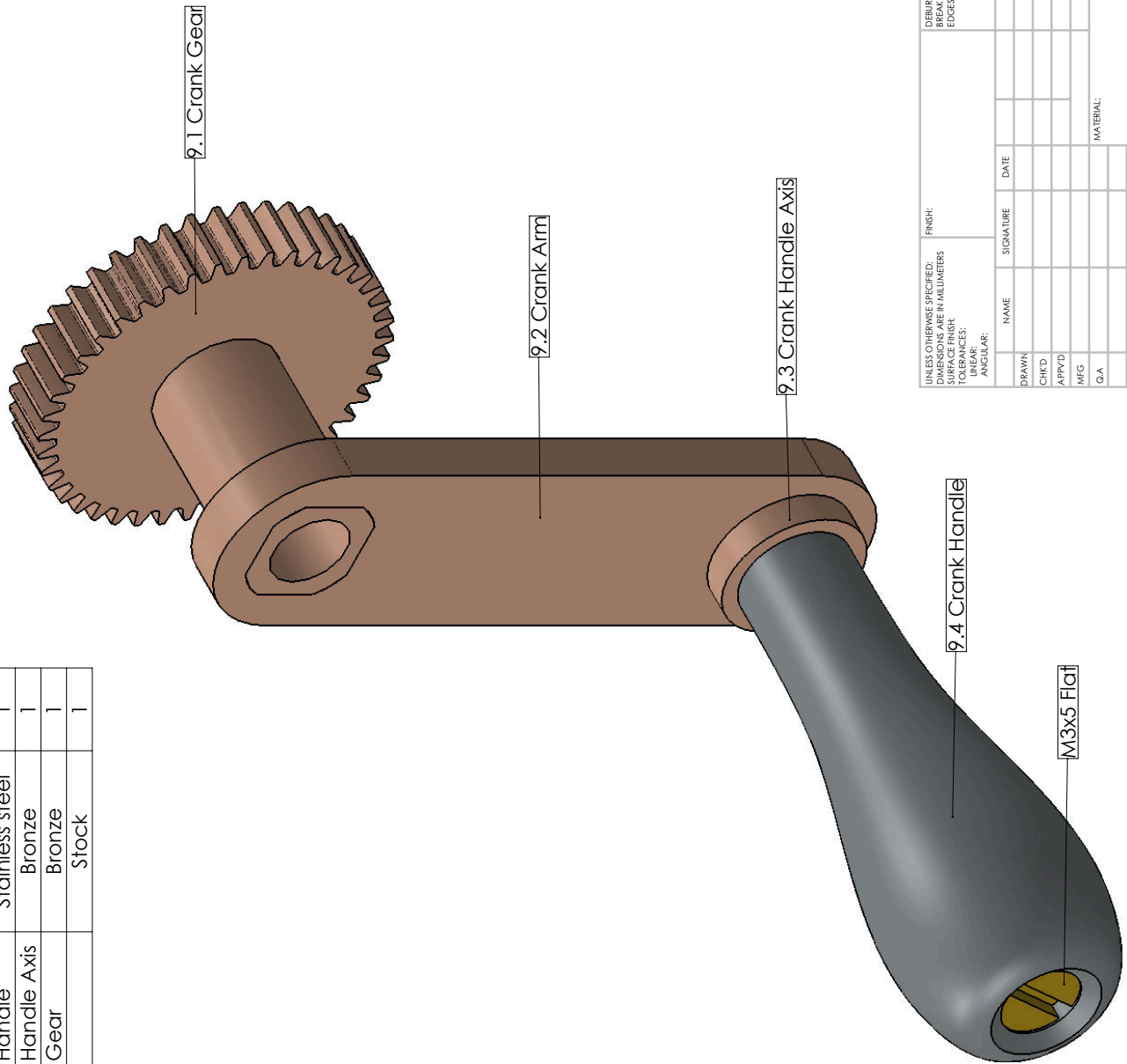
Gear teeth sketch is available digitally in part: "8.6 Cam - Lock - Back"

DETAIL R
SCALE 5 : 1



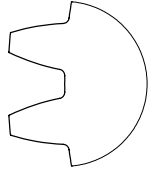
UNLESS OTHERWISE SPECIFIED: DIMENSIONS ARE IN MILLIMETERS		FINISH:		DEBUR AND BREAK SHARP EDGES		DO NOT SCALE DRAWING		REVISION	
SURFACE FINISH:		TOLERANCES:		ANGULAR:		8.6		8.6	
DRAWN		NAME		SIGNATURE		DATE		TITLE	
CHK'D								Cam - Lock - Back	
APP'D								MemoSlide	
MFG								A3	
Q.A								DWG NO.	
								MATERIAL: Bronze	
								WEIGHT:	
								SCALE:2:1	
								SHEET 36 OF 73	
QTY.								1	

ITEM NO.	PART NUMBER	MATERIAL	QTY.
1	9.2 Crank Arm	Bronze	1
2	9.4 Crank Handle	Stainless steel	1
3	9.3 Crank Handle Axis	Bronze	1
4	9.1 Crank Gear	Bronze	1
5	M3x5 Flat	Stock	1



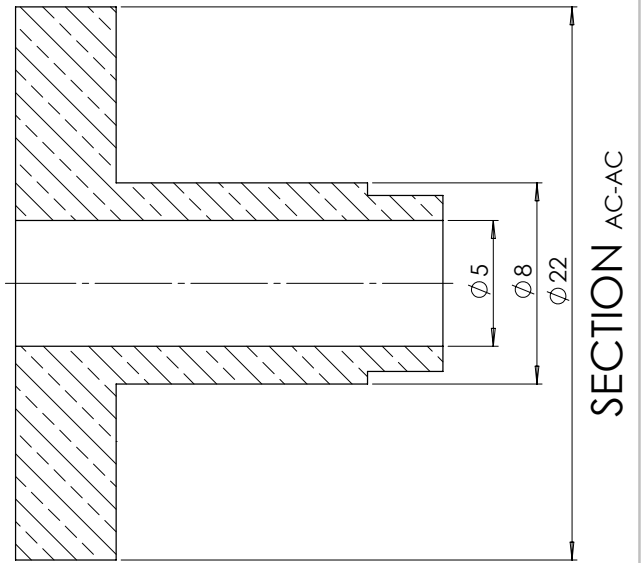
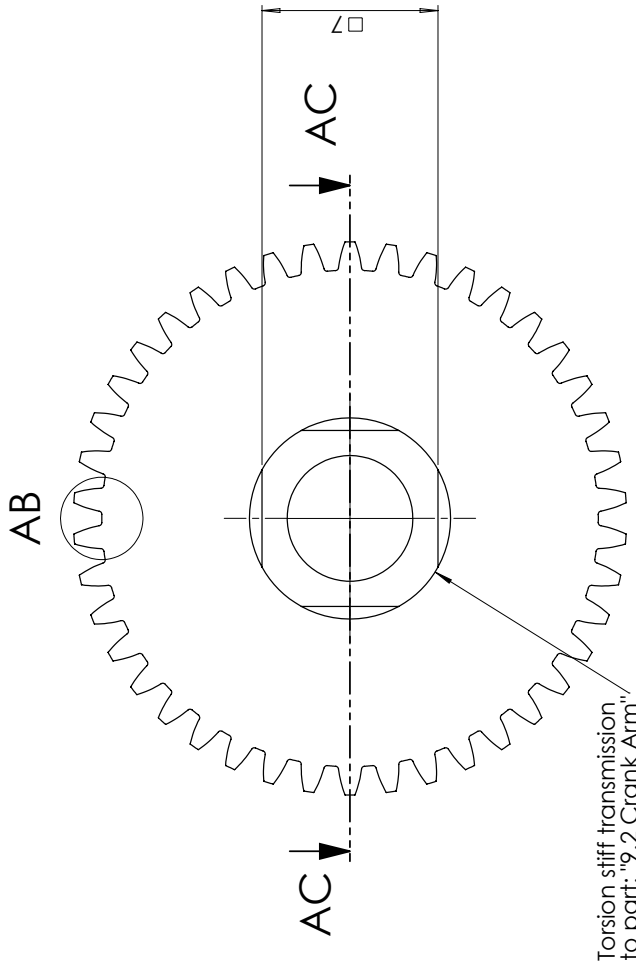
UNLESS OTHERWISE SPECIFIED: DIMENSIONS ARE IN MILLIMETERS		FINISH:		DEBUR AND BREAK SHARP EDGES		DO NOT SCALE DRAWING		REVISION	
SURFACE FINISH:		Roughness:				9			
TOLERANCES:		ANGULAR:							
DRAWN	NAME	SIGNATURE	DATE	TITLE		Crank		DWGS NO.	
CHK'D				MATERIAL:		MemoSlide		A3	
APP'VD				WEIGHT:		SCALE: 1:1		SHEET 37 OF 73	
MFG									
Q.A.									

Gear teeth sketch is available digitally in part: "9.1 Crank Gear"



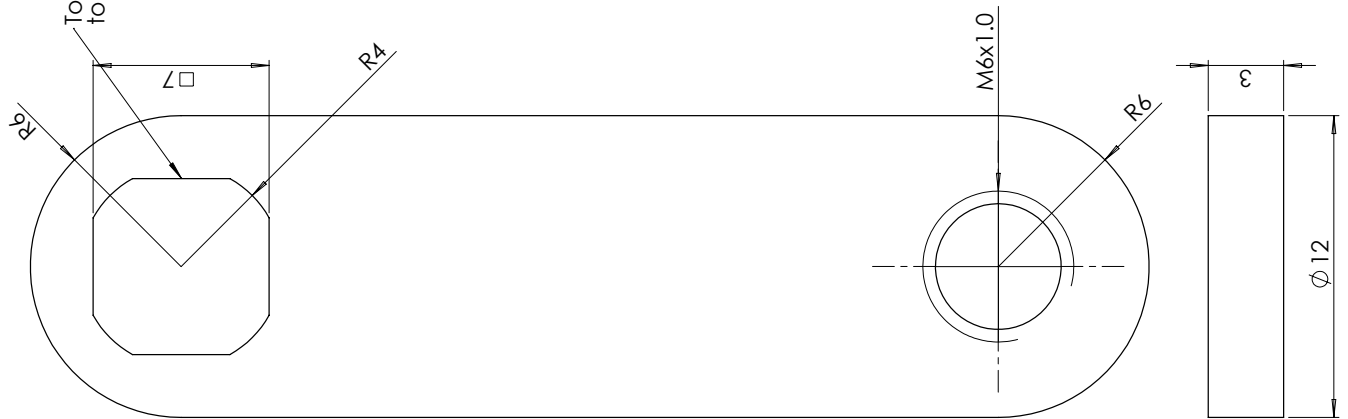
Gear:
module 0.5
teeth: 42

DETAIL AB
SCALE 10:1

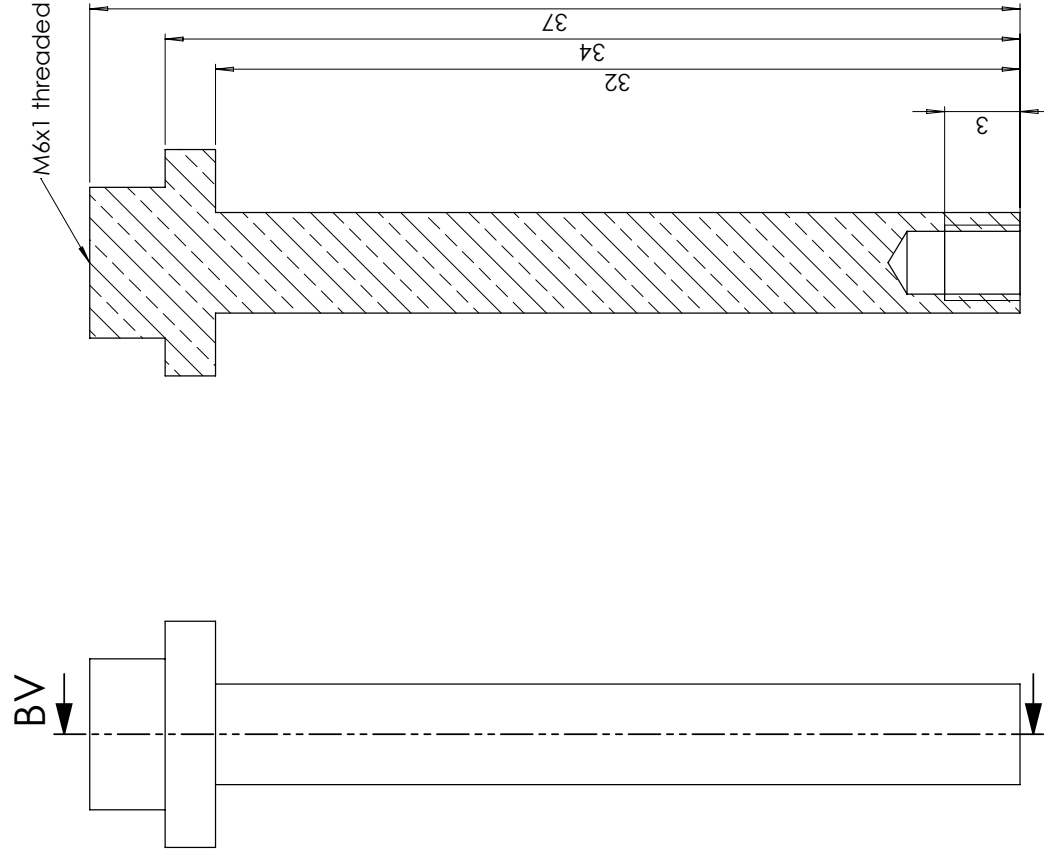


UNLESS OTHERWISE SPECIFIED: DIMENSIONS ARE IN MILLIMETERS		FINISH:		DEBUR AND BREAK SHARP EDGES		DO NOT SCALE DRAWING		REVISION	
SURFACE FINISH:		TOLERANCES:				9.1			
LINEAR:		ANGULAR:				TITLE:		Crank Gear	
DRAWN	NAME	SIGNATURE	DATE	MATERIAL: Brozno		DWG NO. A3		SCALE: 1	
CHK'D				WEIGHT:		SHEET 38 OF 73			
APP'VD									
MEG									
Q.A									

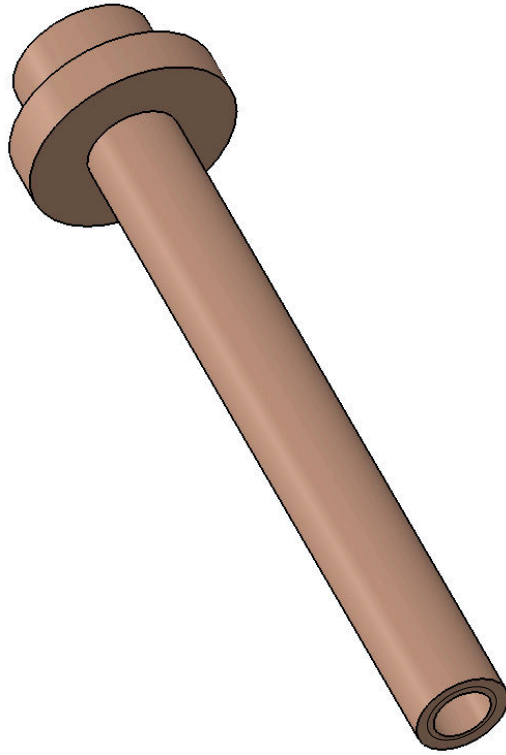
Torsion stiff transmission
to part: "9.1 Crank Gear"



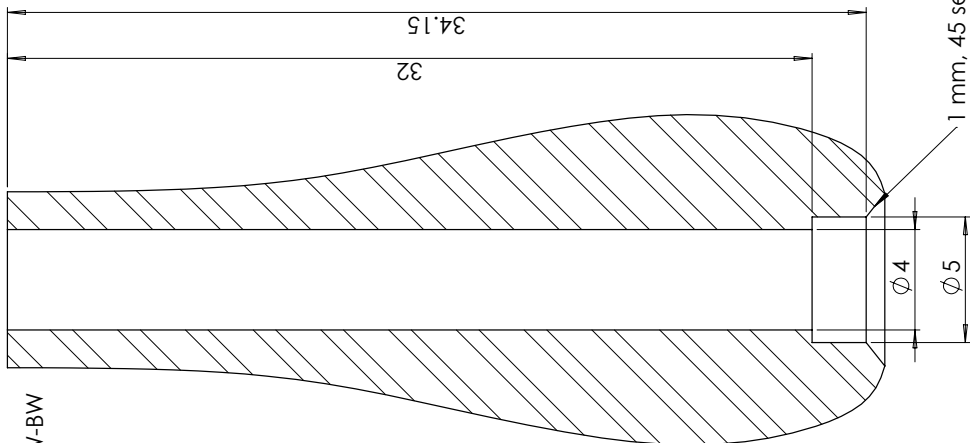
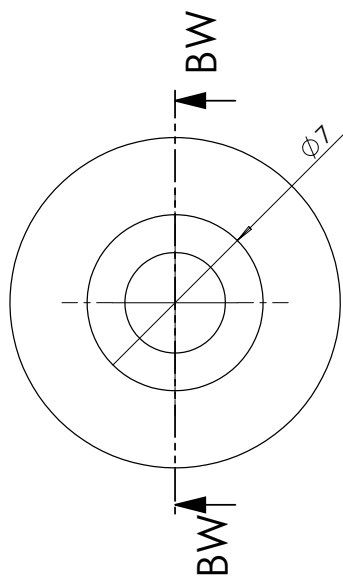
UNLESS OTHERWISE SPECIFIED: DIMENSIONS ARE IN MILLIMETERS		FINISH:		DEBUR AND BREAK SHARP EDGES		DO NOT SCALE DRAWING	REVISION
SURFACE FINISH:		NAME		SIGNATURE		9.2	
TOLERANCES:		DATE		DATE		TITLE	
ANGULAR:		DRAWN		CHK'D		Crank Arm	
		APP'VD		MFG		DWG NO.	
		Q.A.		MATERIAL:		A3	
				Brozno		SCALE: 1:1	
				WEIGHT:		SHEET 19 OF 73	



SECTION BV-BV



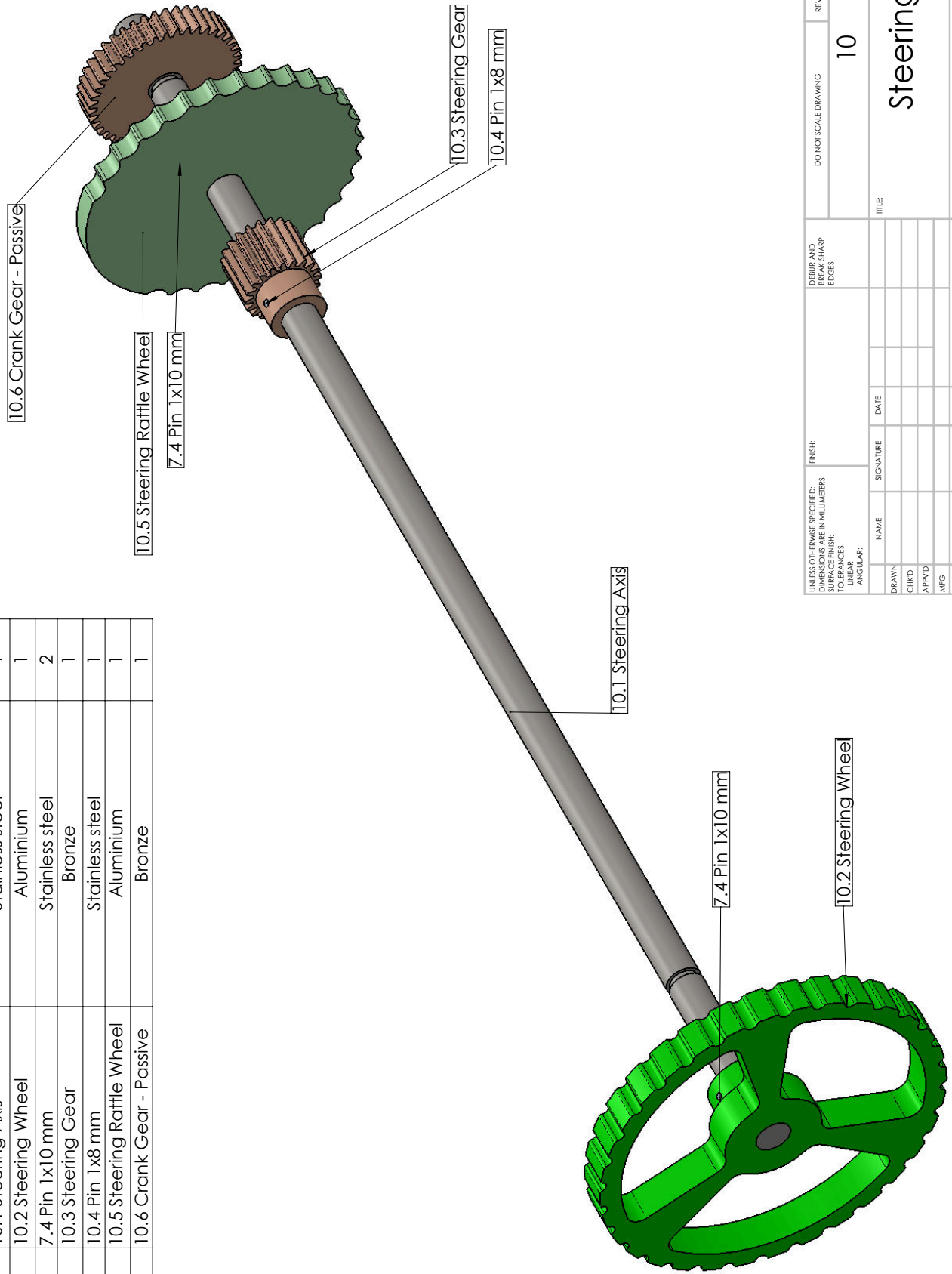
UNLESS OTHERWISE SPECIFIED: DIMENSIONS ARE IN MILLIMETERS		FINISH:		DEBURR AND BREAK SHARP EDGES		DO NOT SCALE DRAWING		REVISION	
SURFACE FINISH:		NAME		SIGNATURE		DATE		9.3	
TOLERANCES:		DRAWN		CHK'D		APP'VD		TITLE	
ANGULAR:		MFG		Q.A.		MATERIAL:		Crank Handle Axis	
						Brozno		DWG NO. A3	
						WEIGHT:		SCALE: 1:1	
								SHEET 40 OF 73	



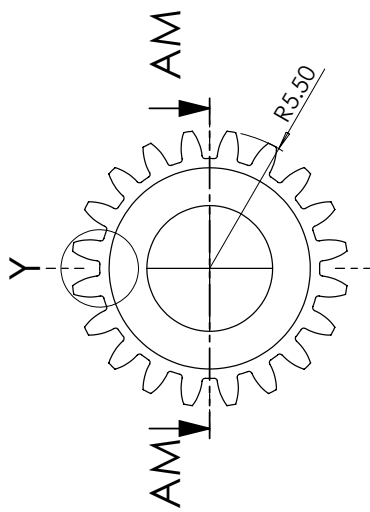
Handle shape is chosen arbitrary.
 Dimensions given ensure compatibility
 with part: '9.3 Crank Handle Axis'

UNLESS OTHERWISE SPECIFIED: DIMENSIONS ARE IN MILLIMETERS		FINISH:		DEBUR AND BREAK SHARP EDGES		DO NOT SCALE DRAWING		REVISION	
SURFACE FINISH:		TOLERANCES:		MATERIAL: Brozno		DWG NO. A3		SHEET 41 OF 73	
TOLERANCES: ANGULAR:		NAME		SIGNATURE		DATE		TITLE	
DRAWN									
CHK'D									
APP'VD									
MFG									
Q.A.									
WEIGHT:		SCALE: 1:1		SCALE: 1:1		SCALE: 1:1		SCALE: 1:1	

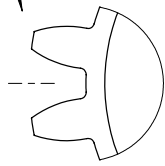
ITEM NO.	PART NUMBER	MATERIAL	QTY.
1	10.1 Steering Axis	Stainless steel	1
2	10.2 Steering Wheel	Aluminium	1
3	7.4 Pin 1x10 mm	Stainless steel	2
4	10.3 Steering Gear	Bronze	1
5	10.4 Pin 1x8 mm	Stainless steel	1
6	10.5 Steering Rattle Wheel	Aluminium	1
7	10.6 Crank Gear - Passive	Bronze	1



UNLESS OTHERWISE SPECIFIED: DIMENSIONS ARE IN MILLIMETERS		FINISH:		DEBUR AND BREAK SHARP EDGES		DO NOT SCALE DRAWING		REVISION	
SURFACE FINISH:		Roughness:				10		10	
TOLERANCES:		ANGULAR:						Steering	
NAME		SIGNATURE		DATE		TITLE		DWG NO.	
DRAWN	CHK'D	APP'VD	MFG	Q.A.					MemoSlide
									A3
MATERIAL:		WEIGHT:		SCALE:2:1		SHEET 42 OF 73			

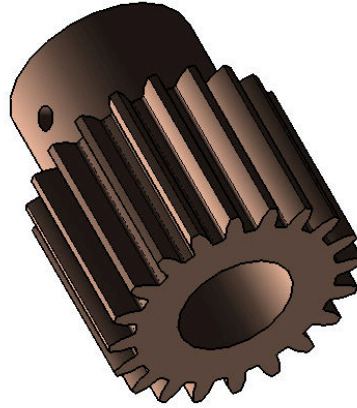
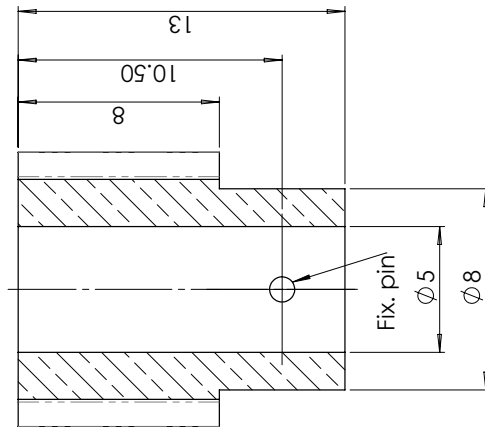


Gearing:
module: 0.5,
teeth: 20

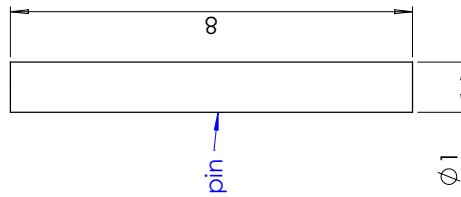
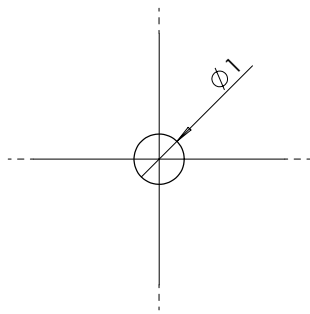


DETAIL Y
SCALE 10 : 1

SECTION AM-AM



UNLESS OTHERWISE SPECIFIED: DIMENSIONS ARE IN MILLIMETERS		FINISH:		DEBUR AND BREAK SHARP EDGES		DO NOT SCALE DRAWING	REVISION
SURFACE FINISH:		NAME		SIGNATURE		10.3	
TOLERANCES:		DRAWN		DATE		TITLE	
ANGULAR:		CHK'D				Steering Gear	
		APP'VD				DWG NO.	
		MFG				MemoSlide	
		Q.A.				MATERIAL:	
						Bronze	
						SCALE: 1	
						SHEET 45 OF 73	
						WEIGHT:	
						A3	



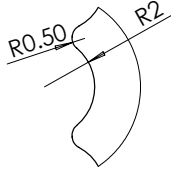
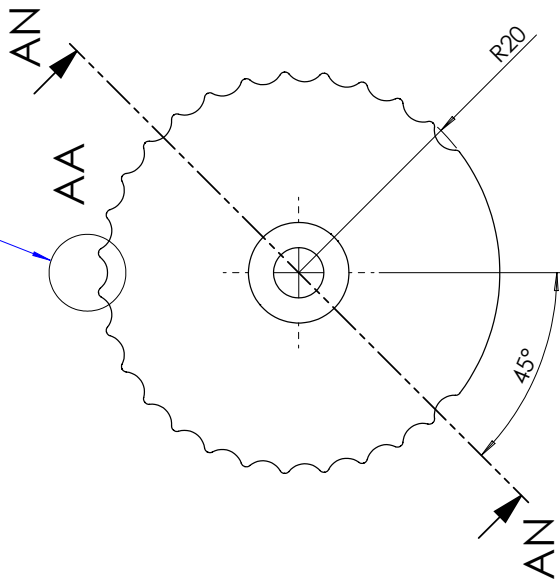
Press fit in 1 mm hole,
to function as locking pin



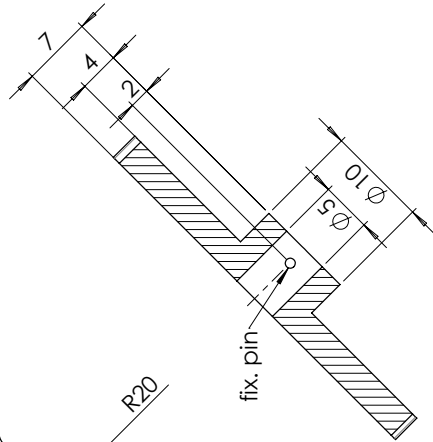
UNLESS OTHERWISE SPECIFIED: DIMENSIONS ARE IN MILLIMETERS		FINISH:		DEBUR AND BREAK SHARP EDGES		DO NOT SCALE DRAWING		REVISION	
SURFACE FINISH:						10.4			
TOLERANCES:									
ANGULAR:									
DRAWN	NAME	SIGNATURE	DATE	TITLE		DWG NO.		A3	
CHKD				Pin 1x8 mm		MemoSlide			
APPVD				MATERIAL: Stainless steel		SCALE: 1:1		SHEET 44 OF 73	
MFG				WEIGHT:					
Q.A									

Radial pattern, every 11.49 degrees, stems from translation between parts: "10.3 Steering Gear" & "14 Shape Active"

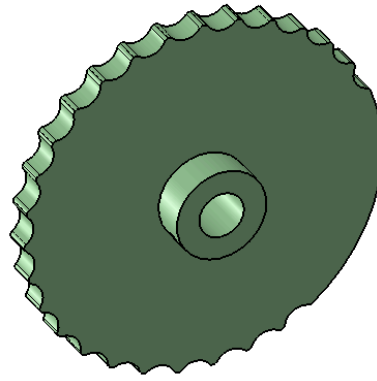
Edge structure is available digitally in part: "10.5 Steering Rattle Wheel"



DETAIL AA
SCALE 5 : 1



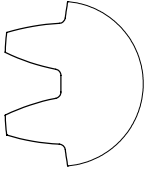
SECTION AN-AN



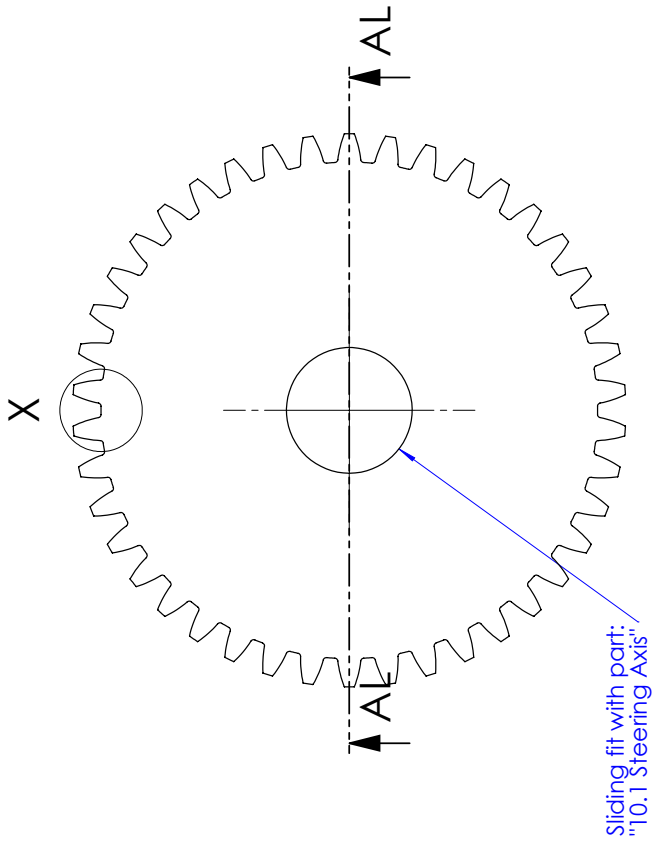
UNLESS OTHERWISE SPECIFIED: DIMENSIONS ARE IN MILLIMETERS		FINISH:		DEBUR AND BREAK SHARP EDGES		DO NOT SCALE DRAWING		REVISION	
SURFACE FINISH:		NAME		SIGNATURE		DATE		10.5	
TOLERANCES:		DRAWN						TITLE	
ANGULAR:		CHK'D						Steering Rattle Wheel	
		APP'VD						DWG NO.	
		MFG						A3	
		Q.A						MATERIAL:	
								Aluminium	
								WEIGHT:	
								SCALE:2:1	
								SHEET 47 OF 73	

Gear teeth sketch is available digitally in part: "9.1 Crank Gear"

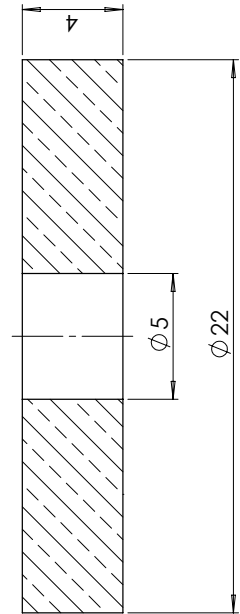
Gear:
module: 0.5
teeth: 42



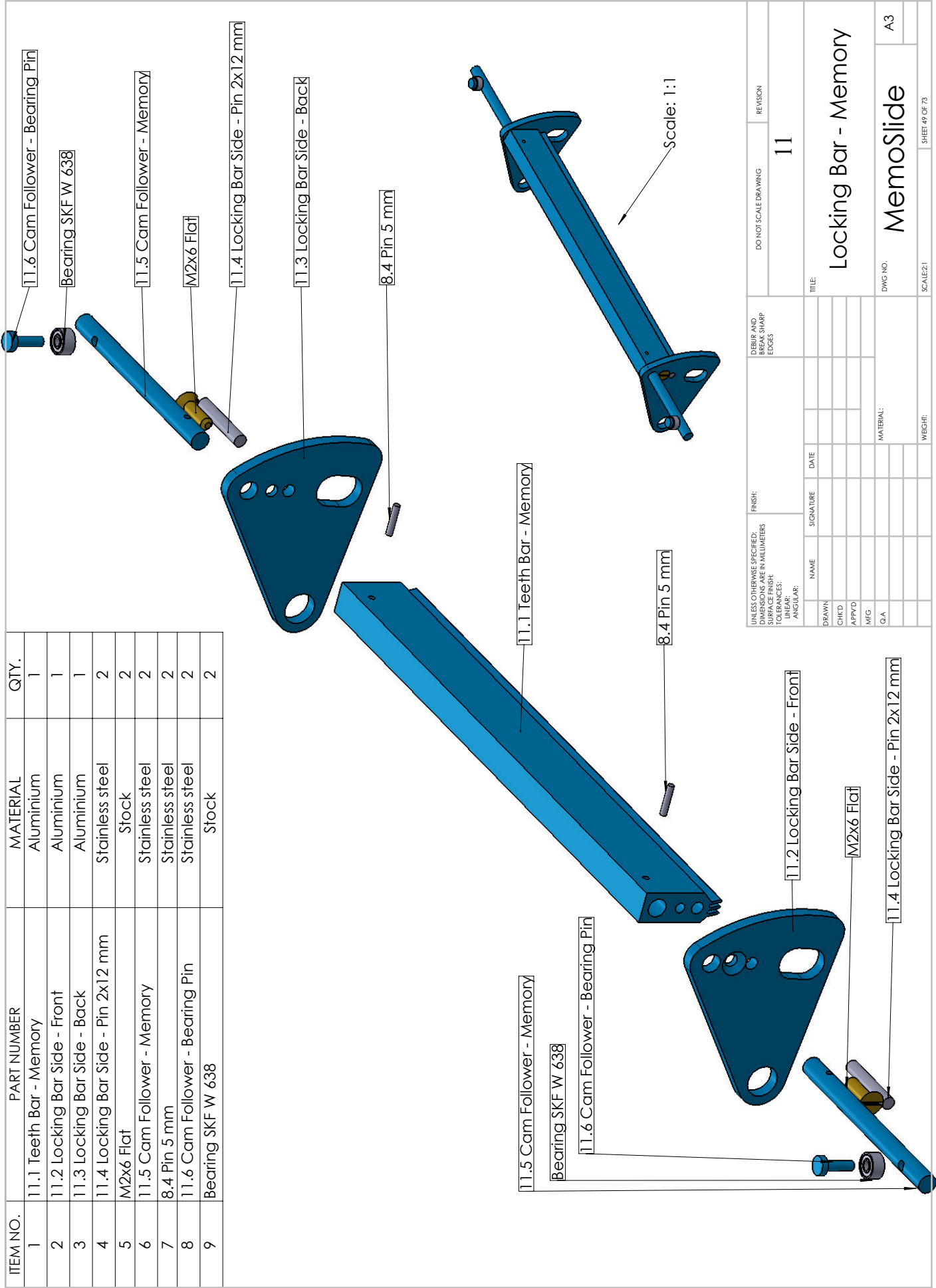
DETAIL X
SCALE 10:1



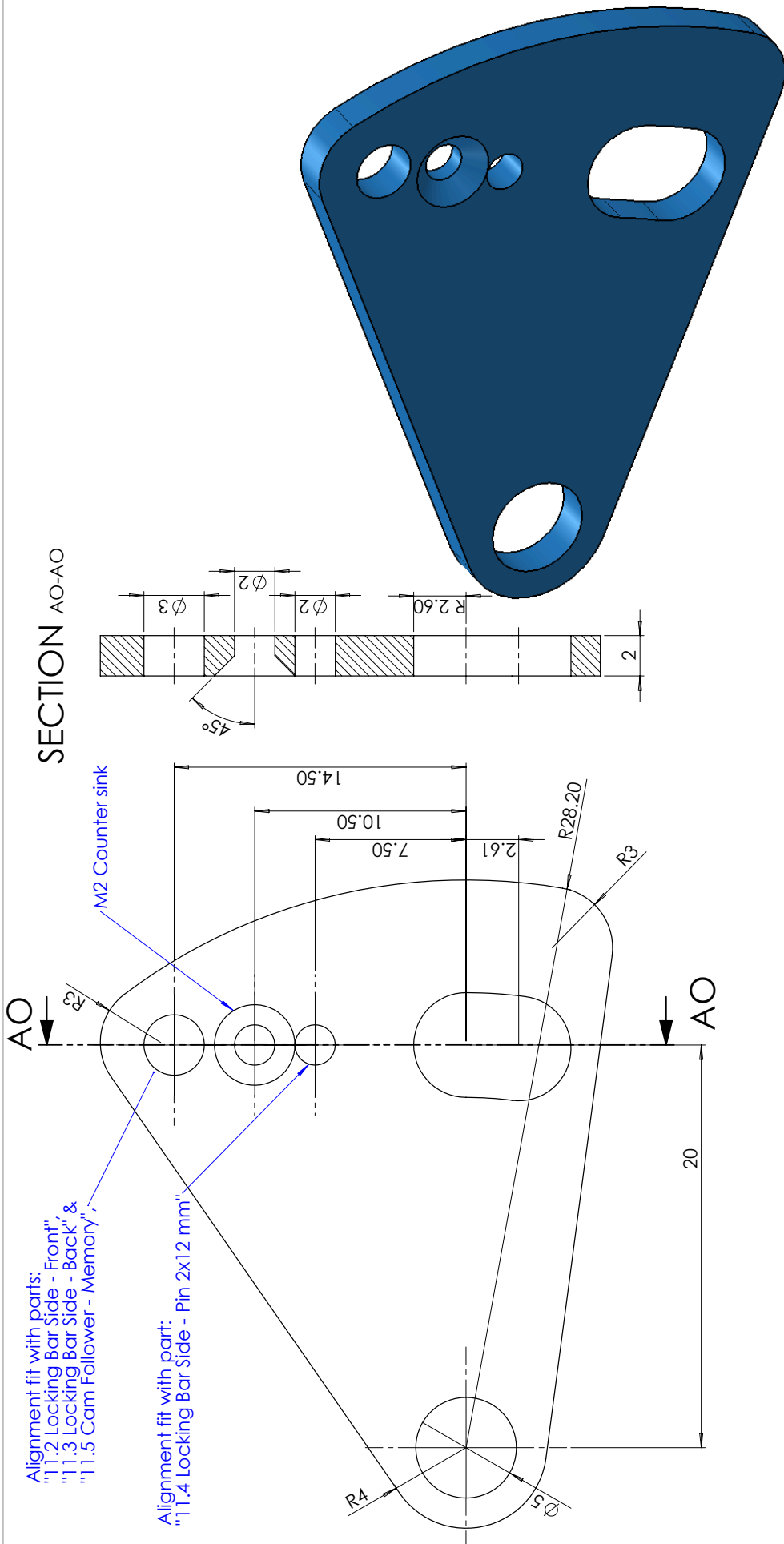
SECTION AL-AL



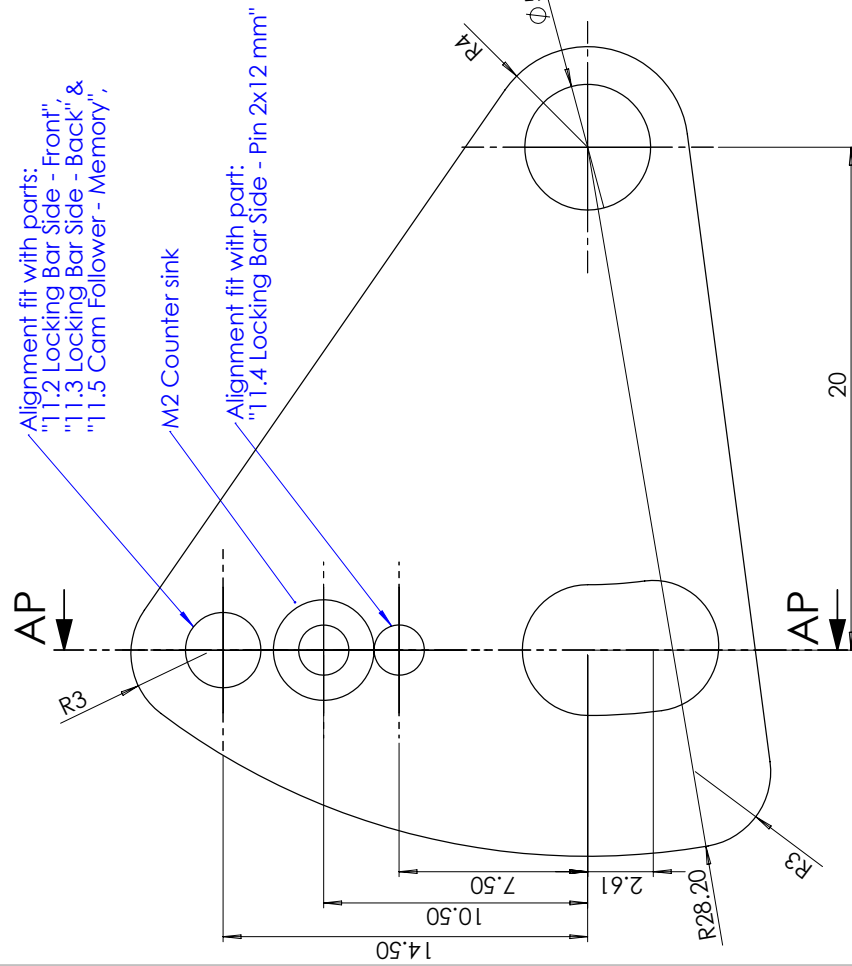
UNLESS OTHERWISE SPECIFIED: DIMENSIONS ARE IN MILLIMETERS		FINISH:	DO NOT SCALE DRAWING		REVISION
SURFACE FINISH:		DEBUR AND BREAK SHARP EDGES	10.6		
TOLERANCES:			TITLE:		
ANGULAR:			Crank Gear - Passive		
DRAWN	NAME	SIGNATURE	DATE	DWG NO.	A3
CHK'D					
APP'VD					
MFG				MATERIAL:	
Q.A.				Bronze	
				WEIGHT:	
				SCALE: 1	SHEET 48 OF 73



UNLESS OTHERWISE SPECIFIED: DIMENSIONS ARE IN MILLIMETERS SURFACE FINISH: TOLERANCES: ANGULAR:	FINISH:	DEBUR AND BREAK SHARP EDGES	DO NOT SCALE DRAWING	REVISION
NAME	SIGNATURE	DATE	11	
DRWN			TITLE	
CHKD			Locking Bar - Memory	
APPVD			DWG NO.	A3
MFG			SCALE: 2:1	SHEET 49 OF 73
QA			MATERIAL:	WEIGHT:

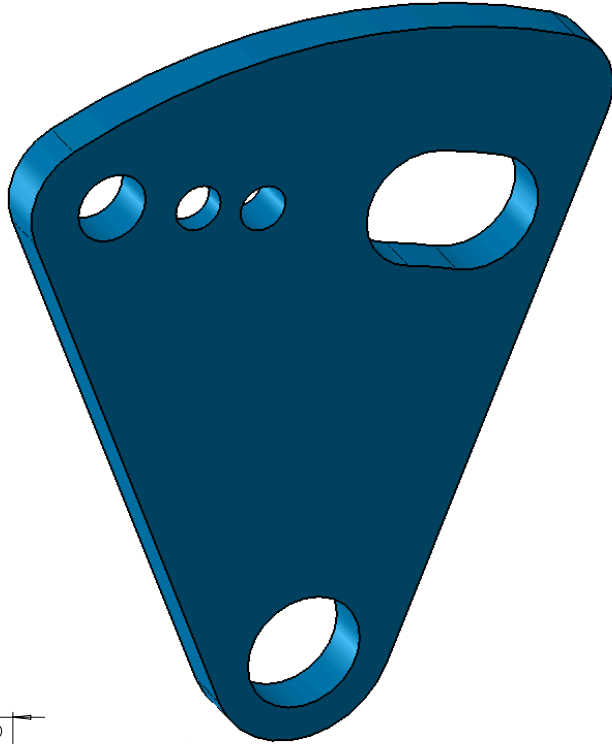
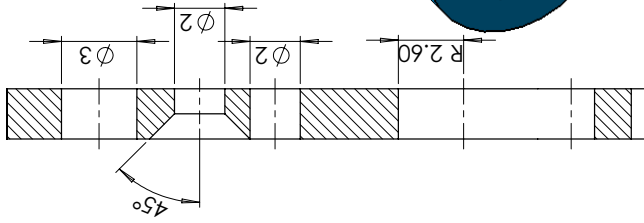


UNLESS OTHERWISE SPECIFIED: DIMENSIONS ARE IN MILLIMETERS SURFACE FINISH: TOLERANCES: ANGULAR:	FINISH: DEBUR AND BREAK SHARP EDGES	DO NOT SCALE DRAWING	REVISION
		11.2	
		Locking Bar Side - Front	
		DWG NO.	A3
		MemoSlide	
		MATERIAL:	Aluminium
		WEIGHT:	
SCALE: 1:1	SHEET 51 OF 73		



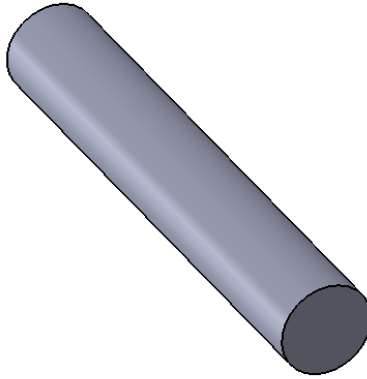
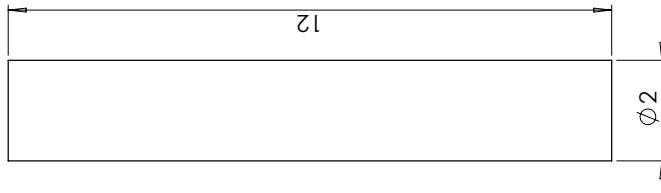
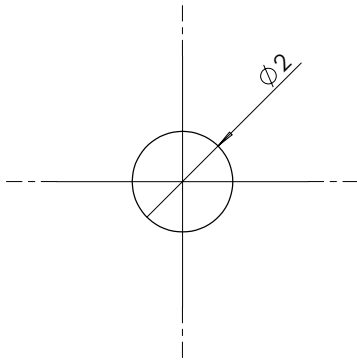
SECTION AP-AP

Completely analogous to part :
 "11.2 Locking Bar Side - Front"
 Except for the counter sink on the other side.



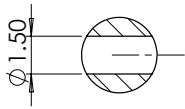
QTY.	2
------	---

UNLESS OTHERWISE SPECIFIED: DIMENSIONS ARE IN MILLIMETERS SURFACE FINISH: TOLERANCES: ANGULAR:	FINISH:	DEBUR AND BREAK SHARP EDGES	DO NOT SCALE DRAWING	REVISION
			11.3	
TITLE			Locking Bar Side - Back	
DRAWN	NAME	SIGNATURE	DATE	
CHK'D				
APP'VD				
MEG				
Q.A				
MATERIAL: Aluminium			DWG NO. MemoSlide	A3
WEIGHT:			SCALE: 1:1	SHEET 52 OF 73

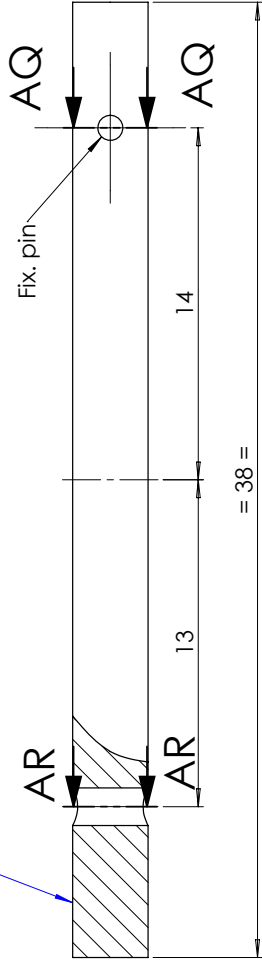


UNLESS OTHERWISE SPECIFIED: DIMENSIONS ARE IN MILLIMETERS		FINISH:	DEBUR AND BREAK SHARP EDGES		DO NOT SCALE DRAWING	REVISION	QTY. 4
SURFACE FINISH: TOLERANCES: ANGULAR:					11.4		
DRAWN	NAME	SIGNATURE	DATE	TITLE Pin 2x12 mm			
CHKD				DWG NO. A3			
APPVD				SCALE: 1:1			
MFG				SHEET 53 OF 73			
Q.A				MATERIAL: Stainless steel			
				WEIGHT:			

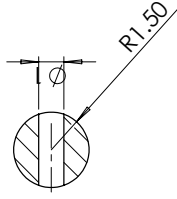
SECTION AR-AR



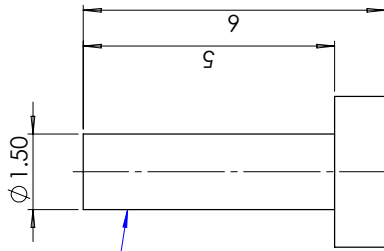
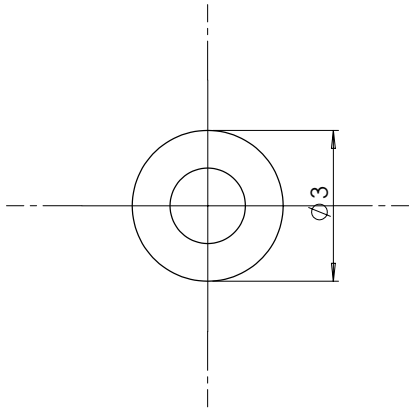
Slicing contact with bronze cams



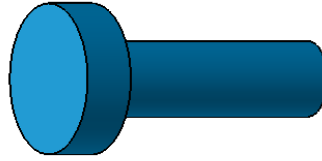
SECTION AQ-AQ



UNLESS OTHERWISE SPECIFIED: DIMENSIONS ARE IN MILLIMETERS		FINISH:		DEBUR AND BREAK SHARP EDGES		DO NOT SCALE DRAWING		REVISION	
SURFACE FINISH:		NAME		SIGNATURE		DATE		11.5	
TOLERANCES:		DRAWN		CHKD				TITLE	
ANGULAR:		APPRD		MFG		Q.A		Cam Follower - Memory	
		MATERIAL:		Stainless steel		DWG NO.		A3	
		WEIGHT:				SCALE: 1:1		SHEET 54 OF 73	
								QTY.	
								2	

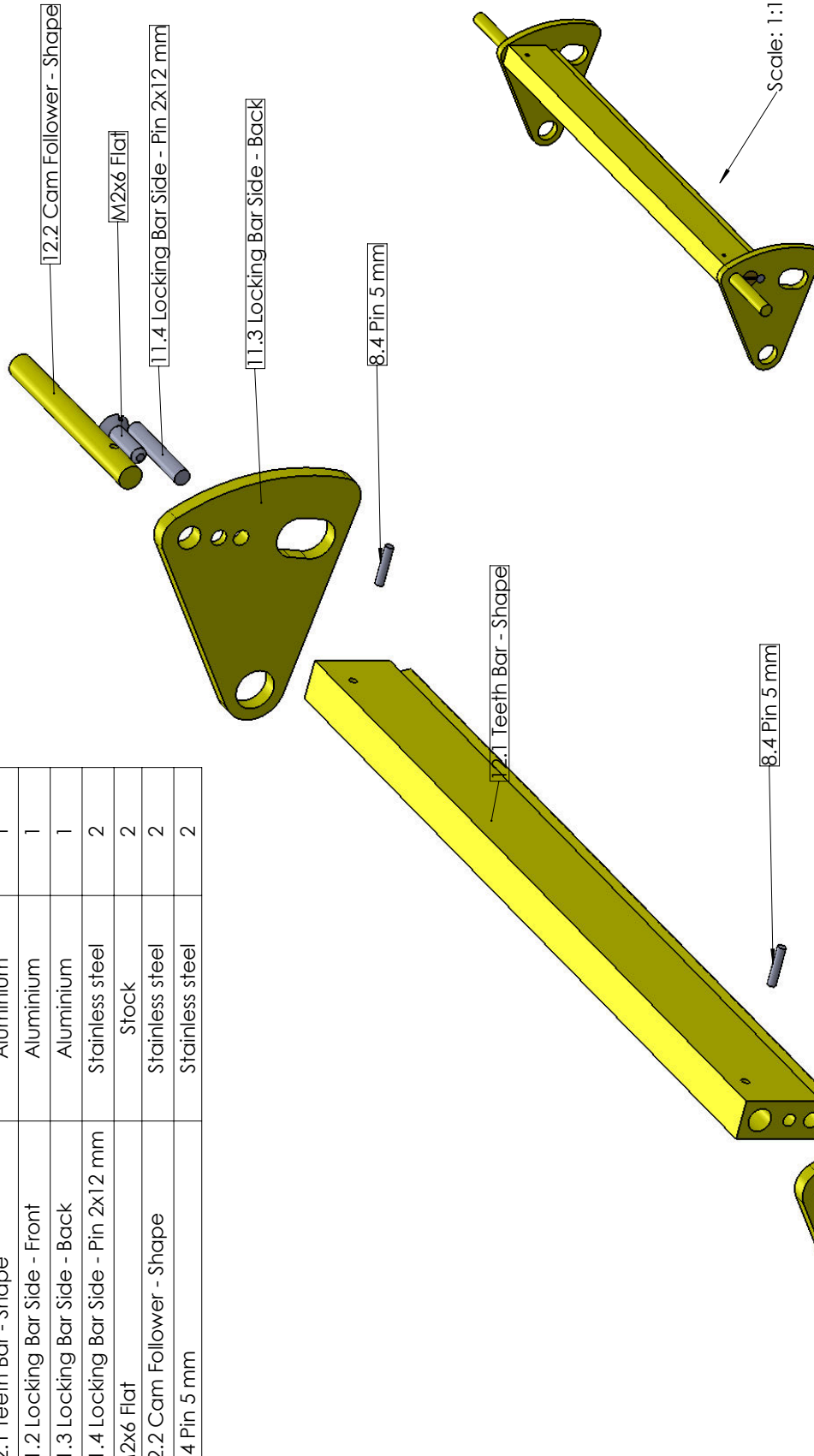


Press fit with parts:
 "1.5 Cam Follower - Memory" &
 "Bearing SKF W 638"

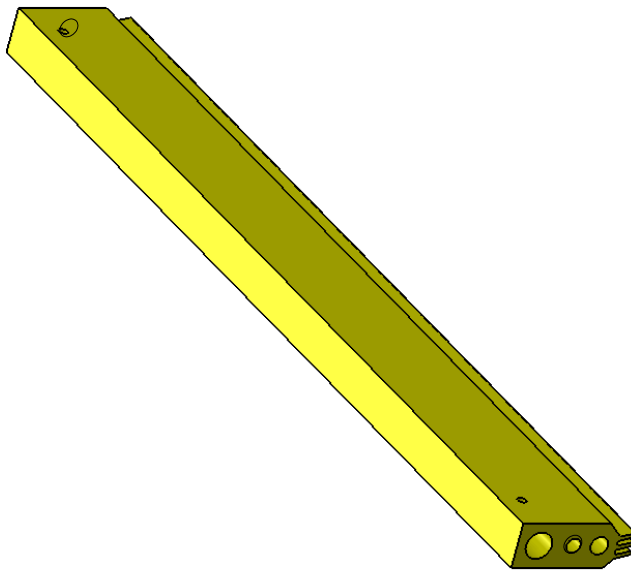
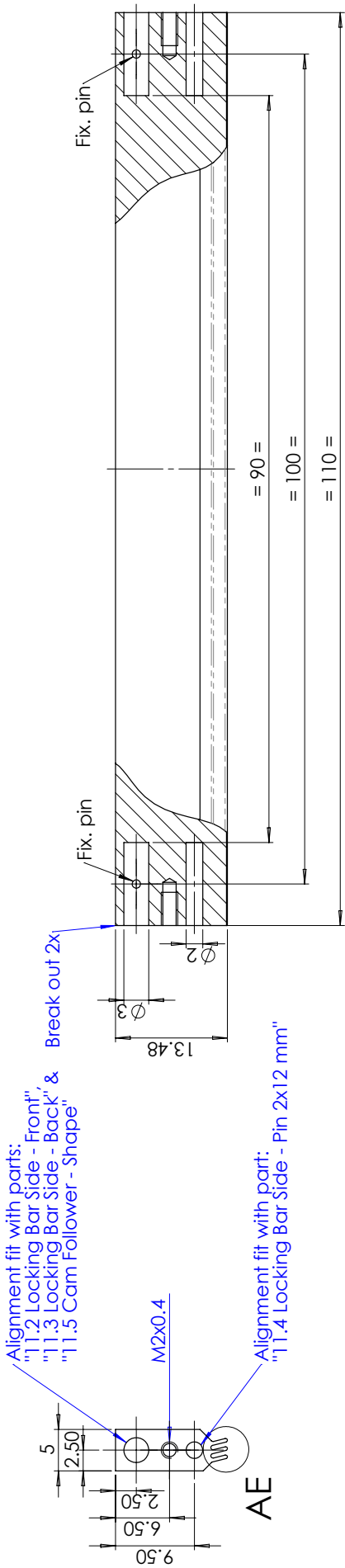


UNLESS OTHERWISE SPECIFIED: DIMENSIONS ARE IN MILLIMETERS		FINISH:		DEBUR AND BREAK SHARP EDGES		DO NOT SCALE DRAWING		REVISION	
SURFACE FINISH:		NAME		SIGNATURE		DATE		TITLE	
TOLERANCES:		DRAWN		CHKD		APPRD		MFG	
ANGULAR:		Q.A		MATERIAL: Stainless steel		DWG NO. A3		SCALE: 1:1	
QTY. 2		11.6		Bearing Pin		MemoSlide		SHEET 55 OF 73	

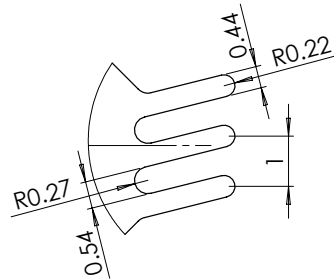
ITEM NO.	PART NUMBER	MATERIAL	Default/QTY.
1	12.1 Teeth Bar - Shape	Aluminium	1
2	11.2 Locking Bar Side - Front	Aluminium	1
3	11.3 Locking Bar Side - Back	Aluminium	1
4	11.4 Locking Bar Side - Pin 2x12 mm	Stainless steel	2
5	M2x6 Flat	Stock	2
6	12.2 Cam Follower - Shape	Stainless steel	2
7	8.4 Pin 5 mm	Stainless steel	2



UNLESS OTHERWISE SPECIFIED: DIMENSIONS ARE IN MILLIMETERS		FINISH:		DEBUR AND BREAK SHARP EDGES		DO NOT SCALE DRAWING		REVISION	
SURFACE FINISH:		Roughness:						12	
TOLERANCES:		ANGULAR:							
NAME	SIGNATURE	DATE	TITLE						
DRAWN			Locking Bar - Shape						
CHK'D			MemoSlide						
APP'VD			A3						
MFG			DWG NO.						
Q.A.			SCALE: 2:1						
MATERIAL:			WEIGHT:						
			SHEET 56 OF 73						



DETAIL AE
SCALE 10 : 1

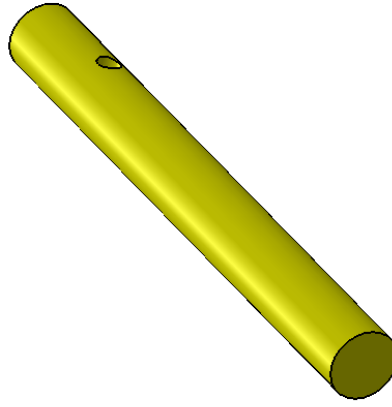
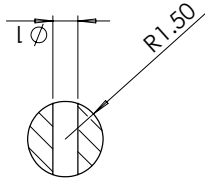
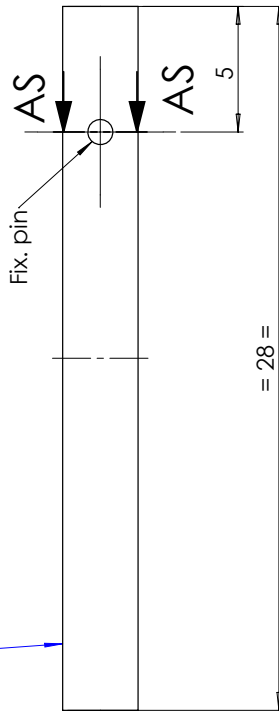


Sketch dimensions are available digitally in part: "12.1 Teeth Bar - Shape".

UNLESS OTHERWISE SPECIFIED: DIMENSIONS ARE IN MILLIMETERS		FINISH:		DEBUR AND BREAK SHARP EDGES		DO NOT SCALE DRAWING		REVISION	
SURFACE FINISH:		NAME		DATE		12.1		Teeth Bar - Shape	
TOLERANCES:		SIGNATURE						Memoslide	
ANGULAR:		DATE						A3	
		DRAWN						DWG NO.	
		CHK'D						SCALE:2:1	
		APP'VD						SHEET 57 OF 73	
		MFG						MATERIAL:	
		Q.A.						Aluminium	
								WEIGHT:	

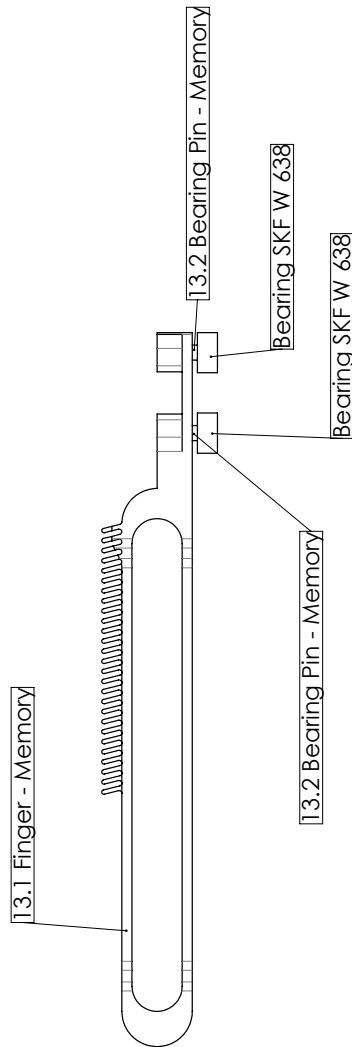
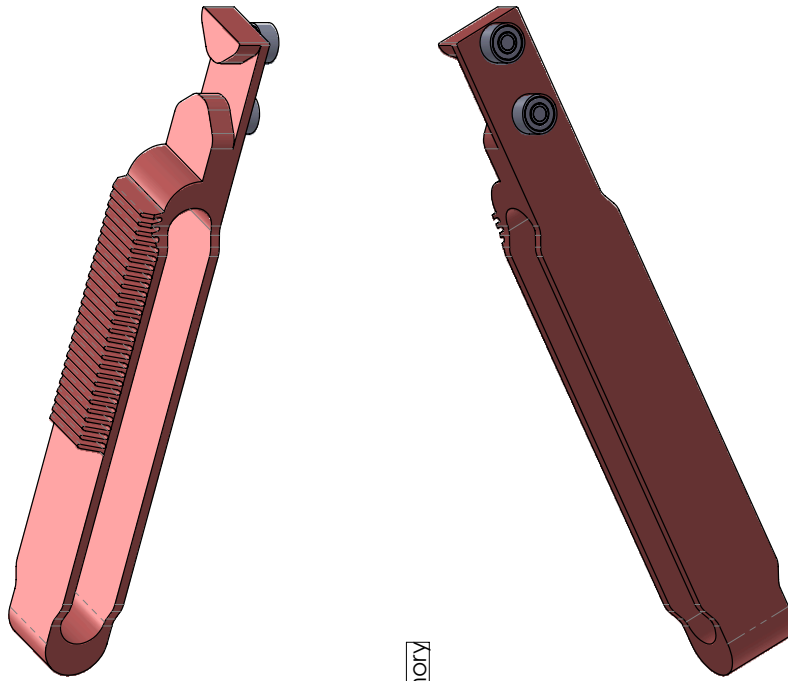
SECTION AS-AS

Sliding contact with bronze cams

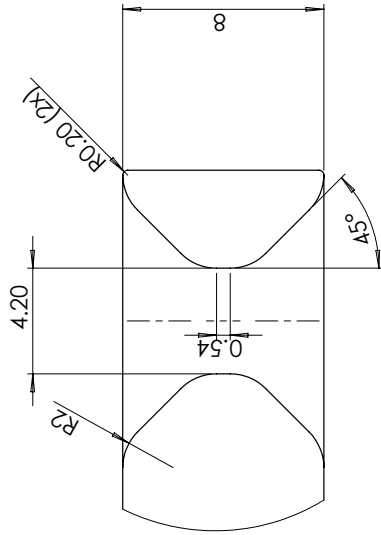


UNLESS OTHERWISE SPECIFIED: DIMENSIONS ARE IN MILLIMETERS		FINISH:		DEBUR AND BREAK SHARP EDGES		DO NOT SCALE DRAWING		REVISION	
SURFACE FINISH:		NAME		SIGNATURE		DATE		12.2	
TOLERANCES:		DRAWN		CHKD		APPRD		TITLE	
ANGULAR:		MFG		Q.A		MATERIAL:		Cam Follower - Shape	
						Stainless steel		DWG NO. A3	
						WEIGHT:		SCALE: 1:1	
								SHEET 58 OF 73	
QTY.		2							

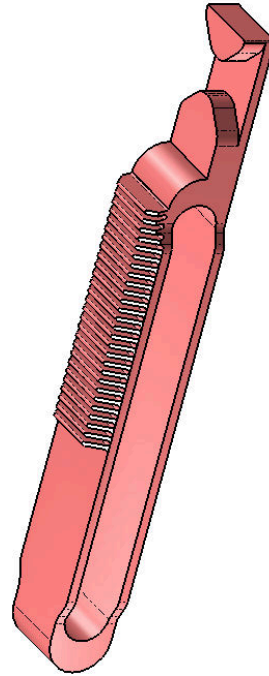
ITEM NO.	PART NUMBER	MATERIAL	QTY.
1	13.1 Finger - Memory	Aluminium	1
2	13.2 Bearing Pin - Memory	Stainless steel	2
3	Bearing SKF W 638	Stock	2



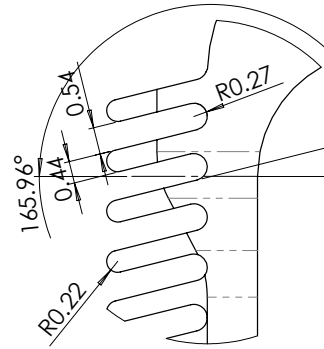
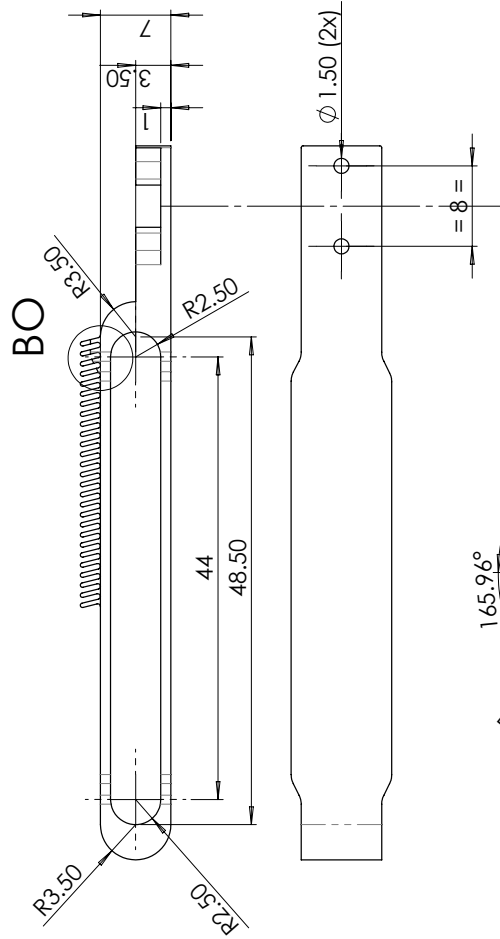
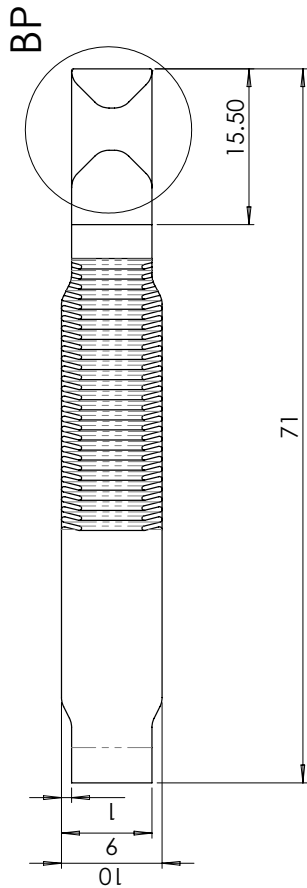
UNLESS OTHERWISE SPECIFIED: DIMENSIONS ARE IN MILLIMETERS		FINISH:		DEBUR AND BREAK SHARP EDGES		DO NOT SCALE DRAWING		REVISION	
SURFACE FINISH:		Roughness:				13			
TOLERANCES:		ANGULAR:							
								TITLE	
								Memory	
								DWG NO.	
								MemoSlide	
								A3	
								SCALE: 2:1	
								SHEET 59 OF 73	
DRAWN		NAME		SIGNATURE		DATE		MATERIAL:	
CHKD								WEIGHT:	
APPVD									
MEG									
Q.A									



DETAIL BP
SCALE 5 : 1

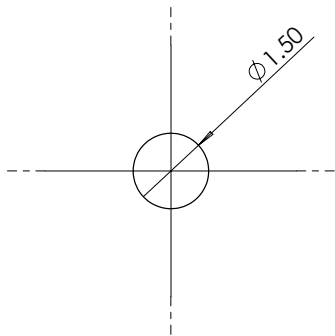


Sketch dimensions are available digitally in part: "13.1 Finger - Memory"

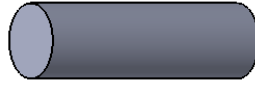
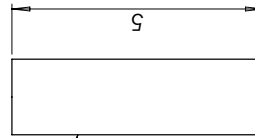


DETAIL BO
SCALE 10 : 1

UNLESS OTHERWISE SPECIFIED: DIMENSIONS ARE IN MILLIMETERS		FINISH:	DO NOT SCALE DRAWING	REVISION
SURFACE FINISH:		DEBUR AND BREAK SHARP EDGES	13	
TOLERANCES:				
ANGULAR:				
DRAWN	NAME	SIGNATURE	DATE	TITLE
CHKD				Finger - Memory
APPVD				
MFG				
QA				
				DWG NO. A3
				MemoSlide
				MATERIAL: Aluminium
				SCALE:2:1
				WEIGHT:
				SHEET 60 OF 73

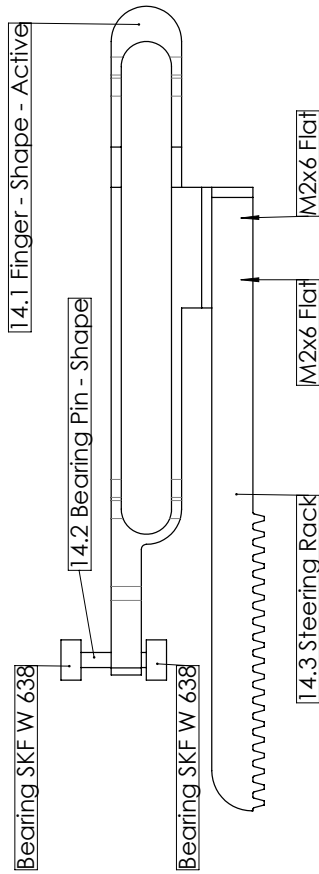


Pressfit between parts:
 "13.1 Finger - Memory" &
 "Bearing SKF W 638"



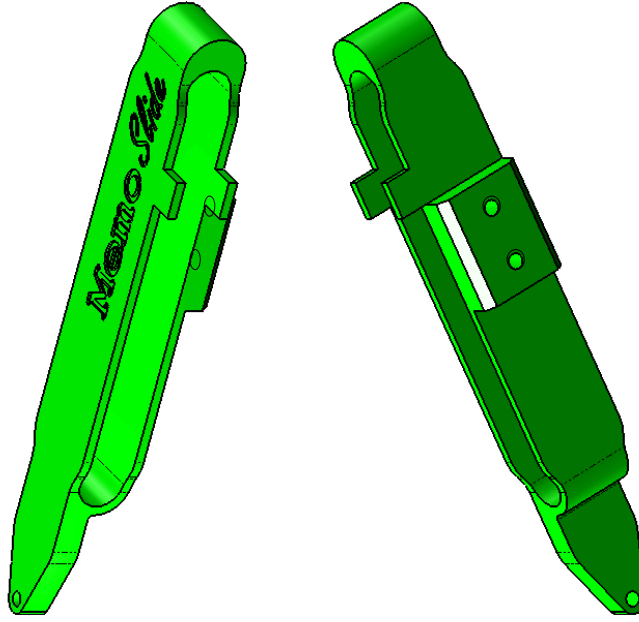
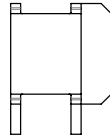
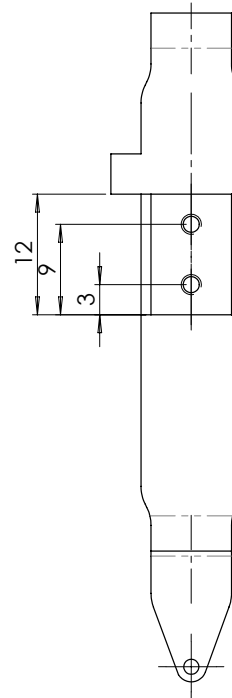
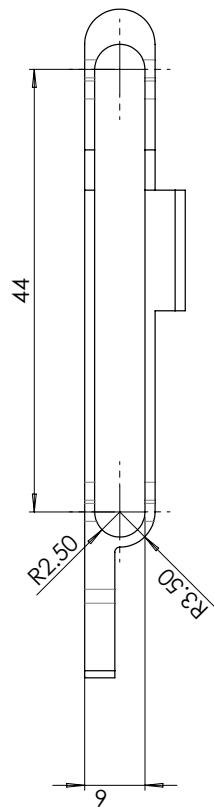
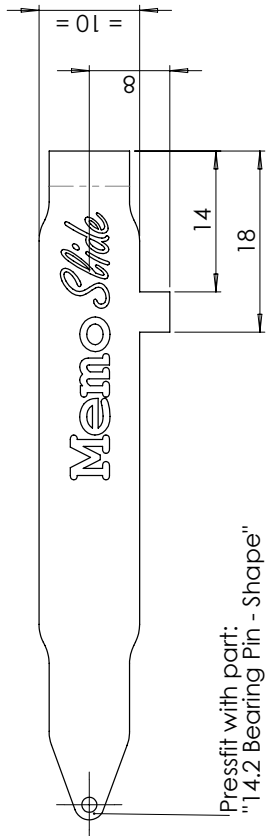
UNLESS OTHERWISE SPECIFIED: DIMENSIONS ARE IN MILLIMETERS		FINISH:		DEBUR AND BREAK SHARP EDGES		DO NOT SCALE DRAWING	REVISION
SURFACE FINISH: TOP SURFACES: ANGULAR:						13.2	
DRAWN	NAME	SIGNATURE	DATE	TITLE			
CHK'D				Bearing Pin - Memory			
APP'VD				DWG NO. A3			
MFG				MATERIAL: Stainless steel			
Q.A.				SCALE: 1:01			
			WEIGHT:		SHEET 61 OF 73		

ITEM NO.	PART NUMBER	MATERIAL	QTY.
1	14.1 Finger - Shape - Active	Aluminium	1
2	14.2 Bearing Pin - Shape	Stainless steel	1
3	Bearing SKF W 638	Stock	2
4	14.3 Steering Rack	Aluminium	1
5	M2x6 Flat	Stock	2

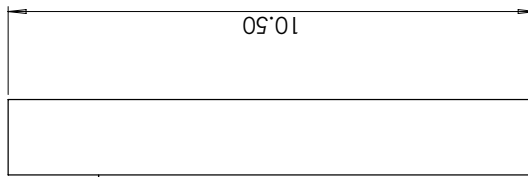
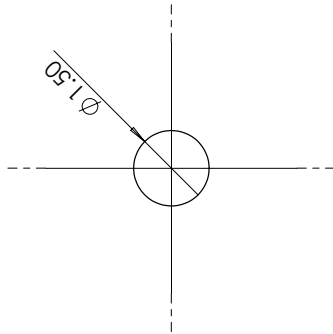


UNLESS OTHERWISE SPECIFIED: DIMENSIONS ARE IN MILLIMETERS		FINISH:		DEBUR AND BREAK SHARP EDGES		DO NOT SCALE DRAWING		REVISION	
SURFACE FINISH:		TOLERANCES:						14	
DIMENSIONS:		ANGULAR:						TITLE	
								Shape Active	
DRAWN		NAME		SIGNATURE		DATE		DWG NO.	
CHK'D								A3	
APP'VD								MemoSlide	
MFG								SCALE: 2:1	
Q.A.								SHEET 62 OF 73	
		MATERIAL:		WEIGHT:					

Sketch containing decorative engraving is available digitally in part: "14.1 Finger - Shape - Active"



UNLESS OTHERWISE SPECIFIED: DIMENSIONS ARE IN MILLIMETERS		FINISH:		DEBUR AND BREAK SHARP EDGES		DO NOT SCALE DRAWING		REVISION	
SURFACE FINISH:		TOLERANCES:				14.1			
DIMENSIONS:		ANGULAR:				TITLE		Finger - Shape - Active	
DRAWN		NAME		SIGNATURE		DATE		DWG NO.	
CHKD								A3	
APPRD								MemoSlide	
MEG								MATERIAL:	
Q.A								Aluminium	
								WEIGHT:	
								SCALE:2:1	
								SHEET 63 OF 73	

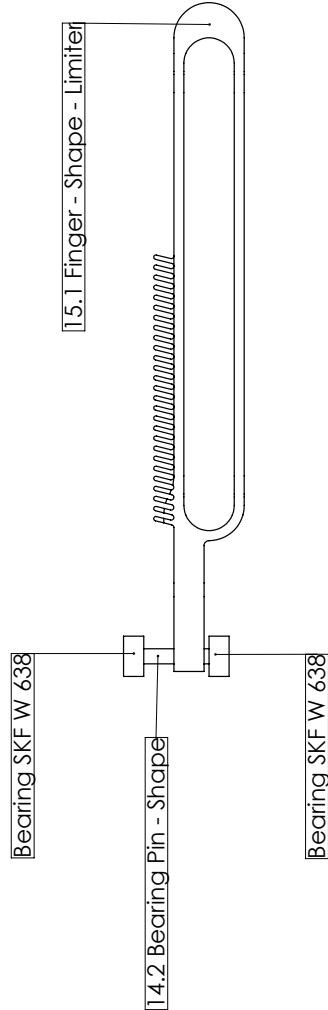
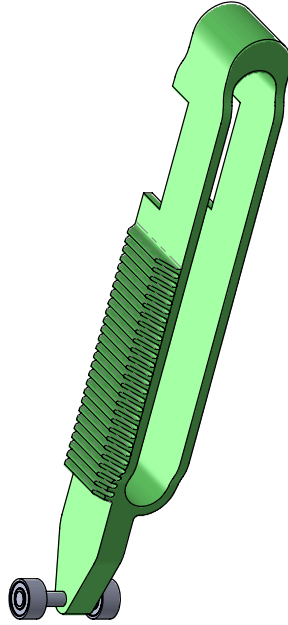


Pressfit between parts:
 "13.1 Finger - Memory" &
 "Bearing SKF W 638"

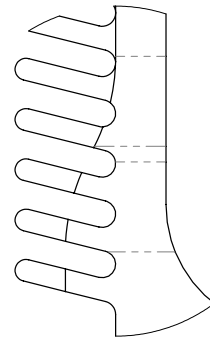
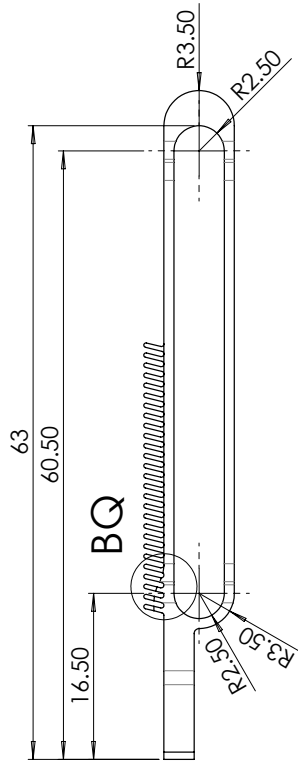
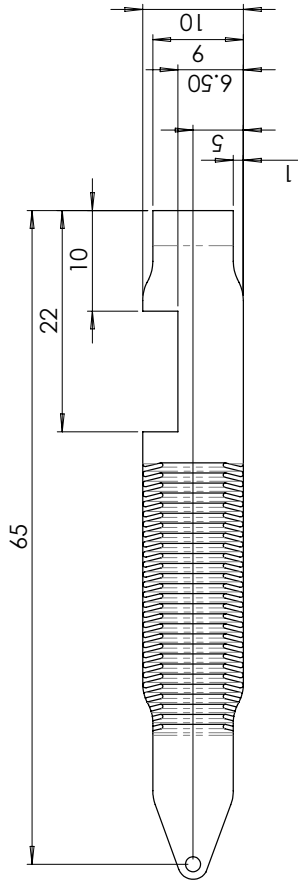


UNLESS OTHERWISE SPECIFIED: DIMENSIONS ARE IN MILLIMETERS		FINISH:		DEBUR AND BREAK SHARP EDGES		DO NOT SCALE DRAWING		REVISION	
SURFACE FINISH:		TOLERANCES:				14.2			
LINEAR:		ANGULAR:							
DRAWN	NAME	SIGNATURE	DATE			TITLE			
CHK'D						Bearing Pin - Shape			
APP'VD						DWG NO.		A3	
MFG				MATERIAL:		MemoSlide			
Q.A				Stainless steel		SCALE:10:1		SHEET 64 OF 73	
				WEIGHT:					

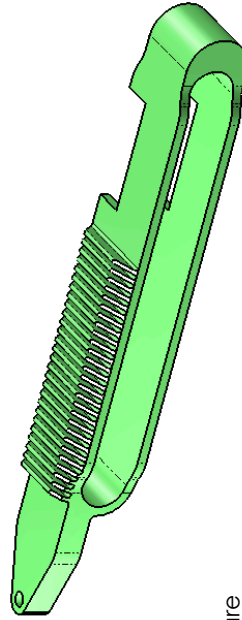
ITEM NO.	PART NUMBER	Material	QTY.
1	15.1 Finger - Shape - Limiter	Aluminium	1
2	14.2 Bearing Pin - Shape	Stainless steel	1
3	Bearing SKF W 638	Stock	2



UNLESS OTHERWISE SPECIFIED: DIMENSIONS ARE IN MILLIMETERS		FINISH:		DEBUR AND BREAK SHARP EDGES		DO NOT SCALE DRAWING		REVISION	
SURFACE FINISH:		TEXTURES:		RADIUS:		SCALE		NO.	
ANGULAR:		ANGULAR:		ANGULAR:		SCALE		NO.	
DRAWN	NAME	SIGNATURE	DATE	TITLE		15		Shape - Limiter	
CHKD				DWG NO.		MemoSlide		A3	
APPVD				MATERIAL:				SCALE:2:1	
MFG				WEIGHT:				SHEET 66 OF 73	
Q.A									



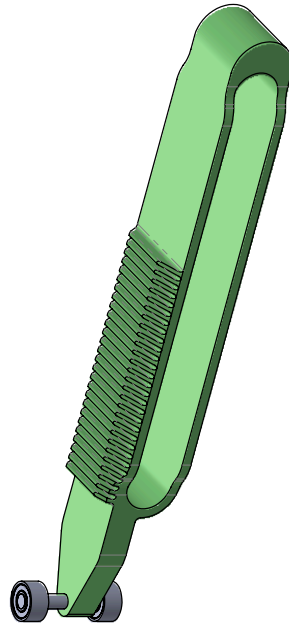
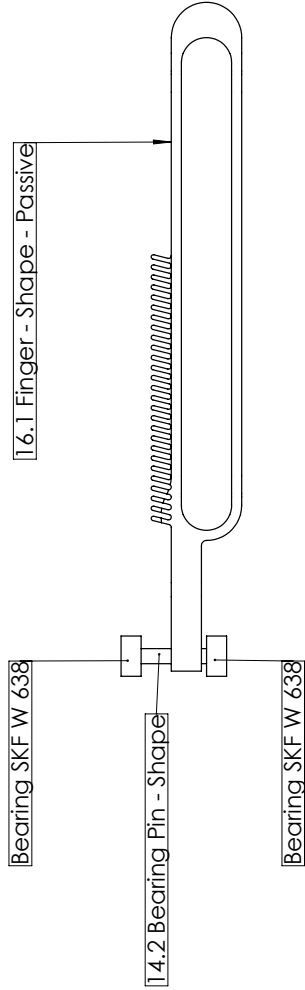
DETAIL BQ
SCALE 10 : 1



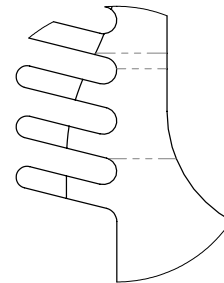
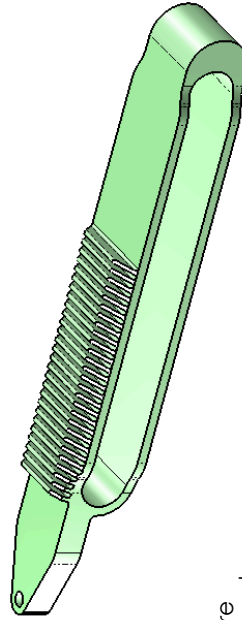
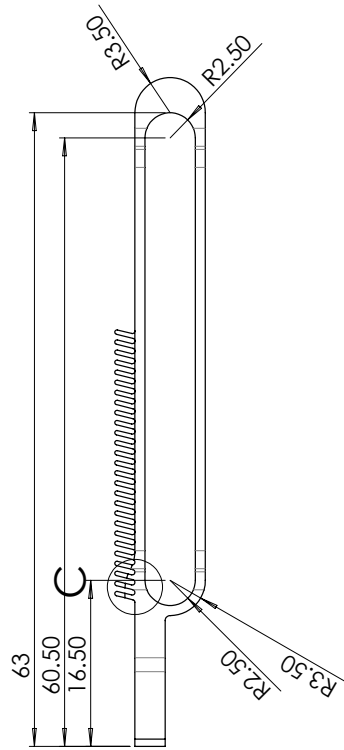
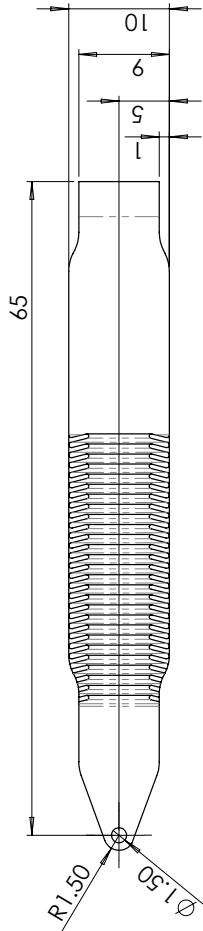
Sketch dimensions are available digitally in part: "13.1 Finger - Shape - Limiter"

UNLESS OTHERWISE SPECIFIED: DIMENSIONS ARE IN MILLIMETERS		FINISH:		DEBUR AND BREAK SHARP EDGES		DO NOT SCALE DRAWING		REVISION	
SURFACE FINISH:		TOLERANCES:				15.1			
DIMENSIONS:		ANGULAR:				TITLE		Finger - Shape - Limiter	
DRAWN	NAME	SIGNATURE	DATE	MATERIAL:		DWG NO.		A3	
CHK'D				Aluminium		MemoSlide			
APP'VD						SCALE:2:1		SHEET 67 OF 73	
MEG				WEIGHT:					
Q.A.									

ITEM NO.	PART NUMBER	Material	QTY.
1	16.1 Finger - Shape - Passive	Aluminium	1
2	14.2 Bearing Pin - Shape	Stainless steel	1
3	Bearing SKF W 638	Stock	2



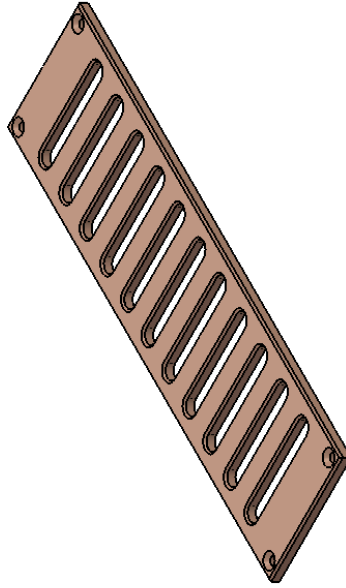
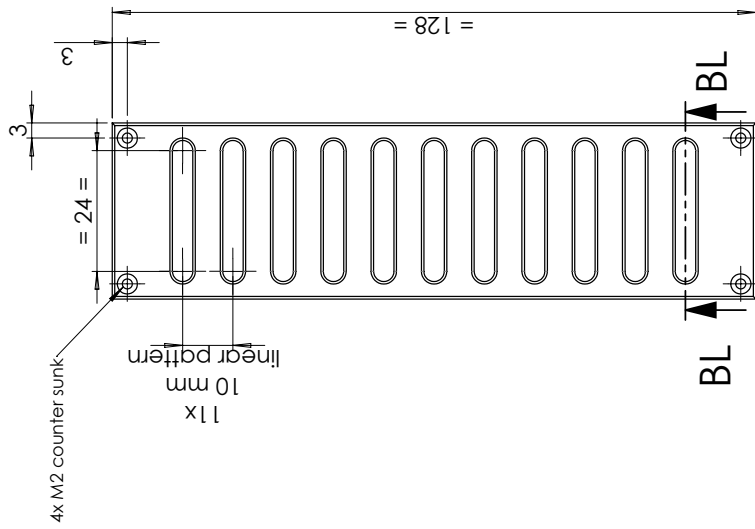
UNLESS OTHERWISE SPECIFIED: DIMENSIONS ARE IN MILLIMETERS		FINISH:		DEBUR AND BREAK SHARP EDGES		DO NOT SCALE DRAWING		REVISION	
SURFACE FINISH:		Roughness:						16	
TOLERANCES:		ANGULAR:						TITLE	
								Shape - Passive	
								DWG NO. A3	
								SCALE:2:1 SHEET 48 OF 73	
NAME	SIGNATURE	DATE	MATERIAL:		WEIGHT:				
DRAWN	CHK'D								
APP'D									
MFG									
Q.A									



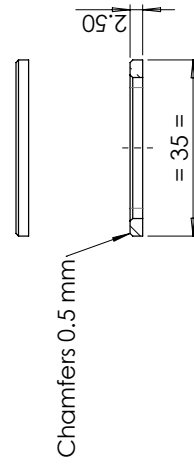
Sketch dimensions are available digitally in part: "16.1 Finger - Shape - Passive"

DETAIL C
SCALE 10 : 1

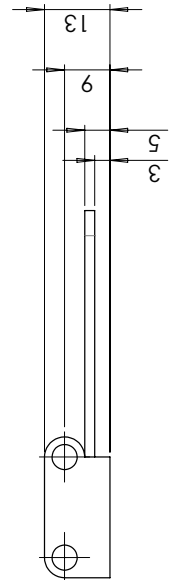
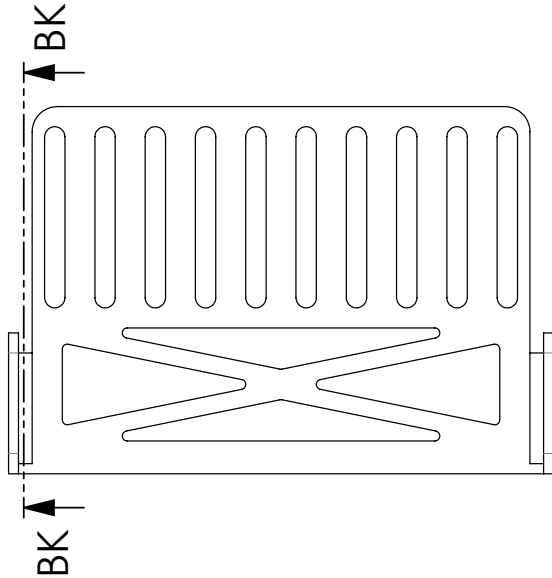
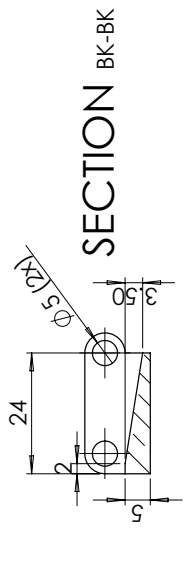
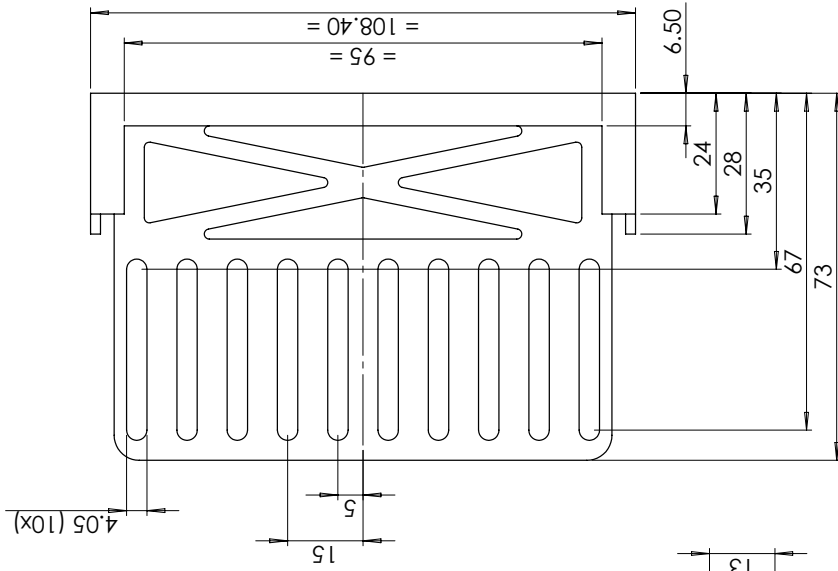
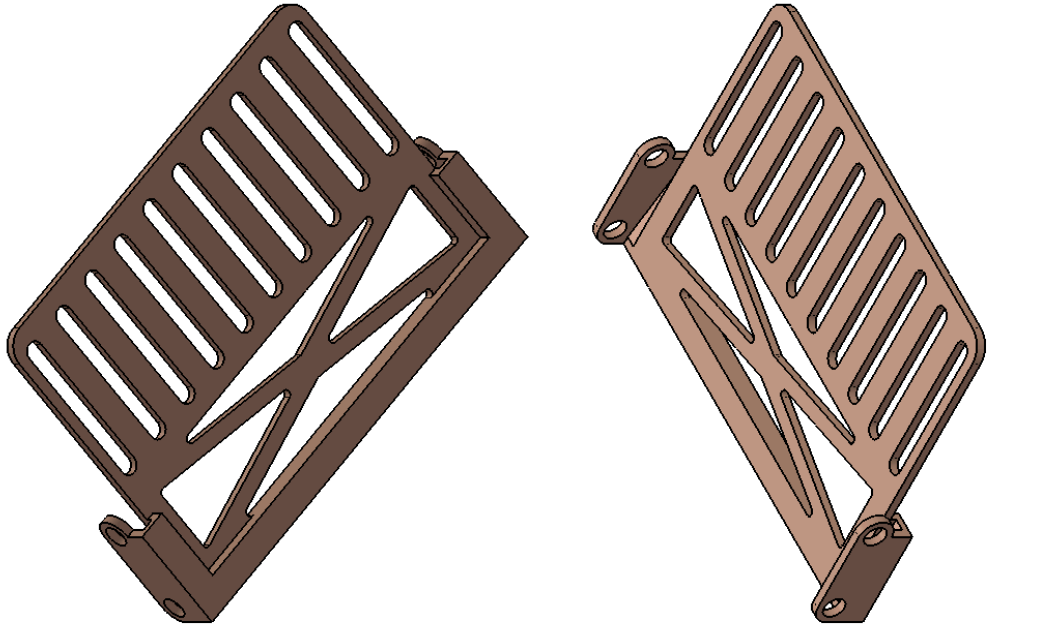
UNLESS OTHERWISE SPECIFIED: DIMENSIONS ARE IN MILLIMETERS		FINISH:		DEBUR AND BREAK SHARP EDGES		DO NOT SCALE DRAWING		REVISION	
SURFACE FINISH:		TOLERANCES:				16.1			
DIMENSIONS:		ANGULAR:						TITLE	
								Finger - Shape - Passive	
DRAWN		NAME		SIGNATURE		DATE		DWG NO.	
CHK'D								A3	
APP'VD								MATERIAL:	
MFG								Aluminium	
Q.A								WEIGHT:	
								SCALE:2:1	
								SHEET 69 OF 73	



Sketch dimensions are available digitally in part: "18 Guide Plate - Bottom"

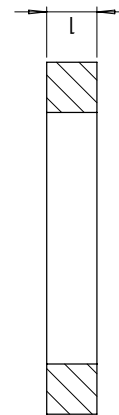
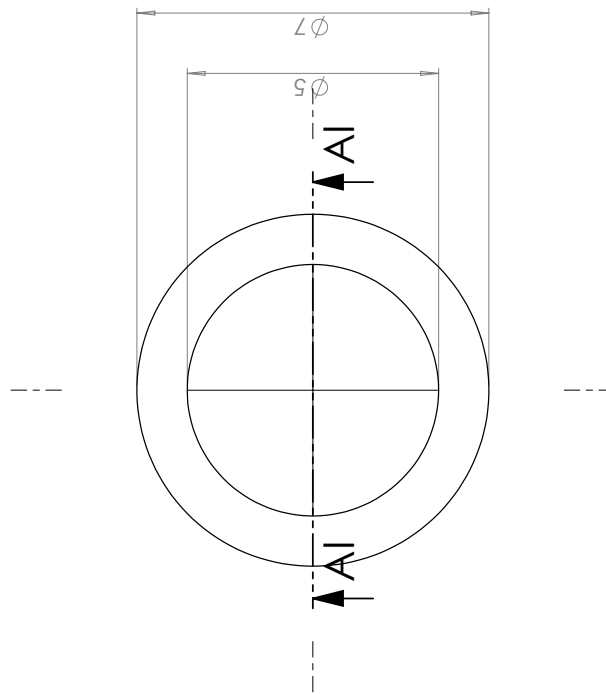
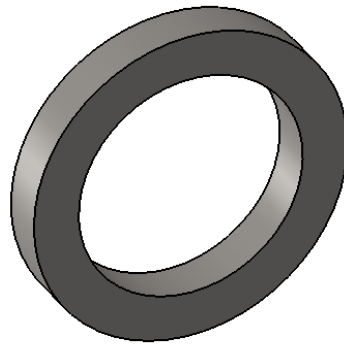


UNLESS OTHERWISE SPECIFIED: DIMENSIONS ARE IN MILLIMETERS		FINISH:		DEBURR AND BREAK SHARP EDGES		DO NOT SCALE DRAWING	REVISION
SURFACE FINISH:		TOLERANCES:				17	
DIMENSIONS:		ANGULAR:					
DRAWN	NAME	SIGNATURE	DATE	TITLE		Guide Plate - Top	
CHK'D						MemoSlide	
APP'D						A3	
MFG				MATERIAL:		Bronze	
Q.A.				WEIGHT:		SCALE:1:1	
						SHEET 70 OF 73	



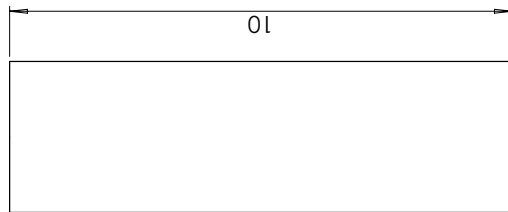
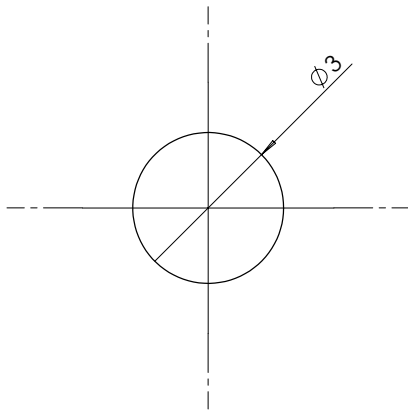
UNLESS OTHERWISE SPECIFIED: DIMENSIONS ARE IN MILLIMETERS SURFACE FINISH: TOLERANCES: ANGULAR:		FINISH:		DEBUR AND BREAK SHARP EDGES		DO NOT SCALE DRAWING	REVISION
DRAWN	NAME	SIGNATURE	DATE			18	
CHKD							
APPVD							
MEG							
Q.A							
				MATERIAL: Bronze		TITLE: Guide Plate - Bottom	
				WEIGHT:		DWG NO. A3	
				SCALE: 1:1		SHEET 71 OF 73	

Sketch dimensions are available digitally in part: "18 Guide Plate - Bottom"



SECTION AI-AI

UNLESS OTHERWISE SPECIFIED: DIMENSIONS ARE IN MILLIMETERS SURFACE FINISH: TOLERANCES: ANGULAR:		FINISH:	DEBUR AND BREAK SHARP EDGES	DO NOT SCALE DRAWING	REVISION	QTY. 2
DRAWN					19	
CHKD						
APPVD						
MFG						
Q.A						
NAME	SIGNATURE	DATE	TITLE Ring 5x1 mm			
			DWG NO. MemoSlide			
			MATERIAL: Stainless steel			
			SCALE: 1:01			
			WEIGHT: SHEET 72 OF 73			



Pressfit between parts:
 "1 Baseplate",
 "2,1 Frame",
 "3,1 Frame",
 "4,1 Frame",
 "5,1 Frame"



UNLESS OTHERWISE SPECIFIED: DIMENSIONS ARE IN MILLIMETERS		FINISH:		DEBUR AND BREAK SHARP EDGES		DO NOT SCALE DRAWING	REVISION
SURFACE FINISH:		NAME		SIGNATURE		20	
TOLERANCES:		DATE		DATE		TITLE	
ANGULAR:		DRAWN		CHK'D		Pin 3x10 mm	
		APPR'D		MFG		DWG NO.	
		Q.A.		MATERIAL: Stainless steel		A3	
				WEIGHT:		SCALE: 1:01	
						SHEET 73 OF 73	
QTY.		8					